Kinetics of Mn-Based Sorbents for Hot Coal Gas Desulfurization

FINAL TECHNICAL REPORT

09/15/1994-09/15/1997

AUTHORS: M.T. Hepworth
J. J. Berns
K. A. Sadecki

REPORT ISSUE DATE: 09/15/1997

DE-FG22-94PC94212 -11

Department of Civil Engineering
500 Pillsbury Dr. S.E.
University of Minnesota
Minneapolis, MN55435-0220

Disclaimer:

ABSTRACT

Mixed manganese oxide sorbents have been investigated for high-temperature removal of hydrogen sulfide (the primary sulfur bearing compound) from hot coal gases. The sorbents were screened by thermodynamic equilibrium considerations for sulfidation. Preliminary experimental work using thermogravimetric analysis (TGA) indicated titania to be a superior substrate than alumina. Four formulations showing superior reactivity in a TGA were then tested in an ambient pressure fixed-bed reactor to determine steady state H_2S concentrations, breakthrough times and effectiveness of the sorbent when subjected to cyclic sulfidation and regeneration testing. Eight tests were conducted with each test consisting of five cycles of sulfidation and regeneration. Sulfidation occurred at 600^oC using a simulated coal gas at an empty-bed space velocity of approximately 12,000 per hour. Manganese-based sorbents with molar ratios > 1:1 Mn:Substrate were effective in reducing the H_2S concentration in simulated coal gases to less than 100 ppmv over five cycles. Actual breakthrough time for formulation C6-2-1100 was as high as 73% of breakthrough time based on wt% Mn in sorbent at 600^oC. Regeneration tests determined that loaded pellets can be essentially completely regenerated in an air/steam mixture at 750^oC with minimal sulfate formation. The leading formulation (designated C6-2) from the fixed-bed tests was then further tested under varying sorbent induration temperature, sulfidation temperature and superficial gas velocity. Four tests were conducted with each test consisting of four cycles of sulfidation and regeneration. Results showed that the induration temperature of the sorbent and the reaction temperature greatly affected the H_2S removal capacity of the sorbent while the superficial gas velocity between 1090 and 1635 cm/min had minimal affect on the sorbent's breakthrough capacity. Testing showed that the sorbent's strength was a strong function of the sorbent induration temperature. Sorbent also showed 30 to 53% loss of its strength over four cycles of sulfidation and regeneration. The former being sorbent indurated at 1115^oC and the prior being sorbent indurated at 1100^oC. A mathematical model was developed to describe the reaction of H_2S with the mixed metal oxide in a fixed-bed reactor, where the individual pellets react according to the shrinking core model. The effective diffusivity within a single pellet was estimated by adjusting its value until a good match between the experimental and model H_2S breakthrough curves was obtained. Predicted sorbent conversion at the conclusion of test FB3A compared well with experimental sulfur analysis.

TABLE OF CONTENTS

EXECUTIVE SUMMARY

Mixed manganese oxide sorbents have been investigated for high-temperature removal of hydrogen sulfide, H_2S, (the primary sulfur bearing pollutant) from hot coal gases. Sorbents were screen by thermodynamic equilibrium considerations for sulfidation. Four formulations were prepared and testing in an ambient pressure fixed-bed reactor to determine desulfurization performance and effectiveness of the sorbent when subjected to cyclic sulfidation and regeneration testing. Eight tests were conducted with each test consisting of five cycles of sulfidation and regeneration. Sulfidation occurred at 600^{o}C using a simulated coal gas at an empty-bed space velocity of approximately 12,000 per hour. Results identified a sorbent containing 4.33 to 1 manganese to titanium on a molar basis as the leading formulation (designated C6-2). Regeneration tests determined that loaded pellets can be essentially completely regenerated in an air/steam mixture at 750^{o}C with minimal sulfate formation. Sorbent strength had decreased, however, over the five cycles. It is not known whether the strength had stabilized or would have continued to decrease. Further testing of sorbent C6-2 in a fixed-bed reactor showed that the sulfidation temperature and the sorbent induration temperature greatly affected the sorbent's H_2S removal capacity while the superficial gas velocity had minimal impact on the sorbent desulfurization performance.

CHAPTER 1. INTRODUCTION

1.1 Introduction

In response to environmental regulations and diminishing petroleum supplies, the production of a clean fuel-gas from coal for use in electric power generation has been gaining attention. Power generation processes such as the integrated gasification combined cycle (IGCC) and the molten carbonate fuel cells (MCFC) are receiving interest because of their potential for superior environmental performance, economics and efficiency in comparison to conventional coal-based power plants.

During the gasification of coal, sulfur pollutants (primarily H_2S and COS) are produced. Coal gas desulfurization is necessary for environmental reasons in addition to protection of turbine components (IGCC) and prevention of electrode poisoning (MCFC). To maintain thermal efficiency hot coal gas desulfurization (HGD) is desired.

Several metal oxides have been investigated as regenerable sorbents for the desulfurization of hot coal gas. The metal oxide should be capable of lowering the H_2S concentration to a level acceptable for IGCC application (100 ppmv). In addition it should regenerate nearly completely to maintain activity over numerous cycles. A general sulfidation reaction is represented by equation 1.1.

$$MO_{(s)} + H_2S_{(g)} = MS_{(s)} + H_2O_{(g)} \qquad (1.1)$$

Where MO and MS refer to a metal oxide and its corresponding sulfide. A typical regeneration reaction is represented by equation 1.2.

$$MS_{(s)} + \frac{3}{2}O_{2(g)} = MO_{(s)} + SO_{2(g)} \qquad (1.2)$$

Due to stability difficulties of single and binary metal oxides, incorporation of an inert secondary metal oxide has been gaining interest. The inert component increases pore structure integrity, stabilizes the active metal against reduction and increases the sorbent durability.

1.2. Objectives

A limited thermodynamic analysis is conducted to determine the potential of manganese oxide sorbents (with and without secondary metal oxides incorporated into them) to lower the H_2S concentration in simulated coal gas. The conditions under which sulfation will occur is also investigated.

Several sorbent formulations are prepared where the amount of substrate (secondary metal oxide) and binder is varied. These formulations are tested in a thermogravimetric apparatus in which weight changes of individual pellets can be measured as a function of reaction time. The superior performing sorbent formulations are then tested in an ambient pressure fixed-bed reactor to determine steady-state H_2S concentrations, breakthrough times and effectiveness of the sorbent when subjected to cyclic testing. The leading formulation of the fixed-bed tests is then further tested. The effects of sulfidation temperature, superficial gas velocity and induration temperature of the sorbent on the desulfurization performance of this leading formulation in a fixed-bed reactor is investigated. In addition, the crush strengths of the sorbent sulfided under varying conditions are compared after 4 cycles of sulfidation and regeneration.

The shrinking core model is also developed to describe the kinetics of sulfidation for single pellets and a mathematical model is derived to describe the sulfidation reaction in a fixed-bed reactor, where individual pellets react according to the shrinking core model. The effective diffusivity within a single pellet is estimated by adjusting its value until a good match between the experimental and model breakthrough curves is obtained. Predicted sorbent conversion as a function of axial length along a packed-bed is compared to experimental sulfur analysis.

CHAPTER 2. LITERATURE REVIEW

2.1 Introduction

The availability of coal in the United States exceeds that of all forms of petroleum and natural gas combined[1]. At current consumption rates, the recoverable coal reserves have been estimated to be adequate over two hundred years. In 1990, 33% of the energy and over half of the electricity that was produced in the U.S. was derived from coal[2]. Table 2.1 shows the contributions of fuel sources in energy and electricity production in the United States.

Table 2.1. Contribution of fuel sources in total energy and electricity production in the U.S. (1990)[2]

Percent of total production in the U.S. (1990 values)						
Fuel	Coal	Petroleum	Natural Gas	Nuclear	Hydro-electric	Other
Energy	33.1	22.9	30.3	13.7		
Electricity	55.5	4.2	9.4	20.5	10.0	0.4

2.2 Coal Characteristics

Coal is derived from the partial degradation of plants. This degradation process varies under varying reaction conditions (microbiological activity, climate) and thus the composition, structure and products of coal vary even for coal mined in the same general location. Coal contains carbon, hydrogen, oxygen and impurities such as sulfur, nitrogen, ash, and trace metals. Major constituents of ash are silica, alumina, iron, calcium, magnesium, sodium, potassium and titanium which are non-combustible. Table 2.2 shows the typical ultimate analysis of major classifications of coal found in the United States.

Table 2.2. Typical ultimate analysis of major classifications of coal found in the U.S. [3]

Type of Coal	Ultimate analysis, mass percent					
	C	H_2	S	O_2	N_2	H_2O
Anthracite	83.9	2.9	0.7	0.7	1.3	2.5
Bituminous (medium volatile)	80.7	4.5	1.8	2.4	1.1	3.3
Subbituminous	58.8	3.8	0.3	12.2	1.3	19.6
Lignite	42.4	2.8	0.7	12.4	0.7	34.8

2.3 Emerging Technologies for Coal Utilization

With diminishing petroleum supplies and stringent environmental regulations, the production of a clean fuel gas from coal for use in electric power generation has been gaining interest. Advanced electric power generation processes such as the integrated gasification combined cycle (IGCC) and molten carbonate fuel cells (MCFC) are receiving attention[4] because of their potential for superior environmental performance, economics, and efficiency in comparison to conventional coal-based power plants.

2.3.1 Integrated Gasification Combined Cycle (IGCC)

IGCC has been identified as an attractive process for the generation of electricity from coal. This is due in part because IGCC can more easily meet the environmental standards for NO_X and SO_X emissions than conventional power plants[5] and the overall efficiency for electric power generation is higher for IGCC than conventional power plants. A simplified diagram of the IGCC process is shown in Figure 2.1.

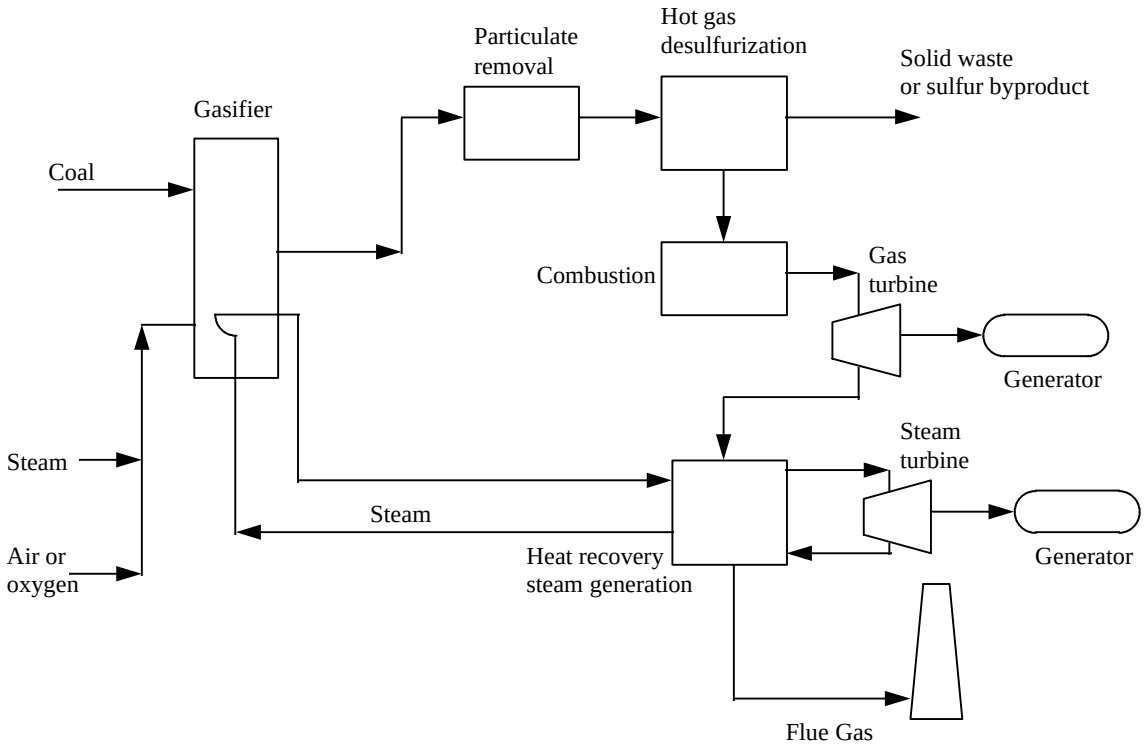

Figure 2.1. Simplified diagram of the ideal integrated gasification combine cycle (IGCC) process.

In the IGCC process, coal is gasified at high temperature (1600-1800^{o}C) and pressure (1 -7 MPa) depending on the process used (reactor type, feed gas composition) then cooled. Gas exiting the gasifier after cooling is at 482-593^{o}C[6]

and is directed to a particulate removal system. The gas is then directed to the hot gas desulfurization system where sulfur pollutants (primarily H_2S and COS) are removed. The gas is then combusted and the resulting hot exhaust is routed through a gas turbine to generate electricity. The residual heat in the exhaust is used to generate steam which then runs a steam turbine to generate additional electricity.

2.3.2 Coal Gasification

Coal gasification has been around for hundreds of years; however, with the emergence of IGCC, it has gained more attention in the past 20 years. During gasification, coal is reacted with steam and oxygen at high temperature and pressure according to equations 2.1 and 2.2.

$$C_{(s)} + H_2O \rightarrow CO_{(g)} + H_{2(g)} \quad (2.1)$$

$$C_{(s)} + O_{2(g)} \rightarrow CO_{2(g)} \quad (2.2)$$

Reaction 2.1 is highly endothermic and will not occur unless the necessary heat of reaction is supplied. This heat can be supplied by burning some of the coal shown in reaction 2.2. Sulfur pollutants are also produced during the gasification process. These sulfur pollutants contain primarily H_2S and COS, with H_2S accounting for approximately 95% of the sulfur pollutants[7].

The composition of a raw fuel gas produced by coal gasification can vary over a wide range, depending on the gasification process (feed gas composition, reactor type) and the type of coal used. The composition of various typical oxygen-blown and air-blown gasifier gases are reported in Table 2.3.

Table 2.3. Typical gasifier exit gas compositions (vol%)[a,8]

	A	B	C	D	E	F	G	H
CO	8	10.55	16.13	11.9	40	24.33	39.1	64
CO_2	11	4.64	7.55	10	12.5	5.16	12.25	0.8
H_2	16	8.26	10.7	17.4	27.84	13.19	30.13	31.6
H_2O	30	27.52	10.94	28.1	18.5	5.35	17.52	1.5
H_2S	3	.06-.5	0.42	1	1.08	0.118	1	1.4
COS	-	-	0.03	-	0.08	-	-	-
N_2	29	48.73	54.22	28.7	-	49.9	-	0.7
CH_4	3	0.24	-	3	-	1.84	-	-
NH_3	0.5	0.2	0.16	0.5	0.2	0.111	-	-
CO/CO_2	0.73	2.27	2.14	1.19	3.2	4.72	3.19	80
H_2/H_2O	0.53	0.3	0.98	0.62	1.5	2.47	1.72	21

[a]Typical air-blown gasifiers: GE fixed-bed (A), KRW fluid bed (B), Texaco entrained-bed (C), and Lurgi fixed-bed (D), Tampella U-gas (F); and typical oxygen-blown gasifiers: Texaco entrained-bed (G) and Shell (H).

2.4 Hot Gas Desulfurization (HGD)

Sulfur pollutants (primarily H_2S and COS) are produced during coal gasification; the concentration of these pollutants must be lowered from several thousand parts per million (ppm) down to the order of 100 ppm for gas turbines (IGCC) and down to 1 ppm for fuel cells[9]. H_2S removal is necessary for environmental reasons in addition to preventing corrosion of the turbine blades (IGCC) and poisoning of the electrodes in a fuel cell. To maintain high thermal efficiency in an IGCC process, H_2S and COS should be removed at the exiting gasifier gas temperatures.

2.5 High Temperature Sorbents

There have been many studies on HGD sorbents. These studies primarily focused on metal oxides as HGD sorbents. The general reaction for H_2S reacting with a metal oxide is given by equation 2.3

$$MO_{(s)} + H_2S_{(g)} = MS_{(s)} + H_2O_{(g)} \qquad (2.3)$$

where M represent a metal. The metal oxide should be capable of reducing the H_2S concentration to an acceptable level for application to IGCC in the temperature range of interest (400°C to 650°C). The upper temperature limit is determined by valve limitations. These valves must be able to withstand high temperatures and pressures under alternating reducing and oxidizing conditions. The lower temperature is limited by thermal efficiency.

Westmoreland and Harrison (1976)[10] studied the thermodynamical feasibility of 28 solids, primarily metal oxides, for high-temperature desulfurization of low-Btu gases. Eleven of these solids showed thermodynamic feasibility for high-temperature desulfurization. These solids (primarily oxides) were based upon the metals: Fe, Zn, Mo, Mn, V, Ca, Sr, Ba, Co, Cu, and W. In a subsequent study[11] the kinetics of 4 metal oxides possessing favorable thermodynamics were investigated. The four metal oxides investigated were CaO, MnO, V_2O_3 and ZnO. Initial rates of chemical reaction were determined over a temperature range of 300-800°C at 1 atm total pressure. It was found that reaction rate of H_2S with MnO is approximately one order of magnitude greater than the reaction rate with either CaO or ZnO and two orders of magnitude greater than the reaction rate with V_2O_3.

Early work on HGD sorbents focused primarily on iron oxide[12-16] and zinc oxide[16-18]. Iron oxide showed favorable reaction kinetics, but unfavorable removal efficiencies (thermodynamics) in comparison to zinc oxide. The two were then combined to form the mixed metal oxide zinc ferrite, $ZnFe_2O_4$[19-23]. This mixed metal oxide possessed H_2S removal efficiency comparable to ZnO but with increased capacity[24].

Studies[25] determined, however, that both ZnO and $ZnFe_2O_4$ had the tendency to reduce in whole or part to zinc metal in coal gas atmospheres which

volatilized, losing valuable sorbent. Sintering and reduction of ZnO by H_2 to volatile Zn limit its operating temperature to approximately 600°C[9]. This led to the incorporation of inert metal oxides into reactive metal oxides. Incorporation of an inert component such as titania, silica or alumina increases pore structure integrity, stabilizes the active metal oxide against reduction and increases the pellet durability.

2.5.1 Zinc-Based Sorbents

Zinc-based sorbents have been extensively researched[4,16,17,19,25-31]. The thermodynamic equilibrium for sulfidation of ZnO is quite favorable, yielding H_2S removal down to a few parts per million[16]. However, as mentioned above, ZnO will reduce to volatile elemental zinc at temperatures greater than 600°C. Tight temperature control is also necessary during regeneration with high temperatures resulting in zinc loss and low temperature resulting in sulfate formation. This has led to the formulation of sorbents containing mixed-metal oxides such as various zinc-titanate formulations. The addition of TiO_2 stabilizes ZnO, thereby increasing the maximum desulfurization temperature to approximately 760°C[7]. Zinc titanate sorbents have been researched for the past 14 years with prices still exceeding $7.00 per pound[32].

2.5.2 Manganese-Based Sorbents

Manganese-based sorbents have also been extensively researched[8,13,33-37]. MnO is not as capable of reducing the H_2S concentration to as low a level as ZnO is, however, manganese-based sorbents do have characteristics that are favorable for coal gas desulfurization. Although ZnO is better at eliminating H_2S than MnO, MnO possesses the advantage of being stable over a wider temperature range under even severely reducing conditions. MnO was found to be stable from temperatures in excess of 1000°C down to 400°C[10], thereby allowing greater flexibility in sulfidation and regeneration temperatures without loss of sorbent. As discussed in section 2.5, the reaction rate of MnO was also found to be higher than that of ZnO, CaO and V_2O_3 under similar sulfidation conditions. The price of manganese pellets made from manganese ore has been predicted to be not less than $3.00 per pound[32].

2.6 Cold versus Hot Sulfur Clean-up

The most commonly used technology for the desulfurization of flue gas from conventional coal-based power plants is the use of a lime-slurry washing process. This technology removes about 90% of the SO_2; however, large volumes of flue gases at low pressure have to be cooled down to ambient temperature and then reheated to 150°C before discharge into the atmosphere[38].

A benefit of coal gasification is that the sulfur is removed at high pressure resulting in lower volumes of gas to be processed through the desulfurization equipment. Other benefits of coal gasification as opposed to conventional coal

processes are that the sulfur is converted to hydrogen sulfide which is easier to remove than SO_2, and elemental sulfur may be recovered as a saleable product[38]. Sulfur removal of greater than 99% may be achievable[39] when using an appropriate metal oxide as the sulfur sorbent.

Economic studies have shown that HGD results in lower capital and operating costs than conventional cold gas desulfurization[40]. A 2-3% increase in efficiency is achieved when desulfurization occurs at 350^{o}C while further increasing the temperature only results in small increases in efficiency[41]. HGD reduces efficiency losses due to cooling and reheating of the fuel gas[16] and minimizes wastewater treatment costs associated with cold gas cleanup.

Advantages that cold sulfur removal has over HGD is that pollutants other than sulfur such as heavy metals will also be removed through condensation and the process has been used for many years making it well established.

2.7. Regeneration

Regeneration of the sorbent is necessary for HGD to be economically viable. A sorbent must be able to undergo numerous sulfidation and regeneration cycles while maintaining strength and reactivity. Sorbent life of one year has been expected in some processes to satisfy economic restraints[42].

Regeneration is typically carried out by oxidizing the loaded sorbent with air by the following general reaction

$$MS_{(s)} + \frac{3}{2}O_{2(g)} \rightarrow MO_{(s)} + SO_{2(g)} \qquad (2.4)$$

Where M is a metal and the SO_2 in the exit regeneration gas can then be used to produce sulfuric acid or elemental sulfur. Sulfuric acid production is only feasible, however, if a nearby plant and market exists. Due to the highly exothermic behavior of oxidation, regeneration in air alone can cause excessive reactor temperatures thereby causing sintering of the pellets and deterioration of the sorbent capacity for H_2S removal[15]. In addition to excessive temperatures, regeneration exit gas composition has been found to vary considerably with time making it difficult to design effective sulfur recovery process[6].

In addition to SO_2 formation, sulfate may also be formed during oxidative regeneration, which is detrimental to the pellet's strength. There are two possible pathways for sulfate formation
path 1:

$$MS + \frac{3}{2}O_2 \rightarrow MO + SO_2 \qquad (2.5)$$

$$MO_{(s)} + SO_{2(g)} + \frac{1}{2}O_{2(g)} \rightarrow MSO_{4(s)} \qquad (2.6)$$

path 2:

$$MS_{(s)} + 2O_{2(g)} \rightarrow MSO_4 \qquad (2.7)$$

where M represents a metal. In path 1, the sulfide is first converted to the oxide with SO_2 evolution and then the oxide reacts with the SO_2 and more O_2 to form the sulfate. In path 2, the oxide is directly converted to the sulfate. Siriwardane and Woodruff (1995)[31] investigated the reaction mechanism of sulfate formation. They found that ZnS reacts according to path 1. Thus to minimize sulfate formation the O_2 should be kept low; however, this will result in low SO_2 formation, making the regeneration exit stream less favorable for sulfuric acid or elemental sulfur production.

Due to the problems of oxidative regeneration, steam regeneration was proposed[13,15,36]. The general reaction is shown in equation 2.8.

$$MS_{(s)} + H_2O_{(g)} = MO_{(s)} + H_2S_{(g)} \qquad (2.8)$$

Atakul et al. (1995)[36] found that sorbent containing MnS supported by g-Al_2O_3 could be completely regenerated in steam at 600^{o}C, however, when regeneration was 90% complete, steam consumption was 8.4 times higher than the theoretical stoichiometric amount of steam required.

A novel regeneration process conducted by Olson et al. (1979)[43] showed that elemental sulfur formation was possible when regenerating sorbent in a steam-air mixture. They reported selectivity for sulfur formation as high as 75% when a mixture of 95 vol% steam and 5 vol% air was used to regenerate iron oxide-silica and iron oxide-fly ash sorbents. Other products formed were H_2S, SO_2 and traces of SO_3. Elemental sulfur production is typically desirable as the sulfur is easy to store, dispose or sell.

2.8 References

1. Nowacki, Perry, *Coal Gasification Processes*, **1981**, Noyes Data Corporation.

2. U.S. Bureau of the Census, *Statistical Abstract of the United States*, **1993**, 113th edition,Washington DC, 571-585.

3. El-Wakil, M.M., Powerplant Technology, McGraw-Hill Book Company, New York, **1984**.

4. Woods, M. C.; Gangwal, S. K.; Jothimurugesan, K.; Harrison, D. P., "Reaction between H_2S and Zinc Oxide-Titanium Oxide Sorbents. 1. Single-Pellets Kinetic Studies", *Ind. Eng. Chem. Res.* **1990**, 29, 1160-1167.

5. Lacey, J. A., "Gasification: a key to the clean use of coal Part 2", *Energy World* **1988**, 156, 2-6.

6. Ayala, R. E.; Kim, B. M., "Modeling and Analysis of Moving-Bed Hot-Gas Desulfurization Processes", *Environmental Progress* **1989**, Vol. 8, No. 1, 19-25.

7. Wang, J. C. P.; Groves, F. R.; Harrison, D. P., "Modeling High Temperature Desulfurization in a Fixed-Bed Reactor", *Chemical Engineering Science* **1990**, Vol. 45, No. 7, 1693-1701.

8. Ben-Slimane, R.; Hepworth, M. T., "Desulfurization of Hot Coal-Derived Fuel Gases with Manganese-Based Regenerable Sorbents. 1. Loading (Sulfidation) Tests", *Energy and Fuels* **1994**, 8, 1175-1183.

9. Ozum, B.; Kovacik,G.; Chambers, A., "Coal Gasification Gas Cleanup", *Int. J. Hydrogen Energy* **1993**, Vol. 18, No. 10, 847-851.

10. Westmoreland, P. R.; Harrison, D. P., "Evaluation of Candidate Solids for High-Temperature Desulfurization of Low-Btu Gases", *Environmental Science and Technology* **1976**, Vol. 10, No. 7, 659-661.

11. Westmoreland, P. R.; Gibson, J.B.; Harrison, D. P. "Comparitive Kinetics of High-Temperature Reaction of H_2S and Selected Metal Oxides", *Environmental Science and Technology* **1977**, Vol. 11, No. 5, 488-491.

12. Sasaoka, E.; et al., "Reactivity and Durability of Iron Oxide High Temperature Desulfurization Sorbents", *Energy and Fuels* **1993**, 7, 632-638.

13. Wakker, J. P.; Gerritsen, A.W.; Moulijn, J.A., "High Temperature H_2S and COS Removal with MnO and FeO on g-Al_2O_3 Acceptors", *Ind. Eng. Chem. Res.* **1993**, 32, 139-149.

14. Schrodt, J. T.; Best, J. E., "Sulfur Recovery from Fuel Gas Desulfurization Sorbents", *AIChE* **1978**, Vol 74, No. 175, 184-189.

15. Tamhankar, S. S.; Garimella, S.; Wen, C. Y., "Kinetic Study on the Reactions Involved in Hot Gas Desulfurization using a Regenerable Iron Oxide Sorbent-III. Reactions of the Sulfided Sorbent with Steam and Steam-Air Mixtures", *Chemical Engineering Science* **1985**, Vol. 40, No. 6, 1019-1025.

16. Tamhankar, S. S.; Bagajewicz, M.; Gavalas, G. R., "Mixed-Oxide Sorbents for High-Temperature Removal of Hydrogen Sulfide", *Ind. Eng. Chem. Process Des. Dev.* **1986**, 25, 429-437.

17. Sasaoka, E.; et al., "Characterization of Reaction between Zinc Oxide and Hydrogen Sulfide", *Energy and Fuels* **1994**, 8, 1100-1105.

18. Hepworth, M. T.; Ben-Slimane, R.; Zhong, S., "Thermodynamic Comparison of Several Sorbent Systems for Hot Coal-Derived Fuel-Gas Desulfurization", *Energy and Fuels* **1993**, 7, 602-609.

19. Gangwal, S. K.; Harkins, S. M.; Woods, M. C., "Bench-Scale Testing of High-Temperature Desulfurization Sorbents", *Environmental Progress* **1989**, Vol. 8, No. 4, 265-269.

20. Karlegard, A.; Bjerle, I., "Kinetic Studies on High Temperature Desulphurization of Synthesis Gas with Zinc Ferrite", *Chem. Eng. Technol.* **1994**, 17, 21-29.

21. Woods, M. C.; Gangwal, S. K.; Jothimurugesan, K.; Harrison, D. P., "Kinetics of the Reaction of a Zinc Ferrite Sorbent in High-Temperature Coal Gas Desulfurization", *Ind. Eng. Chem. Res.* **1991**, 30, 100-107.

22. Swisher, J. H.; Schwerdfeger, K., "Thermodynamic Analysis of Sorption Reaction for the Removal of Sulfur from Hot Gases", *JMEPEG* **1992**, 1, 565-572.

23. Christoforou, S. C.; Efthimiadis, E.A.; Vasalos, I. A., "Sulfidation of Mixed Metal Oxides in a Fluidized-Bed Reactor", *Ind. Eng. Chem. Res.* **1995**, 34, 83-93.

24. Grindley, T.; Steinfeld, G., "Development and Testing of Regenrable Hot Coal Gas Desulfurization Sorbents", Final Report DOE/MC/16545-1125, **1981**, METC, Morgantown, WV.

25. Stephanopoulos, M. F.; et al., "Mixed-Oxide Sorbents for High-Temperature Removal of Hydrogen Sulfide", *Ind. Eng. Chem. Process Des. Dev.* **1986**, 25, 429-437.

26. Jothimurugesan, K.; Harrison, D.P., "Reaction between H2S and Zinc Oxide-Titanium Oxide Sorbents. 2. Single-Pellet Sulfidation Modeling", *Ind. Eng. Chem. Res.* **1990**, 29, 1167-1172.

27. Stephanopoulos, M. F.; et al., " High-Temperature H2S Removal from Fuel Gases by Regenerable Zinc Oxide-Titanium Dioxide Sorbents", *Ind. Eng. Chem. Res.* **1989**, 28, 535-541.

28. Swisher, J. H.; Yang, J., "Attrition-Resistant Zinc Titanate Sorbent for Sulfur", Ind. Eng. Chem. Res. **1995**, 34, 4463-4471.

29. Siriwardane, R. V.; Poston, J. A., "Interaction of H2S with Zinc Titanate in the Presence of H2 and CO", *Applied Surface Science* **1990**, 45, 131-139.

30. Konttinen, J.; Mojtahedi, W., "Gasifier Gas Desulfurization at High Temperature and Pressure", *Kemia Kemi* **1993**, 20, 9-10, 847-851.

31. Siriwardane, R. V.; Woodruff, S., "FTIR Characterization of the Interaction of Oxygen with Zinc Sulfide", *Ind. Eng. Chem. Res.* **1995**, 34, 699-702.

32. Hepworth, M. T.; Ben-Slimane, R., "Hot Coal Gas Desulfurization with Manganese-Based Sorbents", Proceedings of the Advanced Coal-Fired Power Systems '95 Review Meeting, **1995**, Vol. 1, 367-381.

33. Hepworth, M. T.; Ben-Slimane, R., "Desulfurization of Hot Coal-Derived Fuel Gases with Manganese-Based Regenerable Sorbents. 3. Fixed-Bed Testing", *Energy and Fuels* **1995**, 9, 372-378.

34. Hepworth, M. T.; Ben-Slimane, R., "Desulfurization of Hot Coal-Derived Fuel Gases with Manganese-Based Regenerable Sorbents. 2. Regeneration and Multicycle Tests", *Energy and Fuels* **1994**, 8, 1184-1191.

35. Turkdogan, E. T.; Olsson, R. G.; Vinters, J. V., "Sulfate and Sulfide Reactions in the Mn-S-O System",*Metallurgical Transactions B* **1977**, 8B,59-65.

36. Atakul, H.; Wakker, J. P.; Gerritsen, A. W., "Removal of H_2S from Fuel Gases at High Temperatures using MnO/g-Al_2O_3", *Fuel* **1995**, Vol. 74, No. 2, 187-191.

37. Turkdogan, E. T.; Olsson, R.G., "Desulfurization of Hot Reducing Gases with Manganese Oxide Pellets", Proceedings of the Third International Iron and Steel Congress 16-20 April **1978**, Chicago, IL, 277-288.

38. Lacey, J. A., "Gasification: a key to the clean use of coal Part 1",*Energy World* **1988**, 155, 3-7, 9.

39. Mojtahedi, W.; Salo, K.; Abbasian, J., "Desulfurization of Hot Coal Gas in Fluidized Bed with Regenerable Zinc Titanate Sorbents", *Fuel Processing Technology* **1994**, 37, 53-65.

40. Gangwal, S. K.; Gupta, R.; McMichael, W. J., "Hot-Gas Cleanup-Sulfur Recovery Technical, Environmental, and Economic Issues",*Heat Recovery Systems & CHP***1995**, Vol. 15, No. 2, 205-214.

41. Vershoor, M. J. E.; Melman, A. G., "System Study High Temperature Gas Cleaning at IGCC Systems", TNO-Milieu & Energie**1991**, The Netherlands.

42. Gardner, T., DOE/METC, Morgantown, WV, Personal Communication, **1997**.

43. Olson, J. D.; Haynes, M. L.; Shah, V., "Hot Low-Btu Product Gas Desulfurization in Fixed-Bed of Iron Oxide-Fly Ash", USDOE Contract Fe-77-C-01-2757, Final Report, **1979**.

CHAPTER 3. THERMODYNAMIC CONSIDERATIONS

3.1 Introduction

A thermodynamic investigation was conducted to determine the theoretical capability of selected mixed manganese oxide sorbents to eliminate H_2S from coal gas and to determine under what conditions sulfate formation will occur during regeneration. Sulfate formation is an undesirable side reaction for two main reasons. First, manganese sulfate is a larger reaction product than manganese sulfide and will cause the pellets to spall and crack. Second, manganese sulfate will decompose in the presence of a reducing gas during subsequent sulfidations, liberating sulfur dioxide.

3.2 Sulfidation Thermodynamics

The desulfurization of mixed manganese oxide sorbents can be represented by the following reaction

$$H_2S_{(g)} + MnO * M_xO_{y(s)} = H_2O_{(g)} + MnS_{(s)} + M_xO_{y(s)} \qquad (3.1)$$

where M represents a secondary metal. The secondary metal oxides considered were aluminum oxide (Al_2O_3-corundum), silicon oxide (SiO_2-silica) and titanium dioxide (TiO_2-rutile). Excess manganese in the fresh sorbent will exists as Mn_3O_4 or Mn_2O_3; however, upon contact with a reducing coal gas under desulfurization conditions is reduced to MnO. The reaction of MnO with H_2S is given by equation 3.2.

$$H_2S_{(g)} + MnO_{(s)} = H_2O_{(g)} + MnS_{(s)} \qquad (3.2)$$

The equilibrium for the reaction shown in equation 3.2 was determined by Turkdogan and Olsson (1978)[1].

$$\mathrm{Log}\left(\frac{pH_2O}{pH_2S}\right) = \frac{3330}{T} - 0.310 \qquad (3.3)$$

As seen in equation 3.2, the exiting partial pressure of H_2O is equal to the partial pressure of H_2S reacted plus any H_2O vapor in the entering gas. Since the partial pressure of H_2S at equilibrium is typically very low, equation 3.3 can be rewritten to give the exiting equilibrium H_2S concentration for known inlet concentrations of H_2S and H_2O.

$$[H_2S](\text{ppmv}) = \frac{(\%H_2O_{in} + \%H_2S_{in})}{10^{\frac{3330}{T} - 4.310}} \qquad (3.4)$$

Figure 3.1 shows the equilibrium H_2S concentrations as determined from equation 3.4 as a function of temperature for both Shell and KRW coal gas, the compositions of which are given in Table 2.3. These two gases were chosen based on their large difference in H_2O content. As seen in Figure 3.1, the lower the temperature the lower the equilibrium H_2S concentration for both Shell and KRW gas. The dashed line represents the maximum concentration of H_2S acceptable for IGCC application. Shell gas can theoretically be desulfurized with MnO to IGCC specification at temperatures exceeding 900°C, whereas KRW gas can only be desulfurized at temperatures below approximately 610°C. H_2S equilibrium levels are higher for KRW gas than Shell gas at all temperatures because of the higher water vapor content in KRW gas (27.52%) as opposed to Shell gas (1.5%). Therefore, from an equilibrium standpoint a dry gas being desulfurized at as low a temperature as possible is desired. However, thermal efficiencies and kinetics are compromised at lower temperatures.

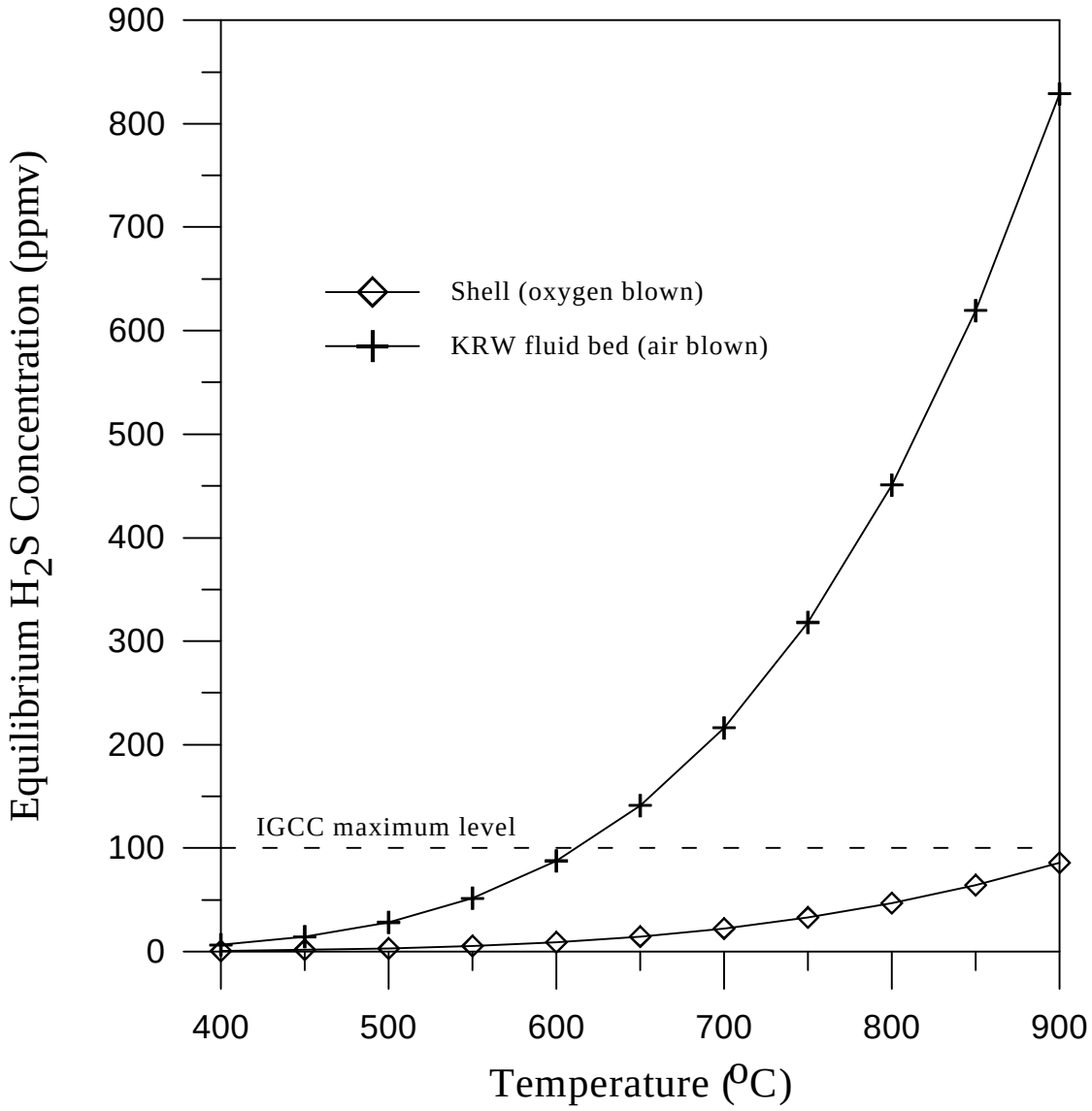

Figure 3.1. H_2S concentration as a function of temperature for Shell and KRW coal gas in equilibrium with MnO and MnS.

Previous equilibrium calculations were based on MnO as the desulfurizing component (equation 3.1). In the following discussion, the desulfurization of a coal gas using selected mixed manganese oxide compounds (equation 3.2) will be presented. A free energy minimization program will be used to calculate the H_2S concentration in equilibrium with various mixed manganese oxide compounds for a simplified Shell gas. This program requires specification of initial composition, temperature and pressure. All possible compounds, of those elements specified in the initial mixture, are considered as possible components of the equilibrium mixture. The amount of each component which minimizes the free energy of the system subject to elemental material balance constraints (defined by the initial mixture) is then determined. The simplified Shell gas has the following compounds and molar percentages: H_2 27, CO 64, H_2O 2, CO_2 2, H_2S 0.5 and N_2 4.5.

The results of the effect of temperature on the equilibrium of various mixed manganese oxide compounds and a simplified Shell gas is depicted in Figure 3.2. As seen in the figure, the lowest H_2S concentration at all temperatures is achieved using MnO as the sorbent while desulfurization with $MnO*Al_2O_3$ allowed the highest H_2S concentration at all temperatures. A sorbent containing an excess of manganese (i.e. four moles of MnO to one mole of TiO_2) is also included for comparison, identified by the + symbol.

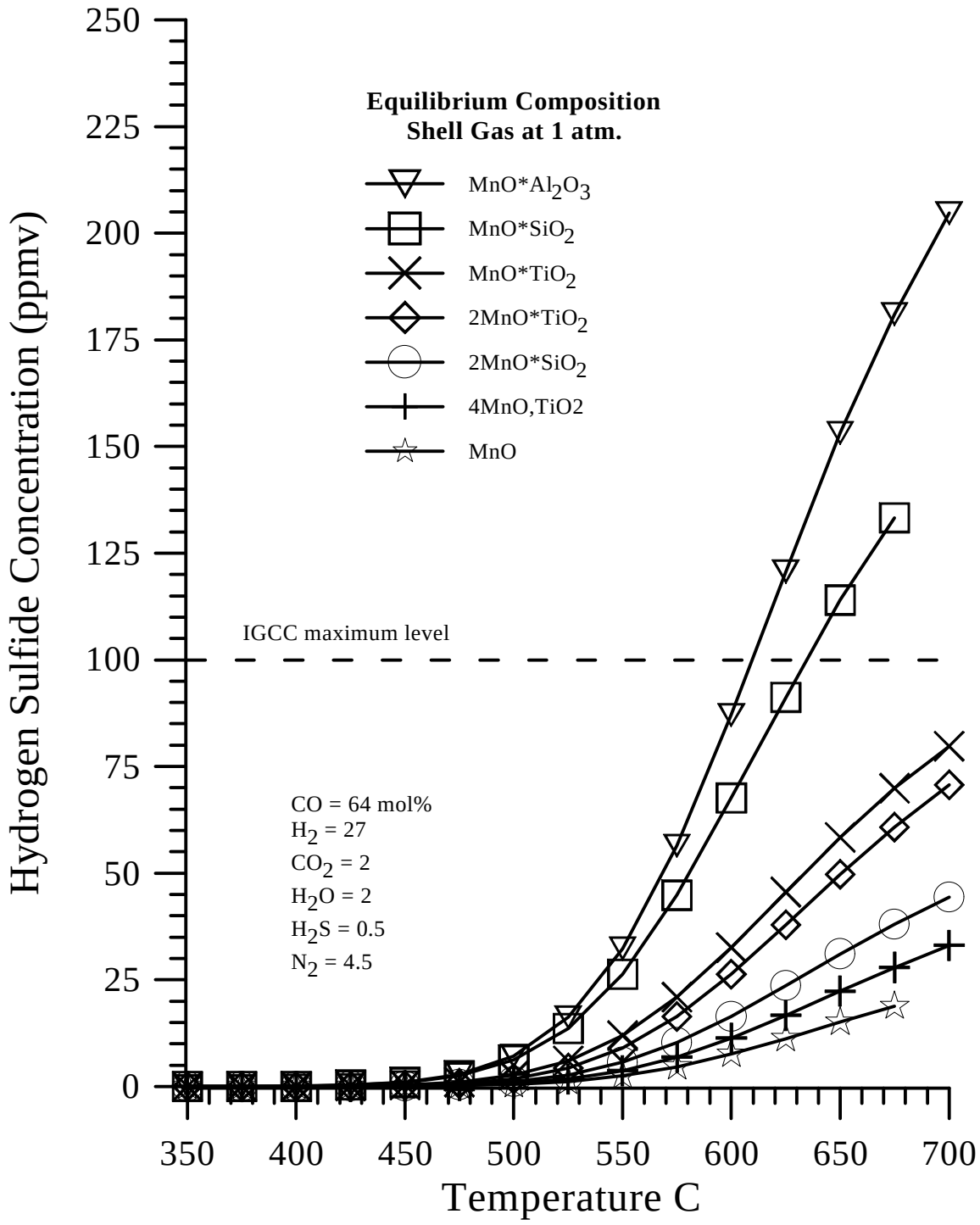

Figure 3.2. H_2S concentration as a function of temperature for Shell gas in equilibrium with various mixed manganese sorbents.

3.3. Regeneration Thermodynamics

A sorbent must be able to undergo many sulfidation and regeneration cycles while maintaining strength and reactivity in order for the sorbent to be economically viable. Regeneration of the sulfided sorbent may be accomplished by oxidizing the sorbent with air. Some reactions that can occur during the regeneration of MnS in air are shown in equations 3.4 to 3.7

$$MnS_{(s)} + \frac{3}{2}O_2 \rightarrow MnO_{(s)} + SO_{2(g)} \quad (3.4)$$

$$MnO_{(s)} + \frac{1}{6}O_{2(g)} \rightarrow \frac{1}{3}Mn_3O_{4(s)} \quad (3.5)$$

$$Mn_3O_{4(s)} + \frac{1}{4}O_{2(g)} \rightarrow \frac{3}{2}Mn_2O_{3(s)} \quad (3.6)$$

$$MnS_{(s)} + 2SO_{2(g)} + O_{2(g)} \rightarrow 2MnSO_{4(s)} \quad (3.7)$$

Equation 3.4 is the most desirable reaction to occur during regeneration because it restores the manganese back to the condition that is ready to react with H_2S again. Further oxidation of manganese as shown in equations 3.5 and 3.6 will result in the consumption of hydrogen from coal gas during the subsequent sulfidation, from the oxidized state back to the reduced state. Alternatively, the Mn_3O_4 and Mn_2O_3 could be reduced to MnO with a furnace off-gas[1] prior to the subsequent sulfidation.

The sulfation of manganese as shown in equation 3.7 is especially undesirable because the production of manganese sulfate will cause the pellets to spall and crack. Manganese sulfate is also slow to decompose resulting in low SO_2 concentrations in the exiting regeneration gases.

To prevent sulfation, the conditions under which it occurs must be avoided. Figure 3.2 shows phase stability diagrams at 600, 800 and 1000^{o}C. It has been determined[2] that regeneration should be conducted at a temperature greater than 900^{o}C when regenerating in air at ambient pressure to prevent sulfation. This is a problem since IGCC valve designs have temperature limits of 1200^{o}F[3] (approximately 650^{o}C). Looking at the phase diagrams, one can see that by lowering the O_2 and/or the SO_2 partial pressure will result in lower $MnSO_4$ stability. Therefore, it may be possible to reduce the regeneration temperature and still keep sulfate formation to a minimum by using a regeneration gas that has lower oxygen potential (i.e. air/steam mixture or oxygen deficient air). This will result in a dilute stream of SO_2 which may favorable from a thermodynamic point of view but unfavorable from an economic point of view. The dilute SO_2 may not be suitable as a marketable byproduct for the production of sulfuric acid or elemental sulfur thereby needing to be treated as a waste stream.

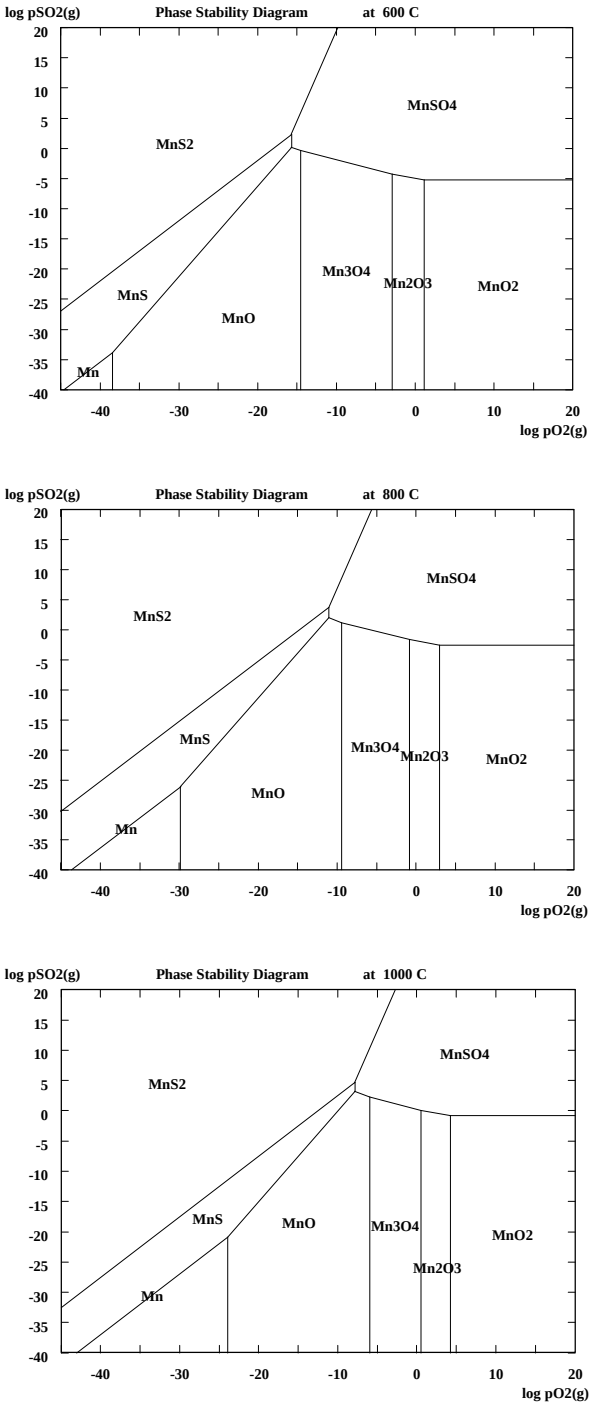

Figure 3.3. Phase stability diagrams* for the Mn-S-O system at 600, 800^{o}C and 1000^{o}C.

Regeneration of the sorbent in steam and nitrogen is also possible. This reaction is just the reverse of the sulfidation reaction.

$$MnS_{(s)} + H_2O_{(g)} = MnO_{(s)} + H_2S_{(g)} \quad (3.8)$$

Steam regeneration can be conducted at lower temperatures without sulfate formation. Also a stream of concentrated H_2S is a more desirable off-gas for the production of sulfur than dilute SO_2. If the H_2S concentration is sufficiently high it may be converted to elemental sulfur by the Claus reaction. However, regeneration reactions are hindered both kinetically and thermodynamically[4] for most metal sulfides of interest.

3.4 References

1. Turkdogan, E. T.; Olsson, R.G., "Desulfurization of Hot Reducing Gases with Manganese Oxide Pellets", Proceedings of the Third International Iron and Steel Congress 16-20 April **1978**, Chicago, IL, 277-288.

2. Hepworth, M. T.; Ben-Slimane, R., "Desulfurization of Hot Coal-Derived Fuel Gases with Manganese-Based Regenerable Sorbents. 2. Regeneration and Multicycle Tests", *Energy and Fuels* **1994**, 8, 1184-1191.

3. Gardner, T., DOE/METC, Morgantown, WV, Personal Communication, **1997**.

4. Gangwal, S. K.; Gupta, R.; McMichael, W. J., "Hot-Gas Cleanup-Sulfur Recovery Technical, Environmental, and Economic Issues",*Heat Recovery Systems & CHP***1995**, Vol. 15, No. 2, 205-214.

CHAPTER 4. KINETIC CONSIDERATIONS

4.1 Introduction

Desulfurization of coal gas using a manganese oxide sorbent can be represented by the following gas-solid reaction:

$$H_2S_{(g)} + MnO_{(s)} = H_2O_{(g)} + MnS_{(s)} \quad (4.1)$$

a generalized gas-solid reaction is shown in equation 4.2

$$A_{(g)} + bB_{(s)} = cC_{(g)} + dD_{(s)} \quad (4.2)$$

This chapter will develop rate expressions for gas-solid reactions of the type shown above. To represent a gas-solid reaction realistically, an appropriate model must be developed. This model can then be used to predict how a reaction will proceed under varying conditions (temperature, gas space velocity) without actually running the experiment. A model must predict reality closely, however, must not be too complicated to be used effectively. Thus a model should be as simple as possible to achieve a reasonable representation of the reaction.

4.2 Single Pellet Modeling: The Shrinking Core Model

The shrinking core model[1,2] (SCM) is a simple idealized model that seems to represent reality in a wide variety of situations[1]. Here the reaction begins at the outer surface of the solid particle and proceeds as a sharp boundary into the interior of the particle. As the boundary moves into the interior of the particle, a product layer is left behind and the unreacted core grows smaller. If the product is a gas or a solid that flakes off as soon as it is formed, then the particle will shrink in size. If the product is a non-flaking solid, then the particle is assumed to remain unchanged in size. The development of the following kinetic expressions assumes the following:

- The particle size is unchanged as the reaction proceeds.
- The unreacted core is non-porous.
- The product layer is porous.
- The particle is spherical.
- The reaction is first order.
- The temperature of the particle remains constant through-out the reaction.

There are three mechanisms that can control the rate of reaction: 1) diffusion through the gas film, 2) diffusion through the product layer and 3)

chemical reaction. These mechanisms and their rate equations are described separately in the following sections. Also a list of variables used in the following sections along with their definitions are given in the Notation section at the end of this report. It should be noted that the rate equations are derived based on the general gas-solid reaction shown in equation 4.2, however, may be easily modified for the reaction of interest in this report, equation 4.1, where A = H_2S, B = MnO and b = 1.

4.2.1 Diffusion Through Gas Film Controls

When the reaction is controlled by gas film diffusion, the gaseous reactant must diffuse through a stagnant gas film, then (relative to the time for diffusion through the gas film) instantaneously diffuses through the product layer and reacts. The resulting concentration profiles of gaseous reactant A are depicted in Figure 4.1. Gas film resistance is dependent on many factors including the relative velocity between the particle and fluid, the fluid properties and the size of the particle.

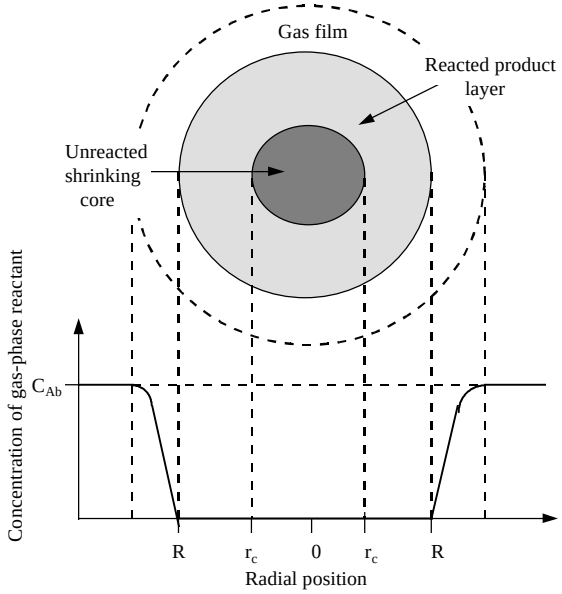

Figure 4.1 Concentration profiles of gaseous reactant A when diffusion through the gas film is the controlling mechanism.

The rate equation, expressed as moles of A disappearing per unit time per particle is related to the mass transfer coefficient, k_g, by

$$-\frac{dN_A}{dt} = 4\pi R^2 k_g (C_{Ab} - C_{Ae}) \qquad (4.3)$$

For an irreversible reaction, the equilibrium concentration, $C_{Ae} = 0$. The number of moles of solid reactant B present in the particle is

$$N_B = \rho_B V_p \tag{4.4}$$

where ρ_B is the molar density of B in the solid and V_p is the volume of the particle. The disappearance of B is related to the decrease in radius of the unreacted core as follows

$$-dN_B = -\rho_B dV = -\rho_B d\left(\frac{4}{3}\pi r_c^3\right) = -4\pi\rho_B r_c^2 dr_c \tag{4.5}$$

Noting that from the stoichiometry of equation 4.2

$$-dN_B = -b dN_A \tag{4.6}$$

Combining equation 4.3, 4.5 and 4.6 gives the rate of reaction in terms of the unreacted core radius

$$-\frac{\rho_B r_c^2}{R^2}\frac{dr_c}{dt} = b k_g (C_{Ab} - C_{Ae}) \tag{4.7}$$

Rearranging and integrating gives

$$t = \frac{\rho_B R}{3b k_g (C_{Ab} - C_{Ae})}\left[1 - \left(\frac{r_c}{R}\right)^3\right] \tag{4.8}$$

The fractional conversion, X, of a sphere is given by

$$X = 1 - \left(\frac{r_c}{R}\right)^3 \tag{4.9}$$

By substituting equation 4.9 into 4.8 we obtain the relationship between time and conversion for a reaction that is gas film diffusion controlled

$$t = \frac{\rho_B R}{3b k_g (C_{Ab} - C_{Ae})} X \tag{4.10}$$

This equation indicates that conversion versus time could be plotted to determine whether the reaction is gas film diffusion controlled as indicated by a straight line. The mass transfer coefficient, k_g, could then be determined from the slope of the line assuming that the radius, R, the molar density, r_B, of the pellet and the reactive gas concentrations, C_{Ab} and C_{Ae}, are known. However, external mass transport usually provides a negligible resistance to the progress of the reaction[2]. In such a case, the mass transfer may also be estimated through various correlations[3] for solids in free fall, packed bed and fluidized beds.

4.2.2 Diffusion Through Product Layer Controls

When the reaction is controlled by product layer diffusion, the gaseous reactant A instantaneously diffuses through the gas film then must diffuse through the product layer, then instantaneously reacts. The resulting concentration profiles of gaseous reactant A are depicted in Figure 4.2. For this analysis, we assume that the concentration gradient of A in the product layer remains in steady state, even though the unreacted core is shrinking slowly with time.

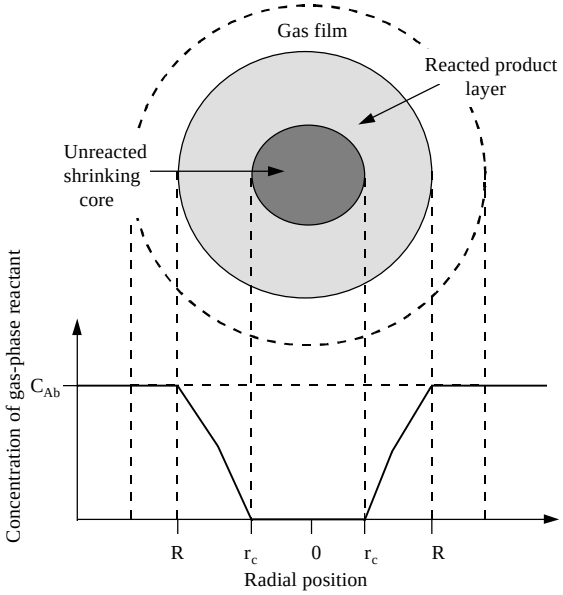

Figure 4.2 Concentration profiles of gaseous reactant A when diffusion through the product layer is the controlling mechanism.

The rate of reaction of A at any instant is related to the flux of A, J_A, to the product layer.

$$-\frac{dN_A}{dt} = 4\pi R^2 J_A \tag{4.11}$$

The flux through the product layer is defined by Fick's Law

$$J_A = D_e \frac{dC}{dr} \tag{4.12}$$

Substituting equation 4.12 into 4.11, separating variables and integrating between R where $C_A = C_{Ab}$ and r_c where $C_A = C_{Ae}$ gives the following rate equation

$$-\frac{dN_A}{dt} = 4\pi D_e (C_{Ab} - C_{Ae}) \left(\frac{1}{r_c} - \frac{1}{R} \right)^{-1} \tag{4.13}$$

Eliminating N_A by substituting equations 4.5 and 4.6 into equation 4.13, separating variables and integrating yields

$$t = \frac{\rho_B R^2}{6bD_e (C_{Ab} - C_{Ae})} \left[1 - 3\left(\frac{r_c}{R} \right)^2 + 2\left(\frac{r_c}{R} \right)^3 \right] \tag{4.14}$$

Remembering that the fractional conversion depends on r_c by equation 4.9, the time to achieve a given fractional conversion for a reaction that is product layer diffusion controlled is thus given by

$$t = \frac{\rho_B R^2}{6bD_e (C_{Ab} - C_{Ae})} \left[1 - 3(1 - X)^{2/3} + 2(1 - X) \right] \tag{4.15}$$

Now a plot of $[1 - 3(1 - X)^{2/3} + 2(1 - X)]$ versus time could be made and if a straight line results, the rate of reaction is controlled by diffusion through the product layer. Diffusion through the product layer has been shown[4] to be the dominant resistance in reactions involving metal oxides with H_2S in the temperature range of 650 - 760^{o}C and a fractional sulfidation greater than approximately 0.20.

4.2.3 Chemical Reaction Controls

When chemical reaction controls the rate of reaction, gaseous reactant A diffuses through the gas film and the product layer much faster than the time it takes to react. The resulting concentration profiles of gaseous reactant A are depicted in Figure 4.3.

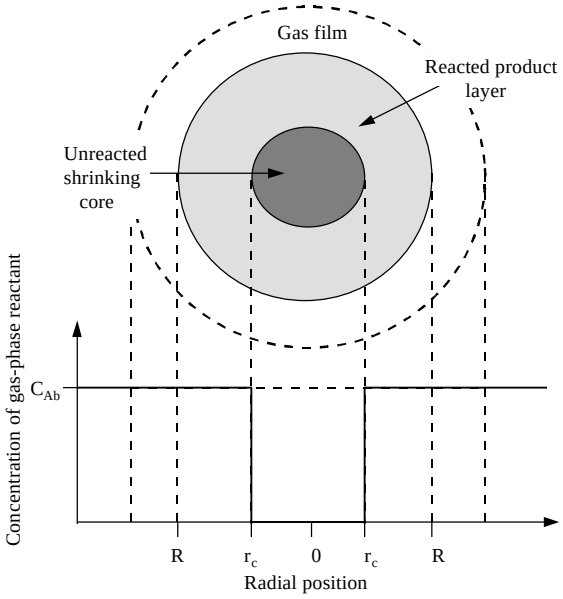

Figure 4.3 Concentration profiles of gaseous reactant A when chemical reaction is the controlling mechanism.

The rate of reaction is now based on the surface area of the unreacted core. The rate of reaction of A, assuming a first order reaction is

$$-\frac{dN_A}{dt} = 4\pi r_c^{\,2} k\left(C_{Ab} - C_{Ae}\right) \tag{4.16}$$

where k is the first-order rate coefficient for a surface reaction. Substituting equation 4.5 and 4.6 into 4.16 yields

$$-\rho_B \frac{dr_c}{dt} = bk\left(C_{Ab} - C_{Ae}\right) \tag{4.17}$$

integrating equation 4.17 from t = 0 to t = t and r_c = R to r_c = r_c gives

$$t = \frac{\rho_B}{bk\left(C_{Ab} - C_{Ae}\right)}\left(R - r_c\right) \tag{4.18}$$

Thus the time to achieve a given conversion of B for a reaction that is chemical reaction limited is

$$t = \frac{\rho_B R}{bk(C_{Ab} - C_{Ae})}\left[1 - \left(1 - X\right)^{1/3}\right] \tag{4.19}$$

4.3 Comparison of Models for Gas-Solid Reactions

The shrinking core model has been used extensively to model gas-solid reactions. This model assumes that the unreacted core is non-porous while the product layer is porous and has a fixed diffusivity coefficient. While there is no such thing as a non-porous solid, there are solids that have very low porosity and the assumption that the solid is non-porous may be acceptable. In cases where this is not true, more sophisticated models that deal with porous solids must be developed. While the shrinking core model may be fitted to experimental data on a particular pellet, its use in extrapolation to pellets of different structure (different porosity) is dangerous in that the model contains no allowance for structural properties[5].

The basic grain model[6] takes into account these structural properties. The grain model is represented by a sphere that is made up of many individual spheres or "grains". These grains all behave as individual shrinking core models. Modifications to the grain model include those that take into account gas-solid reactions that exhibit pore structure evolution during reaction. Mathematical models have been developed for reactions with porous solids that exhibit pore closure behavior[7], diminishing porosity[8] and grain overlapping[9]. These models take into consideration the effects of pore overlapping and non uniform pore length.

Another reason the SCM may fail is that it assumes a constant diffusivity within the product layer which may not be the case as shown by Krishnan and Sotirchos (1993)[10]. They studied the reaction of limestone with SO_2 in a thermogravimetric analyzer (TGA). An attempt was made to fit experimentally observed behavior using the SCM with constant diffusivity in the product layer, but it failed. This led to the development of a variable diffusivity shrinking core model in which the effective diffusivity in the product layer is assumed to vary with the distance from the external surface of the particles.

Reaction may also actually occur between the limits of a diffuse interface or reaction zone situated between the product and reactant as oppose to a sharp interface as described by the SCM. Unlike the SCM, the diffuse interface model[11] includes a measure of the diffusivity of the unreacted solid.

4.4 Fixed-Bed Modeling

It is important to be able to predict the effect of operating parameters such as reaction temperature, superficial velocity of reactant gas and sorbent induration temperature on the desulfurization performance of a sorbent. Therefore, a mathematical model for a fixed-bed is developed where individual pellets react according to the SCM. This will allow parameters such as the effective diffusivity and reaction rate to be fit to experimental data. These parameters can then be used to predict the performance of a sorbent under varying sulfidation conditions and to determine the best operating conditions.

Assuming plug flow of gas, the component A balance is

$$u\frac{\partial C_A}{\partial z}+\varepsilon\frac{\partial C_A}{dt}+r_A=0 \tag{4.20}$$

neglecting the second term on the left hand side[2] gives

$$u\frac{\partial C_A}{\partial z}+r_A=0 \tag{4.21}$$

with

$$C_A = C_{AO} \text{ at } z = 0 \tag{4.22}$$

the component B balance is

$$(1-\varepsilon)\frac{\partial C_B}{\partial t}=-br_A \tag{4.23}$$

with

$$C_B = C_{BO} \text{ at } t = 0 \tag{4.24}$$

where r_A is the rate per unit volume of bed at which moles of component A are reacted or

$$r_A=\frac{1}{V}\frac{dN_A}{dt} \tag{4.25}$$

If the solid reactant B is made up of uniform spheres of radius R, then r_A can be related to the rate at which a single spherical particle reacts

$$r_A=\frac{3(1-\varepsilon)}{4\pi R^3}\frac{dN_A}{dt} \tag{4.26}$$

The rate at which a single particle reacts can be determined from the shrinking core model. As discussed in section 4.2, there are three mechanisms that control the rate of reaction. These three mechanisms are gas film diffusion, product layer diffusion and chemical reaction for which the three rate equations are:

$$N_{gfd} = 4\pi R^2 k_g (C_{Ab} - C_{Ae}) \quad \text{gas film diffusion} \tag{4.27}$$

$$N_{pld} = 4\pi D_e (C_{Ab} - C_{Ae}) \left(\frac{1}{r_c} - \frac{1}{R} \right)^{-1} \quad \text{product layer diffusion} \tag{4.28}$$

$$N_{rxn} = 4\pi r_c^2 k (C_{Ab} - C_{Ae}) \quad \text{chemical reaction} \tag{4.29}$$

The global reaction rate per particle will incorporate the three reaction rates given in the above equations as shown

$$\frac{dN_A}{dt} = \frac{1}{\frac{1}{N_{gfd}} + \frac{1}{N_{pld}} + \frac{1}{N_{rxn}}} \tag{4.30}$$

The global reaction rate can then be substituted into equation 4.25 and assuming an irreversible reaction ($C_{Ae} = 0$) yields

$$r_A = \frac{3(1-\varepsilon) C_{Ab}}{R} \left[\frac{1}{k_g} + \frac{R}{D_e} \left[(1-X)^{-1/3} - 1 \right] + \frac{1}{k(1-X)^{2/3}} \right]^{-1} \tag{4.31}$$

Substituting equation 4.31 into 4.21 and 4.23 and introducing dimensionless variables yields the following equations

$$\frac{\partial C_A^*}{\partial z^*} = -\frac{r_A L}{C_{AO} u} \tag{4.32}$$

$$\frac{\partial X}{\partial t^*} = \frac{r_A L}{C_{AO} u} \tag{4.33}$$

The dimensionless variables are defined in the Notation. Hence equations 4.32 and 4.33 establish C_A^* (t^*, z^*) and X(t^*, z^*). These equations may be solved numerically with the boundary conditions

$$C_A^* = 1 \text{ at } z^* = 0 \text{ at all } t^* \quad (4.34)$$

$$X = 0 \text{ at } t^* = 0 \text{ at all } z^* \quad (4.35)$$

4.5 References

1. Levenspiel, O. *Chemical Reaction Engineering*, p. 361-368, 2nd Edition, John Wiley & Sons, Inc., New York, **1972**.

2. Szekely, J., Evans, J.W., Sohn, H.Y., *Gas-Solid Reactions*, Academic Press, New York, **1976**.

3. Geankoplis, C. J., *Transport Processes and Unit Operations*, 3rd edition, P T R Prentice-Hall, Inc., Englewood Cliffs, NJ, **1993**.

4. Jothimurugesan, K.; Harrison, D.P., "Reaction between H_2S and Zinc Oxide-Titanium Oxide Sorbents. 2. Single-Pellet Sulfidation Modeling", *Ind. Eng. Chem. Res.* **1990**, 29, 1167-1172.

5. Evans, J. W.; Song, S., "Application of a Porous Pellet Model to Fixed, Moving, and Fluidized Bed Gas-Solid Reactors", *Ind. Eng. Chem. Process Des. Develop.* **1974**, Vol. 13, No. 2, 146-152.

6. Szekely, J.; Evans, J. W., *Chem Eng. Sci.* **1971**, 26, 1901.

7. Sotirchos, S. V.; Yu, H., "A Generalized Pore Model for Gas-Solid Reactions Exhibiting Pore Closure", *AIChE Journal* **1987**, Vol. 33, No. 3, 382-392.

8. Sotirchos, S.V.; Zarkanitis, S., "A Distributed Pore Size and Length Model for Porous Media Reacting with Diminishing Porosity", *Chemical Engineering Science* **1993**, Vol. 48, No. 8, 1487-1502.

9. Sotirchos, S. V.; Efthimiadis, E. A., "A Partially Overlapping Grain Model for Gas-Solid Reactions", *Chemical Engineering Science* **1993**, Vol. 48, No. 7, 1201-1212.

10. Sotirchos, S. V.; Krishnan, S. V., "A Variable Diffusivity Shrinking-Core Model and its Application to the Direct Sulfation of Limestone", *The Canadian Journal of Chemical Engineering* **1993**, 71, 734-745.

11. Mutasher, E. I.; Khan A. R.; Bowen, J. H., "A Generalized Diffuse Interface Model of Gas-Solid Non-Catalytic Reaction in a Fixed Bed", *Chem. Eng. Res. Des.* **1989**, 67, 66-75.

CHAPTER 5. EXPERIMENTAL PROCEDURE

5.1 Pellet Manufacture

The manganese-based sorbent used in all experiments consisted of spherical pellets that were 1.2 to 3.36 mm in diameter. The spherical shape provided for optimum packing and strength characteristics. The feed materials used and the process for manufacturing the manganese-based pellets are described below.

5.1.1 Feed Materials

Exploratory investigation of Mn-based sorbent began with the consideration of the following parameters of feed materials and preparation techniques. Composition variables were:

- Manganese source,
- Substrate composition,
- Mn to substrate molar ratio,
- Non-volatile binder wt%,
- Porosity enhancer composition,
- Porosity enhancement wt%.

The manganese sources were chosen from a commercially available $MnCO_3$ and a pyrolusite ore. Substrates were chosen based on thermodynamic equilibrium between mixed metal oxide sorbent ($Mn.M_xO_y$) and hydrogen sulfide. Substrates considered included titanium dioxide, alundum, bauxite and silica. The manganese carbonate was obtained from Chemetals, Baltimore, MD. The manufacturer assay is given in Table 5.1. The titanium dioxide was obtained from Fisher Scientific, Fair Lawn, NJ. The average titanium dioxide particle size was 0.3 to 1.0 mm. The impurity assay is given in Table 5.2. The alundum was provided by Norton Industrial Ceramics Corporation, Worchester, MA. The manufacture assay is presented in Table 5.3. Bentonite was used as a non-volatile binder and was obtained from Aldrich Chemical, Milwaukee, WI. Bentonite particles were less than 47 mm in size.

Table 5.1. Manufacturer assay of $MnCO_3$, Chemetals, Baltimore, MD.

Component	Weight %
$MnCO_3$	93.73
MnO_2	0.25
CaO	0.124
Na_2O	0.056
H_2O	2.1
Fe	-

Table 5.2. Titanium dioxide impurity from manufacture, Fisher Scientific, Fair Lawn, NJ.

Impurity	Weight Percent
Fe	0.003
Pb	0.006
Water Soluble Salts	0.03
Zn	0.002

Table 5.3. Manufacture assay of alundum source material; Norton Industrial Ceramics, Worchester, MA.

Component	Weight Percent
Al_2O_3	96.6
TiO_2	2.6

5.1.2 Formula Designations

Formula designations are described by listing sequentially; a letter, a number, a dash, a second number, a second dash, and finally a third number (ex. C6-2-1100). The first letter corresponds to the manganese source (C for $MnCO_3$, and A for MnO_2-ore). The first number refers to the molar ratio of Mn to substrate and the substrate composition (1,2,4,5,7,11 for alundum, 6,8,9 for titania, and 10 for bauxite). The second number is the weight percent bentonite binder. Note, some C4-2 formulations have letters following the weight percent bentonite. These letters refers to porosity promoters added, i.e., C4-2x (A for activated carbon, D for dextrin, and M for MoO_3). A summary of the formulations tested in the fixed-bed reactor is given in Table 5.4.

Table 5.4. Initial formulations of manganese-based sorbents

Formulation Designation	Molar Ratio Mn:Substrate	Substrate	Wt% Bentonite	Induration Temperature (^oC)
C4-2-1175	4.33:1	Alundum	2	1175
C6-2-1100	4.33:1	Titania	2	1100
C8-0-1200	2:1	Titania	0	1200
C11-0-1160	1:1	Alundum	0	1160
C6-2-1115	4.33:1	Titania	2	1115

5.1.3 Preparation

Feed powder consisting of manganese carbonate, titanium dioxide, and bentonite was hand mixed in a 1 liter plastic container. Titanium dioxide tended to self-agglomerate, forming white streaks and clumps in the mixture. Therefore the mixture was hand-ground until the powder had a uniform consistency and color.

The powder was then pelletized in a balling tire. The balling tire was 13 inches in diameter, rotated at 35 rpm and formed a 60^{o} angle with the horizontal. Approximately 20 g of powder was initially added to the tire. Water was then sprayed in small amounts (less than 0.5 mL) at the powder. This formed small spherical "seeds". Approximately 5 g of powder was then added to the tire followed by additional sprays of water to grow the seeds and keep them moist respectively. This process was continued two or three times at intervals of 30 to 60 seconds until "green" pellets that were at least 2 mm in size were formed. The "green" pellets were removed from the tire and screened. Pellets that were 1.6 to 3.5 mm in size were retained for further preparation. These pellets were 10-30% by weight water and had crush strengths of less than 1 lb/pellet.

Green pellets of the appropriate size (1.6 to 3.5 mm) were allowed to air dry overnight and then dried to a constant weight at 105^{o}C. Dry pellets were calcined for four hours at 350^{o}C. Calcination provided for evolution of CO_2 and hydrated water at moderate rates. Calcined pellets were still very weak (crush strength of less than 1 lb/mm). Calcined pellets were allowed to cool overnight then were placed in a high-temperature furnace to provide for sintering and therefore to increase the strength of the pellet (induration). The temperature was ramped up for 2 to 2.5 hours to a desired temperature (approximately 1100^{o}C). The pellets were indurated at this temperature for 2 hours. The temperature was verified with a type R (Rh-Pt) thermocouple and was maintained within ± 2 degrees of the desired temperature. The indurated pellets were 1.2 to 3.36 mm in size after size reduction due to sintering. Average crush strengths of freshly indurated pellets were 1.4 to 5 lb/mm.

5.2 Pellet Characterization

Pellet characterization consisted of TGA testing, (section 5.2.1), fixed-bed testing (section 5.2.2), strength testing (section 5.2.3), x-ray diffraction (section 5.2.4), manganese analysis (section 5.2.5), sulfur analysis (section 5.2.6) and pore structure analysis (5.2.7). All freshly indurated pellets were stored in a vacuum dessicator until use.

5.2.1 Thermogravimetric Analysis (TGA)

Pellets with requisite strength (see section 5.2.3) were tested via TGA to determine the reaction kinetics of sulfidation. The reaction variables included sulfidation temperature in the range of 500^{o}C to 900^{o}C and pellet diameter in the range of 1.69 to 3.36 mm. Each TGA test sample consisted of three pellets.

The pellets were placed into the reaction chamber of the cold zone. The reactor was then heated to the desired temperature in a flowing nitrogen atmosphere. When the desired temperature was achieved, the sample was lowered into the hot zone. The pellets were then reduced in H_2 flowing at 1 L/min for 30 to 60 minutes at the desired temperature. The pellets were than sulfided in a 3% H_2S and 97% H_2 mixture for 60 minutes at the desired temperature. The pellets were then regenerated in air flowing at 1 L/min. The conditions for TGA analysis are summarized in Table 5.5.

Table 5.5. Conditions of TGA experiments for all formulations

Average pellet diameter	1 - 3 mm
Sample mass	200 - 800 mg
Reduction duration T > 550^{o}C T < 550^{o}C	 30 min 60 min
Sulfidation duration	120 min
Sulfidation gas composition and flow rate	1 L/min H_2; 30,000 ppmv H_2S
Sulfidation pressure	1 atm
Regeneration duration	60 min
Regeneration gas composition and flow rate	1 L/min air
Regeneration pressure	1 atm

5.2.2 Fixed-bed Testing

Indurated pellets were tested in an ambient pressure fixed-bed reactor to determine pre-breakthrough H_2S concentrations, breakthrough times (reaction kinetics), and effectiveness of the sorbent when subjected to multiple sulfidation and regeneration cycles. Figure 5.1 is a schematic diagram of the fixed-bed experimental apparatus. The reactor consisted of a 2.54 cm (1") ID quartz tube positioned vertically in a two-zone furnace. Figure 5.2 is a schematic of the reactor. The preheat zone was maintained at 200^{o}C. The reaction temperature was 500 to 600^{o}C and was monitored using a type K thermocouple positioned directly above the sorbent bed. Sulfidation and regeneration gases entered the reactor in an upward direction. Mixing of the gases was achieved through quartz packing followed by an alumina gas distributor disk supporting the sorbent bed. Exit gases were cooled in a cold trap where vapors such as water and sulfur were condensed and collected. The gases were then scrubbed in a sodium hypochlorite solution (sulfidation) or a hydrogen peroxide and sodium hydroxide solution (regeneration) prior to flaring and venting.

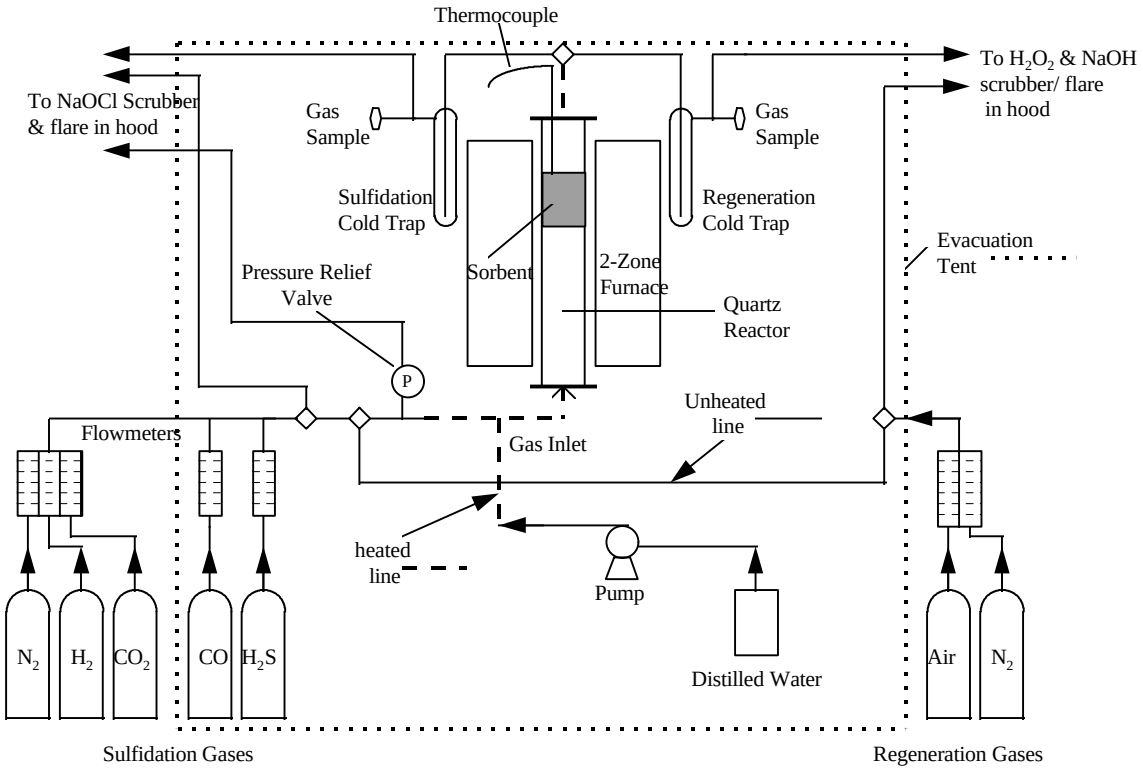

Figure 5.1. Experimental equipment for fixed-bed testing.

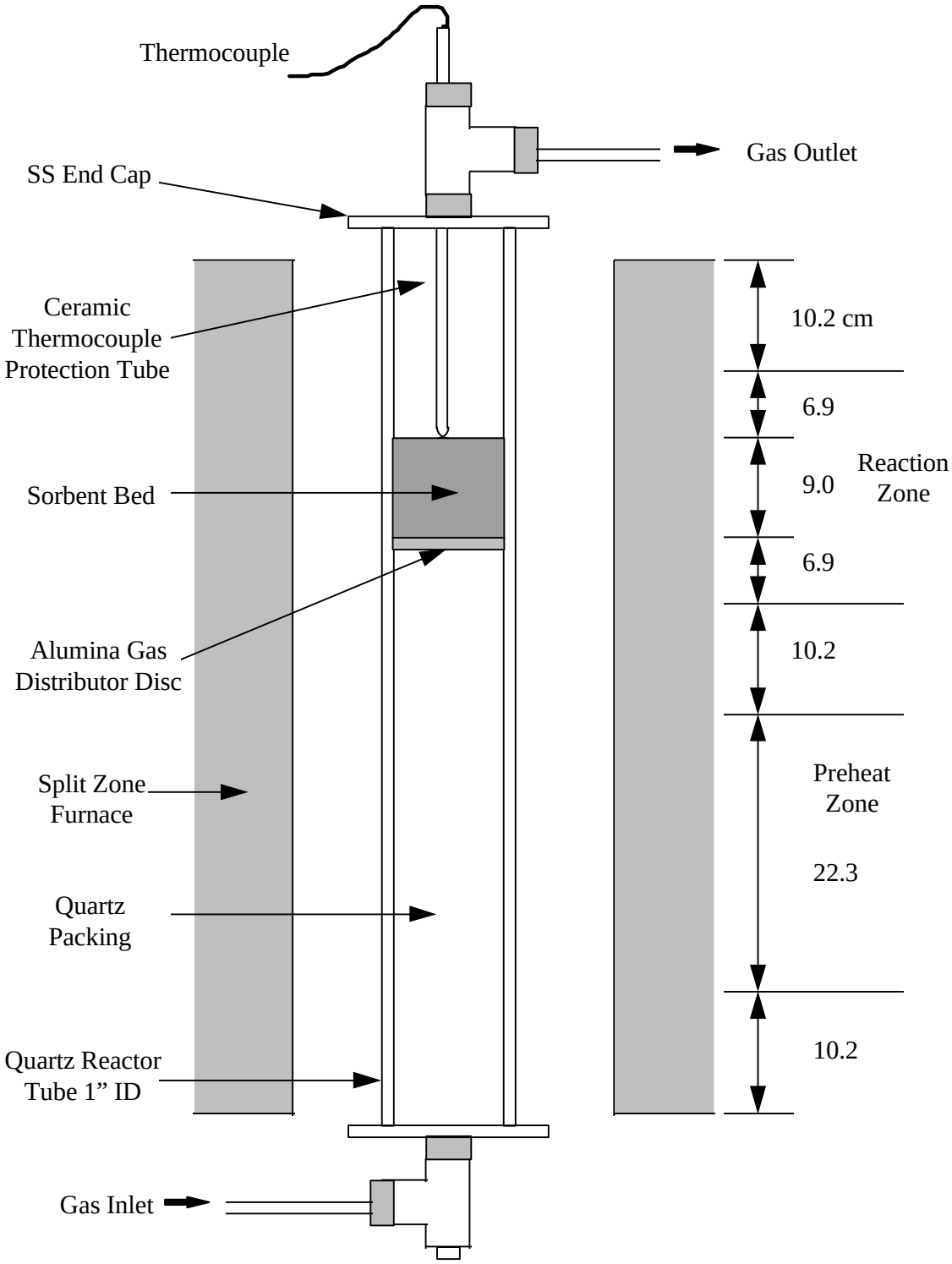

Figure 5.2. Schematic diagram of the fixed-bed desulfurization reactor.

For each test, 89 to 95 mm (3.5 to 3.75 ") of sorbent was added to the reactor tube in the reaction zone. The reactor was heated in a nitrogen atmosphere to the desired operating temperature. A simplified Shell gas spiked with 1.8 to 2.8 mol% H_2S was then introduced into the reactor at 2 to 3 L/min (STP). Volumetric flow rates of the gases were calibrated with rotameters using a wet-test meter. Elevated H_2S concentrations were employed to reduce the sulfidation breakthrough time. Exit gases were sampled after the cold trap and were analyzed using detector tubes for H_2S until breakthrough occurred.

Twelve tests were conducted using four sorbent formulations with varying sulfidation and regeneration conditions. Four or five cycles of sulfidation and regeneration were conducted for all four tests to determine the sorbents' strength and activity retention. The test conditions for sulfidation for the twelve tests are summarized in Table 5.6.

Table 5.6. Fixed-bed operating conditions for sulfidation

Test Designation	Sorbent Used	Temperature (^oC)	Gas Composition	Gas Flow Rate (L/min, STP)
1FB	C6-2-1100	600	Shell[a]	3
2FB	C6-2-1100	600	Shell[a]	3
3FB	C6-2-1100	600	Shell[a]	3
4FB	C4-2-1175	600	Shell[a]	3
5FB	C8-0-1200	600	Shell[a]	3
6FB	C8-0-1200	600	Shell[a]	3
7FB	C6-2-1100	600	Shell[a]	3
8FB	C11-0-1160	600	Shell[a]	3
FB1A	C6-2-1100	550	Shell[a]	3
FB2A	C6-2-1100	550	Shell[a]	2
FB3A	C6-2-1100	500	Shell[a]	3
FB4A	C6-2-1115	600	Shell[a]	3

[a]Refers to a simplified Shell gas with the following composition (mol%): 64 CO, 2 CO_2, 27 H_2, 2 H_2O, 1.8 - 2.8 H_2S, balance N_2.

The sorbent was regenerated in an air/steam mixture for all tests. The regeneration temperature was 650 to 750^{o}C. The regeneration gas flow rate was 1 to 1.25 L/min (STP). The test conditions for regeneration for all twelve tests are summarized in Table 5.7.

Table 5.7. Fixed-bed operating conditions for regeneration

Test Designation	Sorbent Used	Temperature (^{o}C)	Gas Composition (mol %)	Gas Flow Rate (L/min, STP)
1FB	C6-2-1100	900	100 air	1
2FB	C6-2-1100	750	90 N_2, 10 O_2	1
3FB	C6-2-1100	750	95 N_2, 5 O_2	1
4FB	C4-2-1175	750	60 air, 40 steam	1
5FB	C8-0-1200	750	60 air, 40 steam	1
6FB	C8-0-1200	750	20 N_2, 80 steam	1
7FB	C6-2-1100	750	60 air, 40 steam	1
8FB	C11-0-1160	750	20 N_2, 80 steam	1
FB1A	C6-2-1100	750	50 air, 50 steam	1
FB2A	C6-2-1100	750	50 air, 50 steam	1.25
FB3A	C6-2-1100	650	40 air, 60 steam	1
FB4A	C6-2-1115	750	50 air, 50 steam	1

5.2.3 Strength Testing

Crush (compressive) strength testing was conducted on all freshly indurated pellets. To determine strength retention, pellets that had undergone cyclic fixed-bed testing were also tested for crush strength. Crush strength was measured with a radial compressive test using a John Chatillon and Sons, New York, NY, crusher, model TCM-TT. Testing was done in accordance with ASTM designation 4179-88a. The pellet diameter was measured using a vernier caliper. The lbs-forces it took to crush the pellet was then divided by the diameter. Due to strength variations in pellets prepared identically, crush strength was determined as an average of 15 crush strengths for pellets with similar diameters.

5.2.4 X-ray Diffraction (XRD)

Wide angle XRD using a Siemens D-500 apparatus was employed to determine what crystalline phases were present in the manganese-based sorbent. Four tests were conducted using fresh, reduced fresh, regenerated, and sulfided sorbent. Reduced fresh sorbent was prepared in a fixed-bed at 600^{o}C with H_2 flowing at 1 L/min for 45 minutes. Phases search for included: hausmannite (Mn_3O_4), bixbyite (Mn_2O_3), manganosite (MnO), rutile (TiO_2), pyrophanite ($MnO.TiO_2$), manganese titanium oxide (Mn_2TiO_4), alabandite (MnS), manganese sulfate ($MnSO_4$) and sulfided spinels such as $MnS.TiO_2$.

5.2.5 Manganese Analysis

The weight percent manganese in the fresh sorbent was measured through Inductively Coupled Plasma analysis. Staff in the Geology Department of the University of Minnesota performed this analysis.

5.2.6 Sulfur Analysis

The weight percent sulfur in sulfided and regenerated sorbent was measured by a coulometric titration method with iodine. Sample sizes of 20 to 125 mg were used. Staff in the Civil Engineering Department of the University of Minnesota performed this test.

5.2.7 Pore Structure Analysis

Freshly indurated pellets were examined for internal structural properties via Hg porosimetry. Sorbent exposed to fixed-bed operating conditions was sampled from the center of the sorbent bed, along the axial dimension. Sample sizes of approximately 1 gram of sorbent (approximately 25 pellets) were required for porosimetry. Results are reported as incremental intrusion volume versus equivalent pore diameter.

CHAPTER 6. RESULTS AND DISCUSSION

6.1 Introduction

In addition to TGA and fixed-bed testing, a number of tests were conducted to characterize and determine the performance of the sorbent. These tests included strength testing, in addition to sulfur, x-ray diffraction and pore structure analysis. The TGA results are presented first then the fixed-bed test results. Finally each of the additional tests are discussed.

6.2 TGA RESULTS

The reaction of various mixed manganese oxides in a TGA has been investigated. Details of the TGA experimental equipment are available elsewhere[1]. Briefly, the apparatus consists of a automatic recording balance which hold up to twelve pellets. The balance is lowered into the reaction zone when the unit has reached the desired temperature. Reaction gases are flowed through the reaction zone and the dimensionless weight (W/W_o) changes of the pellets are recorded as the reaction proceeds. These dimensionless weight changes were used to calculate sorbent conversion, X, as a function of time. Table 5.5 summarizes the test conditions for reduction and sulfidation in a TGA.

There are three main groups of formulations tested. They are $MnCO_3$ supported with TiO_2 (with or without bentonite), $MnCO_3$ supported with Al_2O_3 (with or without porosity enhancers) and MnO_2 ore supported with Al_2O_3 (with or without bentonite). Figure 6.1 shows reactivity (given as W/W_o versus time) of various $MnCO_3/TiO_2$ formulations at 900^{o}C. Figure 6.2 shows the conversion versus time plot, generated from the dimensionless weight changes, for various Mn-based formulations. All Mn-Ti formulations react rapidly initially at 500^{o}C, with C6-2-1100 obtaining the highest fractional conversion. Formulation C9-2, which has a higher Mn:Ti molar ratio than C6-2-1100, did not produce greater sulfidation kinetics or sulfur capacity.

With bentonite as a bonding agent, it is believed that Mn:Ti ratios greater than 7:1 produced less reactive pellets. This may be explained by porosimetry data (see section 6.8) which suggests that C6-2-1100 has higher surface area than C9-2-1110. All rates on the $MnCO_3$-TiO_2 formulations decreased rapidly between 12-20% conversion. This kinetic deceleration may be due to plugging of the pellet pores with sulfur creating inaccessible pore volume or a large increase in diffusional resistance from MnO to MnS.

Sintering during the first reduction and sulfidation cycle is believed to be negligible. Further testing of C6-2-1100 was conducted to determine the strong dependence of preparation temperature on sulfidation fractional conversion, shown in Figure 6.3.

Figure 6.4 show the effect of pellet diameter on reactivity at 500^{o}C for sorbent C6-2-1100. As seen in the figure, the smaller the pellet diameter, the

higher the conversion after the completion of the test. This effect suggests intra-particle rate limitations.

Figure 6.5 shows the results of TGA testing at various reaction temperature (400 to 900^{o}C) for formulation C6-2-1100. Higher temperature led to higher conversions at the completion of the test. This phenomena was also seen in tests done in the fixed-bed reactor (see section 6.3).

Formulation C9-2-1110 was eliminated from regeneration testing while C8-0-1230 was included. Both $MnCO_3$-TiO_2 sorbents are completely regenerated as shown in Figures 6.6 and 6.7 for formulations C6-2-1100 and C8-0-1230 respectively.

Reduction/sulfidation test results for $MnCO_3$-Al_2O_3 formulations are presented in Figure 6.8. As the weight percentage of bentonite (indicated by the second number in the formulation designation) is increased, the required induration temperature for a given strength criteria is markedly decreased (see section 6.6). To reduce the induration temperature, formulations high is Al_2O_3 and bentonite were produced. This proved unsuccessful as presumably the bentonite reduces capacity and $MnO.Al_2O_3$ equilibrium with H_2S in unfavorable.

The required induration temperature for MnO_2 ore-Al_2O_3 formulations is generally much less than for $MnCO_3$-Al_2O_3 formulations as the gangue constituents (primarily silicates) have a relatively low sintering temperature. The reactivities for all ore-based pellets is given in figure 6.9. Formulations A2-2-1175 has 2% bentonite and relatively less alundum than A1-0-1150. Interestingly, their reduction and sulfidation curves look qualitatively identical at 900^{o}C. The exception is that A1-0-1150 reduces more completely as expected from lack of bentonite.

It appears from the previous results that titania is a superior substrate than alumina probably because the manganese/titania bond is weaker than the manganese/alumina bond. This means the manganese which is tied up in forming a spinel has a higher activity in the titania form than in the alumina form and is more effective in reacting with sulfur.

6.3 Fixed-bed Testing

Twelve tests were conducted in an ambient pressure fixed-bed reactor with each test consisting of either four or five cycles of sulfidation and regeneration. The first eight tests were conducted using four different sorbent formulations and varying regeneration conditions. The last four tests were conducted using the superiour performing formulation from the previous testing and varying sulfidation conditions. Sulfidation results for all twelve tests will be presented first then the regeneration results will be presented. Finally, the effects of sulfidation temperature, superficial gas velocity and the sorbent induration temperature on the desulfurization performance of the sorbent C6-2-1100 will be presented.

6.3.1 Sulfidation

The operating conditions of all twelve tests for sulfidation are summarized in Table 5.6. H_2S concentration in the reactor effluent was measured as a function of time using detector tubes. Reactor effluent was sampled after the cold trap, thereby giving H_2S concentrations on a dry basis.

The fixed-bed sulfidation breakthrough curves for all twelve tests are shown in figures 6.10 to 6.24. T_{th} is the theoretical time to breakthrough based on the moles of manganese in the packed-bed. The theoretical breakthrough time was calculated assuming one mole of manganese per mole of sulfur and exit H_2S concentrations prior to breakthrough of zero. The equation used to determine the theoretical breakthrough time is given in the Notation section at the end of this report. The sulfidation breakthrough curves for tests FB1A, FB2A, FB3A and FB4A are followed by sulfidation breakthrough curves plotted against dimensionless time (time/theoretical breakthrough time). When the H_2S concentration in the exit stream is low, the dimensionless time approximates the conversion of the total mass of MnO. Thus, the desulfurization performance of a sorbent tested under varying conditions can be compared.

The breakthrough time was defined to be the time at which the concentration of H_2S reached and stayed above 100 ppmv. This concentration was chosen because it is the maximum level of H_2S acceptable for IGCC. Each test was terminated shortly after this concentration had been reached to minimize corrosion of downstream equipment and H_2S release. The sulfidation gas composition for all tests was a simulated Shell fuel-gas. The fixed-bed results are divided into two groups: the results from tests 1FB to 8FB and the results from tests FB1A to FB4A.

6.3.1.1 Fixed-Bed Tests 1FB to 8FB

Figures 10 to 17 show the results of the fixed-bed sulfidation testing for tests 1FB to 8FB. Eight tests were conducted using four different formulations. Results from each formulation are describe separately below. A summary of the steady-state H_2S concentrations achieved in the fixed-bed and the breakthrough times for all tests conducted is given in Table 6.1. The breakthrough time based on the wt% Mn in the sorbent was calculated assuming a steady-state H_2S concentration of zero. Five cycles of sulfidation and regeneration were conducted for each test.

Table 6.1. Steady-state H_2S concentrations and breakthrough times of sorbent in fixed-bed

Formulation Test Designation	Amount of Sorbent (g)	Steady-State H_2S (ppmv)	Breakthrough time based on wt% Mn (min)	Actual Breakthrough Time (min) Cycle 1	2	3	4	5
C6-2-1100 1FB	54.94	26.1	183.8	107	72	79	90	90
C6-2-1100 2FB	NA	46.3	179.2	112	116	122	128	125
C6-2-1100 3FB	53.76	22.3	181.5	115	122	127	132	133
C6-2-1100 7FB	52.92	23.8	178.7	107	112	116	123	124
C8-0-1200 5FB	43.66	58.0	131.3	15	21	23	24	24
C8-0-1200 6FB	41.93	24.0	126	9	1	1	5	7
C4-2-1175 4FB	NA	24.7	178.7	67	71	75	77	77
C11-0-1160 8FB	49.48	*	79	0	0	0	NA	NA

NA = not available; *no apparent steady-state was achieved during test 8FB.

Figures 10-13 are sulfidation breakthrough plots for formulation C6-2-1100. Four tests were conducted on this formulation. The conditions for each test are the same except that the sorbent was regenerated differently. The steady-state H_2S concentrations for each sulfidation cycle of each test ranged between 20 and 50 ppmv.

Figure 10 shows the breakthrough curves for sorbent regenerated in air at 900^{O}C. As can be seen in this figure the sorbent did not regenerate completely. The second sulfidation cycle had a breakthrough time much earlier than the first sulfidation. This is most likely due to sintering of the pellets during regeneration.

Figures 11 and 12 show the breakthrough curves for sorbent regenerated in oxygen depleted air and lower temperature. The breakthrough times are progressively better with progressing number of cycles. Cycle number 5 of Figure 12 shows a breakthrough time of 133 minutes which is 73% of the breakthrough time based on wt% Mn in sorbent.

Figure 13 shows the breakthrough curve for sorbent regenerated in steam and air. Again the breakthrough times are progressively better with progressing number of cycles.

Figures 14 and 15 are the sulfidation breakthrough plots for formulation C8-0-1200. Two tests were conducted on this formulation. For the first test, the sorbent was regenerated in air and steam, while the second was regenerated in steam and nitrogen. As can be seen in Figures 14 and 15, the sorbent did not regenerate as fully in steam and nitrogen as it did in air and steam.

Figure 16 is the sulfidation breakthrough plot of formulation C4-2-1175. This sorbent was regenerated in steam and air. As can be seen from the figure, the breakthrough times become progressively better with progressing cycle numbers, however the steady-state H_2S concentration isn't as good for cycles 2-5 (60 ppmv) as compared to the first cycle (25 ppmv). Also, there is a large H_2S concentration early in cycles 2-5 that reduce to the steady-state after a short time. This may indicate the formation of sulfates during regeneration. When the sorbent is subsequently sulfided, the sulfates are reduced to SO_2 and is measured by the detector tubes incorrectly as H_2S.

Figure 17 is the sulfidation of a 1:1 molar ratio of Mn to substrate (alundum). As can be seen from the plot, this formulation was less effective in reducing the H_2S concentration than the sorbents that had >1:1 molar ratios of Mn:substrate. This is because the substrate combines with the Mn and is less effective as a reactant than MnO which is still present in sorbents with molar ratios >1:1.

Formulation C6-2 appears to possess the most favorable sulfur capacity and equilibrium H_2S levels over five cycles of sulfidation and regeneration. Therefore, further testing of C6-2 was conducted to determine the effects of sulfidation temperature, sulfidation gas superficial velocity and sorbent induration temperature on the desulfurization performance of the sorbent. These tests are discussed in the next section and are designated FB1A to FB4A.

6.3.1.2 Fixed-Bed Tests FB1A to FB4A

Tests FB1A, FB2A and FB3A all used C6-2-1100 as the desulfurization sorbent while test FB4A used C6-2-1115. The only difference in these two sorbents is the induration temperature (1100 and 1115^{o}C respectively).

Sulfidation of the sorbent in test FB1A was conducted at 550^{o}C with a superficial gas velocity of 1635 cm/min (3 L/min, STP). Sulfidation in test FB2A was conducted at 550^{o}C with superficial gas velocity of 1090 cm/min (2 L/min, STP). This test was conducted to determine the effect of the superficial gas velocity on the desulfurization performance of sorbent C6-2-1100. Sulfidation in test FB3A was conducted at 500^{o}C and a gas flow rate of 3 L/min to determine the effect of temperature on desulfurization performance. Sulfidation in test FB4A was conducted at 600^{o}C and a gas flow rate of 3 L/min. This test was conducted to determine the effect of the sorbent induration temperature on the desulfurization performance of the sorbent. Results from test FB4A were compared to a test from a previous section, 7FB. Sulfidation conditions in test 7FB were the same as those in FB4A; the only difference in the two tests was the induration temperature of the sorbent.

The temperature profile during sulfidation is shown in the upper plot of figures 6.18, 6.21 and 6.23. This was done to show that the desulfurization process is relatively isothermal. A temperature rise of only 25^{o}C occurred during the sulfidations of test FB1A. The temperature spikes at the beginning of the sulfidations of test FB4A were assumed to be due to the reduction of Mn_2O_3 to MnO. The temperature returned to the original temperature for each sulfidation and remained steady.

Prior to breakthrough, the H_2S concentration (dry basis) was below 100 ppmv for all sulfidations of all tests. The typical pre-breakthrough H_2S concentration was 10 to 75 ppmv. During the first sulfidations of tests FB1A and FB3A, very low H_2S concentrations (10 ppmv) were achieved, however, during subsequent sulfidations, higher concentrations (up to 75 ppmv) were realized. A possible reason for this is that sulfate could have been formed during previous regenerations and this sulfate was then reduced to SO_2 during subsequent sulfidations. The SO_2 could have been incorrectly detected by the detector tube as H_2S.

The lowest H_2S concentrations achieved during sulfidation did decrease as expected from thermodynamic analysis as the temperature decreased; however, the lowest concentration in some tests was accompanied by higher concentrations. In test FB1A, pre-breakthrough concentrations of H_2S as high as 75 ppmv were achieved whereas in test FB4A, pre-breakthrough concentration as high as 40 ppmv were only achieved. This despite the fact that test FB1A was conducted at 550^{o}C and test FB4A was conducted at 600^{o}C and thermodynamics (Chapter 3) predicts higher H_2S concentrations at higher temperatures. Therefore, the effect of reaction temperature on equilibrium concentration was minimal in the temperature range of 500 to 600^{o}C.

The observed breakthrough sorbent conversion was determined by dividing the actual time to achieve breakthrough by the theoretical time to breakthrough. Observed sorbent conversion ranged from 0.18 to 0.41, with the lowest conversion being attained for cycle 1 of test FB3A and the highest for cycle 4 of test FB2A. All sulfidation tests showed improved sorbent conversions at breakthrough from cycle 1 to cycle 4 except FB4A. This may be due to a small amount of sulfate formation during regeneration. This sulfate formation may have caused small cracks and these cracks may help to decrease transport resistances. Test FB4A did not show improvement in sulfidation conversion, which may be due to the fact that the sorbent used in this test was indurated at a higher temperature than the sorbent in all other test, giving it a stronger crush strength (see section 6.6) and thus more resistance to cracks. Table 6.2 summarizes the results for all fixed-bed sulfidation tests.

Table 6.2. Lowest H_2S concentrations achieved and observed sorbent conversions in fixed-bed tests

Test Designation	Cycle	Lowest H_2S Concentration Achieved (ppmv)	Observed Sorbent Conversion at Breakthrough	Relative Percent Change*
FB1A	1	10	0.28	
FB1A	4	15	0.38	+36
FB2A	1	10	0.30	
FB2A	4	20	0.41	+37
FB3A	1	10	0.18	
FB3A	4	30	0.27	+50
FB4A	1	25	0.28	
FB4A	4	25	0.28	0

*Percent change is defined as (cycle 1 conversion - cycle 4 conversion)/cycle 1 conversion

6.3.2 Regeneration

After each sulfidation process, the sorbent was regenerated in air or an air/steam or steam/N_2 mixture flowing at approximately 1 L/min. The operating conditions of all twelve tests for regeneration are summarized in Table 5.7. The regeneration curves are shown in Figures 6.25 to 6.36.

6.3.2.1 Tests 1FB to 8FB

Figures 6.25 to 6.32 show the results from the fixed-bed regeneration testing for tests 1FB to 8FB. Eight tests were conducted using four different formulations. Five cycles of sulfidation and regeneration were conducted for each test. Results from each formulation are described separately. A summary of the SO_2 or H_2S concentrations achieved in the exit gases and the time for regeneration is given in Table 6.3. Regeneration time is based on the time to achieve an exit SO_2 or H_2S gas concentration of less than 10% of the highest concentration achieved. The regeneration times were then average over five cycles.

Table 6.3. Highest Concentration of SO_2 or H_2S Achieved in Exit Gases and Average Regeneration Times.

Formulation Test Designation	Highest concentration of SO_2 (or H_2S) achieved in exit gases, mol%	Average regeneration time (min)
C6-2-1100 1FB	8.3	95
C6-2-1100 2FB	4.5	190
C6-2-1100 3FB	2.1	435
C6-2-1100 7FB	7.8	115
C8-0-1200 5FB	9.0	45
C8-0-1200 6FB	(1.5)	280
C4-2-1175 4FB	7.2	76
C11-0-1160 8FB	(0.8)	150

Figures 6.25-6.28 are the regeneration breakthrough plots for formulation C6-2-1100. Figure 6.25 shows the regeneration curves for sorbent regenerated in air at 900^{o}C. Regeneration in air produced a dry SO_2 concentration of 8.3 mol% in the exit gases and an average regeneration time of 95 minutes, however due to the exothermic character of the desulfurization reaction, high temperatures were also produced. This is undesirable because of sintering effects. As described in section 6.3.1.1, the sorbent's capacity was reduced considerably from the first sulfidation cycle to the second cycle. A regeneration temperature similar to the sulfidation temperature is also desirable, however to prevent sulfate formation, which may cause the pellets to crack, a higher temperature is needed when regenerating in air.

A lower temperature is possible when regenerating in atmospheres with lower oxygen potentials. Figures 6.26 and 6.27 show the regeneration curves for sorbent C6-2-1100 regenerated in oxygen depleted air at 750^{o}C. The pellets were shown to be completely regenerated, however, the exit SO_2 concentration is lower and the average regeneration time is longer than regeneration in air. The SO_2 at this concentration may not be economically recoverable.

Figure 6.28 shows the regeneration curves for sorbent C6-2-1100 regenerated in an air/steam mixture. Regeneration in 60% air and 40% steam regenerated the sorbent completely while minimizing sulfate formation and large

increases in temperature. The highest SO_2 concentration achieved in the exit gases was 7.8 mol%.

Figure 6.29 shows the regeneration curves for sorbent C8-0-1200 regenerated in air and steam. The sorbent was regenerated completely with exit SO_2 concentrations as high as 9 mol%, however, some sulfate formation was indicated during subsequent sulfidation testing.

Figure 6.30 shows the regeneration curves for sorbent C8-0-1200 regenerated in steam and nitrogen. Steam regeneration produced low concentrations of H_2S in the gas exit stream and did not completely regenerate the pellets.

Figure 6.31 shows the regeneration curves for sorbent C4-2-1175 regenerated in air and steam. The sorbent was regenerated completely with exit SO_2 concentrations as high as 7.2 mol%. Some sulfate formation was indicated, however, this was minimal.

Figure 6.32 shows the regeneration curves for sorbent C11-0-1160 regenerated in steam and nitrogen. Again steam regeneration produced low concentrations of H_2S in the gas exit stream and did not fully regenerate the pellets.

Tests FB1A to FB4A

The regeneration curves for tests FB1A to FB4A are shown in Figures 6.33 to 6.36. After each sulfidation process, the sorbent was regenerated in an air/steam mixture flowing at approximately 1 L/min.

A thermocouple placed at the exit of the packed-bed indicated that the temperature rose as much as 125^oC. This increase in temperature occurred immediately prior to a sudden drop in SO_2 exit gas concentration as seen in Figure 6.33. This is due to the placement of the thermocouple. The thermocouple, which is positioned right at the sorbent bed exit, reads high temperatures in the vicinity of the reaction zone. Thus when the temperature gets very high, it indicates that the reaction is occurring near the exit of the bed, near the completion of regeneration. Although, the thermocouple only read a rise in temperature of 125^oC, it is suspected that the temperature actually rose higher since regeneration temperatures as low as 650^oC were used with minimal sulfate formation (the fact that the pellets remained intact and did not show noticeable cracks was an indication for minimal sulfate formation).

Another important aspect of regeneration besides sulfate formation is the off-gas composition. As seen in figures 6.33 to 6.36, the maximum SO_2 concentration achieved in all four tests for all regeneration processes was at least 5 % (dry basis) with more typical concentrations of approximately 6 %. This SO_2 concentration held fairly steady until a sharp decrease in the concentration occurred, indicating regeneration breakthrough. The breakthrough occurred rapidly when the bed was almost completely regenerated. The remaining low concentrations of SO_2 following breakthrough

were attributed to small amounts of sulfate being formed during regeneration, decomposing back to SO_2.

6.3.3 Effects of Varying Sulfidation Conditions

To determine the best operating conditions, the effects of sulfidation temperature, superficial gas velocity and sorbent induration temperature on the desulfurization performance of the sorbent were investigated. To compare the sorbent's performance under varying conditions, the first sulfidation results of each test were used.

Figure 6.37 shows the effect of sulfidation temperature on the desulfurization performance of the sorbent (C6-2-1100). As discussed in section 6.3.1.2, the sulfidation temperature had a negligible affect on the pre-breakthrough concentration of H_2S. Pre-breakthrough concentrations ranged from 10 to 75 ppmv, all of which are acceptable for IGCC application.

The observed sorbent breakthrough conversion as approximated by the dimensionless time, however, is greatly affected by the sulfidation temperature. The sorbent conversion at breakthrough increased as the sulfidation temperature increased. This is because the reaction and transport kinetics (discussed in Chapter 4) improve with increasing temperature. The observed sorbent breakthrough conversion increases from 0.18 at 500^{o}C to 0.60 at 600^{o}C. Thus a small change in the sulfidation temperature results in a large increase in the capacity without much compromise in the pre-breakthrough concentration.

Figure 6.38 shows the effect of the superficial gas velocity on the desulfurization performance of the sorbent. As seen in the figure, there is a slight increase in the observed sorbent breakthrough conversion as the velocity is decreased. This can be explained by the nature of the reaction. There is more than one reaction mechanism (reaction, gas film diffusion, product layer diffusion) occurring. One mechanism may be very fast and independent of time while another needs time to proceed (time dependent). As the gas velocity increases the contribution of the time dependent mechanisms becomes less, and consequently the breakthrough conversion is lower. However, between superficial gas velocities of 1090 cm/min and 1635 cm/min the difference in breakthrough conversion is minimal.

Figure 6.39 shows the effect of the sorbent induration temperature on the desulfurization performance of the sorbent. The sorbent induration temperature greatly affected the observed sorbent conversion at breakthrough. The observed sorbent breakthrough conversion was 0.60 for sulfidation of sorbent indurated at 1100^{o}C (C6-2-1100). The conversion dropped to 0.28 when sulfiding sorbent that was indurated at 1115^{o}C (C6-2-1115). This is a considerable drop for such a small change in induration temperature. The much lower conversion of C6-2-1115 must be attributed to a difference in physical properties as compared to C6-2-1100. The higher induration temperature of C6-

2-1115 caused more sintering to occur which decreased the pore sizes, thereby increasing transport resistances.

6.4 Fixed-bed Modeling

A mathematical model was developed in Chapter 4 to describe a gas-solid reaction in a fixed-bed reactor. The individual pellets (solid) were assumed to react according to the shrinking core model. In this section, the final model equations (equations 4.32 and 4.33) are used to describe the desulfurization process.

There were several assumptions made in the derivation of these equations that should be addressed. The pellets were assumed to remain unchanged in size during sulfidation. This assumption is reasonable because the manganese-based pellets contain sufficient amount of non-reactive (inert) components (titanium matrix and inorganic binder) that remain as non-flaking materials. Also, the sulfidation reaction forms a firm product (MnS) which has only a slightly larger specific volume. The reaction was assumed to be first order with respect to H_2S. This has been experimentally verified in a previous study[2]. The reaction was considered to be irreversible. This is a reasonable assumption since the pre-breakthrough exit H_2S levels between 500^oC and 600^oC were typically less than 75 ppmv, down from 22,000 ppmv. The equations are limited to H_2S being the only gaseous reactant. This is not a serious limitation since approximately 95% of the sulfur in coal derived gas is H_2S. Other reactions are ignored such as the reduction of Mn_2O_3 to MnO. This reaction is assumed to occur instantaneously upon sorbent exposure to the reducing coal gas and does not affect the reaction of H_2S with MnO. Finally no energy balance has been included. Although the sulfidation reaction is exothermic, the low H_2S concentration results in low heat evolution, thus, the pellets and fixed-bed reactor may be considered to be isothermal. This isothermal behavior has been verified experimentally (see Figure 6.10).

The fixed-bed operating conditions for each test are summarized in Table 5.6. The values of all model parameters used in equations 4.32 and 4.33 are summarized in Table 6.4 with the exception of the intrinsic reaction rate constant, k, and the effective diffusivity within the product layer, D_e. The intrinsic rate constant was assumed to be significantly large such that would drop out of the rate equations, leaving the rate dependent only on transport resistances. This assumption has been utilized by other investigators[3]. The mass transfer coefficient was estimated from an empirical correlation[4]. The effective diffusivity can also be estimated; however, the available models are at best approximate[3]. Therefore, the value of D_e was estimated by adjusting the value until a good match between the predicted H_2S breakthrough curves and the experimental breakthrough curves was obtained. This was done for the first and fourth sulfidation of each test.

Table 6.4. Model Parameter Values for Fixed-Bed Sulfidation Tests

Test Designation	FB1A	FB2A	FB3A	FB4A	7FB
Sorbent	C6-2-1100	C6-2-1100	C6-2-1100	C6-2-1115	C6-2-1100
R (cm)	0.20	0.20	0.20	0.20	0.20
L (cm)	9.0	9.0	9.0	9.0	9.0
u (cm/min)	1635.1	1090.1	1535.8	1734.5	1734.5
e (dimensionless)	0.34	0.34	0.34	0.34	0.34
G (cm^3/min), STP	3000	2000	3000	3000	3000
C_{AO} (mol/cm^3) 10^7	3.26	2.66-3.40	4.41	3.07	3.07
kg (cm/min)	1268	1022	1191	1430	1430

A numerical procedure based on Euler's method was implemented. Equation 4.32 was first solved at $t^* = 0$ and $X = 0$ for all z^* to obtain $C_A^*(0, z^*)$. Time was then incremented by solving equation 4.33 using $X = 0$ and $C_A^*(0, z^*)$ to determine $X(t_1^*, z^*)$ This entire procedure was then repeated until the final desired conditions were reached.

The predicted H_2S breakthrough curves could be matched well to the experimental breakthrough curves thus providing an estimate of the effective diffusivity, D_e. The predicted and experimental breakthrough curves are shown in Figure 6.40 and 6.43. A summary of the D_e values obtained from the fixed-bed modeling is shown in Table 6.5.

Table 6.5. D_e values and percent change for fixed-bed sulfidation tests.

Test Designation	Cycle	Gas Flow Rate, STP (cm^3/min)	Temperature (^oC)	Sorbent Used	D_e (cm^2/min)	Relative Percent Change*
FB1A	1	3000	550	C6-2-1100	0.77	
FB1A	4	3000	550	C6-2-1100	1.07	+39.0
FB2A	1	2000	550	C6-2-1100	0.53	
FB2A	4	2000	550	C6-2-1100	0.75	+41.5
FB3A	1	3000	500	C6-2-1100	0.38	
FB3A	4	3000	500	C6-2-1100	0.70	+84.2
FB4A	1	3000	600	C6-2-1115	0.86	
FB4A	4	3000	600	C6-2-1115	0.86	0
7FB	1	3000	600	C6-2-1100	2.45	
7FB	4	3000	600	C6-2-1100	2.84	+39.0

*Percent change is defined as (4th cycle D_e - 1st cycle D_e)/1st cycle D_e

The sulfidation cycles of tests FB1A, FB3A and 7FB were conducted at 550, 500 and 600^{o}C respectively while all other conditions remained the same. Values of D_e were obtained for both the 1st and fourth sulfidations of each test. These values were then used to determine the temperature dependence of D_e. Figure 6.44 shows D_e (on a log scale) plotted against reciprocal temperature. The best-fit straight line through the data for the first and fourth sulfidations is given by:

$$\mathrm{Ln}(D_e) = \frac{-12{,}500}{T} + 15.12 \qquad \text{First sulfidation} \qquad (6.1)$$

$$\mathrm{Ln}(D_e) = \frac{-9364}{T} + 11.66 \qquad \text{Fourth sulfidation} \qquad (6.2)$$

The low R^2 values seen in figure 6.44 may be due to sorbent preparation. Although the sorbent was prepared with the same materials and manufacturing procedure, the sorbent used in test 7FB was prepared by a different investigator and came from a different batch than the other tests. Any slight variation of the structural properties of the sorbent can alter the results. This can be seen from test FB4A where the only difference from test 7FB is a small change in the

induration temperature (1115 versus 1100^{o}C), while there is a large difference in the value of D_e obtained.

The only difference in the conditions of tests FB1A and FB2A is the sulfidation superficial gas velocity. The effective diffusivity should not be dependent on the gas velocity since it involves diffusion within the pellet. Therefore the same value of D_e should be obtained for tests FB1A and FB2A. The D_e values obtained (see Table 6.5) are indeed similar for the two tests. The differences are attributed to experimental error.

It appears from the above results that the mathematical model can be used to approximate the reaction of H_2S with MnO in a fixed-bed reactor. Although the model does not allow for structural variations, it may be useful for establishing design guidelines and interpreting experimental data.

6.5 Sulfur Analysis

As an independent check of the conversions predicted by the mathematical model, experimental sulfur analysis was conducted on sulfided pellets from test FB3A (after 3.5 cycles). Three samples from different axial positions in the packed-bed were analyzed for sulfur. Samples were taken from the bottom (gas inlet) one-third**,** middle one-third and top (exit) one-third of the packed-bed. Figure 6.45 displays the sorbent conversion as a function of the dimensionless distance from the gas inlet for both experimental results and the model prediction. The model prediction was calculated using the estimated D_e value found from the previous modeling results (0.70 cm^2/min) and the time at the termination of test FB3A (37 minutes). The three horizontal lines represent the experimental sorbent conversion at the three fixed axial positions.

As seen in Figure 6.45, samples taken from the top and bottom one-third of the packed-bed compared very well to model predictions while the middle one-third sample was a little high. A possible reason for this may be that when the sorbent was removed from the reactor, some of the pellets may have been axially mixed. Pellets from the bottom of the packed-bed may have ended up in the middle, resulting in higher sulfur loading. The good comparison between predicted and experimental sorbent conversions is another indication that the mathematical model does indeed approximate the reaction of H_2S with MnO in a fixed-bed reactor.

Sulfur analysis was also used to determine the regenerability of the sorbent. If the amount of sulfur left in the sorbent is low, then it can be assumed that the sorbent was satisfactorily regenerated. For this reason, the sorbent from tests 1FB to 7FB after five cycles of sulfidation and regeneration were analyzed for sulfur. Figure 6.46 shows the sulfur profiles for sorbent from tests 1FB-7FB after the 5th regeneration. Sorbent from these tests all had approximately the same weight percent of sulfur remaining in the sorbent, all of which are low, indicating essentially complete regeneration. Sorbent from tests 3FB and 6FB did, however, have slightly less weight percent of sulfur remaining.

Regeneration of test 3FB was conducted using very oxygen depleted air (50 cc/min O_2 and 950 cc/min N_2) and thus probably did not form as much sulfate as tests with regeneration in higher oxygen concentration (e.g. test 1FB).

6.6 Strength Testing

An important factor in the ability of a sorbent to be used effectively in the desulfurization of coal gas is the structural integrity of the sorbent. In order for the sorbent to be economically viable, it must be able to withstand many cycles of sulfidation and regeneration. The sorbent resistance to attrition must be high especially if desulfurization is to occur in a fluidized bed. Due to equipment limitations attrition testing was not possible. However, all freshly indurated and cycled sorbents were subjected to crush (compressive) strength testing.

The crush strength of freshly indurated pellets were found to be highly sensitive to the temperature at which it was indurated. This is illustrated in Figure 6.47. As can be seen in the figure, a small increase in temperature can result in a large difference in crush strength. Induration time for all sorbents tested was restricted to two hours due to time constraints. The sensitivity of the crush strength to induration temperature could possibly be minimized with longer induration times at lower temperature and needs to be further investigated.

The crush strength of cycled sorbent (sorbent that had undergone 4 or 5 cycles of sulfidation and regeneration in a fixed-bed reactor) was also measured. Cycled samples used for strength testing were collected from the middle one-third, along the axial dimension, of the sorbent bed. The crush strength of all sorbent after several cycles of sulfidation and regeneration decreased. Figure 6.48 shows the crush strengths of pellets after 5 sulfidation and regeneration cycles for formulations C4-2-1175 and C8-0-1200. The crush strength of the fresh sorbent is also given for comparison reasons. Sorbent from test 5FB had the largest decrease in crush strength (57.9%) while sorbent from test 4FB had only and 17.9% decrease. The sulfidation and regeneration conditions were the same (sulfidation at 600^{o}C using Shell gas and regeneration at 750^{o}C, using a steam/air mixture), however, the sorbent formulations were different. C4-2-1175 contains 2% bentonite binder while C8-0-1200 does not contain any bentonite. Sorbent from test 6FB had the smallest decrease in crush strength. This test used C8-0-1200 formulation, however, the sorbent was regenerated with a steam/N_2 mixture. These regeneration conditions does not allow for the formation of sulfates as does the steam/air mixture and may be why it had the smallest decrease in crush strength after 5 cycles.

Figure 6.49 shows the crush strengths of freshly indurated pellets and pellets after 4 or 5 sulfidation and regeneration cycles (5 cycles for 1FB-7FB and 4 cycles for FB1A and FB2A) for formulation C6-2-1100. Sorbent from test 1FB had the largest decrease in crush strength. In this test, regeneration was carried out at 900^{o}C using pure air. However, sorbent from tests 2FB, and 3FB using oxygen depleted air had less decrease in crush strength (21.8% and 14.6%

respectively). Sorbent from test 7FB had used air/steam mixture for regeneration and had a 24.1% decrease in crush strength. Sorbent from test FB1A and FB2A had a decrease in crush strength after four cycles of 40.0% and 46.7%. The difference in these two tests is the sulfidation gas flow rate (3L/min and 2L/min). As seen in the above results, there isn't any significant difference in the crush strength of the two sorbents after 4 cycles.

Figure 6.50 shows the results of crush strength testing on sorbent C6-2-1100 and sorbent C6-2-1115 after four cycles of sulfidation and regeneration. Note that the sorbent from FB3A is actually the crush strength of the sorbent after 3.5 cycles (sulfided state) whereas FB1A, FB2A, and FB4A are crush strengths of the sorbent after four full cycles (regenerated state). The largest loss of sorbent strength (53 %) occurred during test FB2A. This test utilized sorbent C6-2-1100 (indurated at 1100^{o}C). The smallest loss in sorbent strength (30 %) occurred during test FB4A. This test utilized sorbent C6-2-1115 (indurated at 1115^{o}C)

It is not known whether the sorbent would have continued to lose strength after additional cyclic testing or if the sorbent strength had stabilized. A minimum required pellet strength is typically establish for desulfurization processes. Therefore, if the pellet strength had stabilized, the minimum strength could be achieved and maintained. This could be accomplished by indurating the pellets at the minimum temperature that will achieve a sorbent crush strength that is approximately 50 % greater than the minimum strength requirement.

6.7 X-Ray Diffraction (XRD)

Figures 6.51 through 6.54 represent the x-ray diffraction patterns for fresh, fresh reduced, sulfided and regenerated pellets for formulation C6-2-1100. The top plot is the experimental x-ray diffraction patterns, while the bottom plot represents the "cards" or peaks that correspond to the pure substance. The fresh reduced pellets were prepared in a fixed-bed at 600^{o}C with H_2 flowing at 1 L/min for 45 minutes. Cycled sorbent was collected from the middle one-third, along the axial dimension, of the sorbent bed.

As seen in figures 6.51 through 6.54, the background is moderately high which is an indication that there is a non-crystalline phase present. Crystalline phases identified in fresh sorbent were bixbyite-C (Mn_2O_3) and pyrophanite, syn ($MnO.TiO_2$). Crystalline phases present in fresh reduced pellets were pyrophanite and manganosite (MnO). As discussed in Chapter 3, the reduction of Mn_2O_3 to MnO was expected. Also, as expected, no crystalline phase of metallic Mn was detected in the reduced sample.

The sulfided sample was obtained from test FB3A after 3.5 cycles. Crystalline phases identified in this sample were rutile, syn (TiO_2) and alabandite (MnS). No sulfided spinel was detected ($MnS.TiO_2$) therefore, it appears that the pyrophanite dissociates in the presence of H_2S. Also compounds that contain more than one mole of sulfur to Mn were not detected.

The regenerated sample was obtained from test FB1A after 4 cycles. Crystalline phases identified in this sample were Mn_2O_3 and TiO_2. A significant finding is that the sorbent was regenerated to Mn_2O_3, a higher oxide than both MnO and Mn_3O_4. This is somewhat undesirable in that the higher oxide will consume hydrogen from the fuel-gas during subsequent sulfidations. Another important finding is that no $MnSO_4$ was detected, in fact no compounds containing sulfur were detected. This is an indication of essentially complete regeneration.

6.8 Pore Structure Analysis

Mercury porosimetry was used to analyze the internal structure of fresh sorbent. A summary of the results is presented in Table 6.6. Comparing fresh C6-2-1100 and fresh C9-2-1110, the former has a larger intrusion volume while having similar mean pore diameter. This points to more surface area in C6-2-1100 pellets than in C9-2-1110.

Table 6.6. Results of mercury porosimetry of freshly indurated pellets

Pellet Properties	A1-2-1125	C6-2-1100	C9-2-1110	C5-2-1250
Total Intrusion Volume, mL/g	0.2220	0.2328	0.1618	0.2901
Total Pore Area m^2/g	0.490	---	0.199	0.103
Median Pore Diameter (volume), mm	4.7579	4.1741	4.1157	10.9701
Median Pore Diameter (area), mm	0.0142	---	2.9058	10.0270
Average Pore Diameter (4V/A), mm	1.8116	---	3.2474	11.3167
Bulk Density, g/mL	---	2.1073	2.4126	1.8807
Apparent Density (skeletal), g/mL	---	4.1357	3.9580	4.1390
Porosity, %	---	49.05	39.05	54.56

6.9 References

1. Hepworth, M.T. "Hot Coal-Gas Desulfurization with Manganese-Based Sorbents" Final Report for the period of the contract: September 18, 1992 to December 17, 1994. DE-AC21-92MC29246, **1994**.

2. Westmoreland, P. R.; Gibson, J.B.; Harrison, D. P. "Comparative Kinetics of High-Temperature Reaction of H_2S and Selected Metal Oxides", *Environmental Science and Technology* **1977**, Vol. 11, No. 5, 488-491.

3. Wang, J. C. P.; Groves, F. R.; Harrison, D. P., "Modeling High Temperature Desulfurization in a Fixed-Bed Reactor", *Chemical Engineering Science* **1990**, Vol. 45, No. 7, 1693-1701.

4. Geankoplis, C. J., *Transport Processes and Unit Operations*, 3rd edition, P T R Prentice-Hall, Inc., Englewood Cliffs, NJ, **1993**.

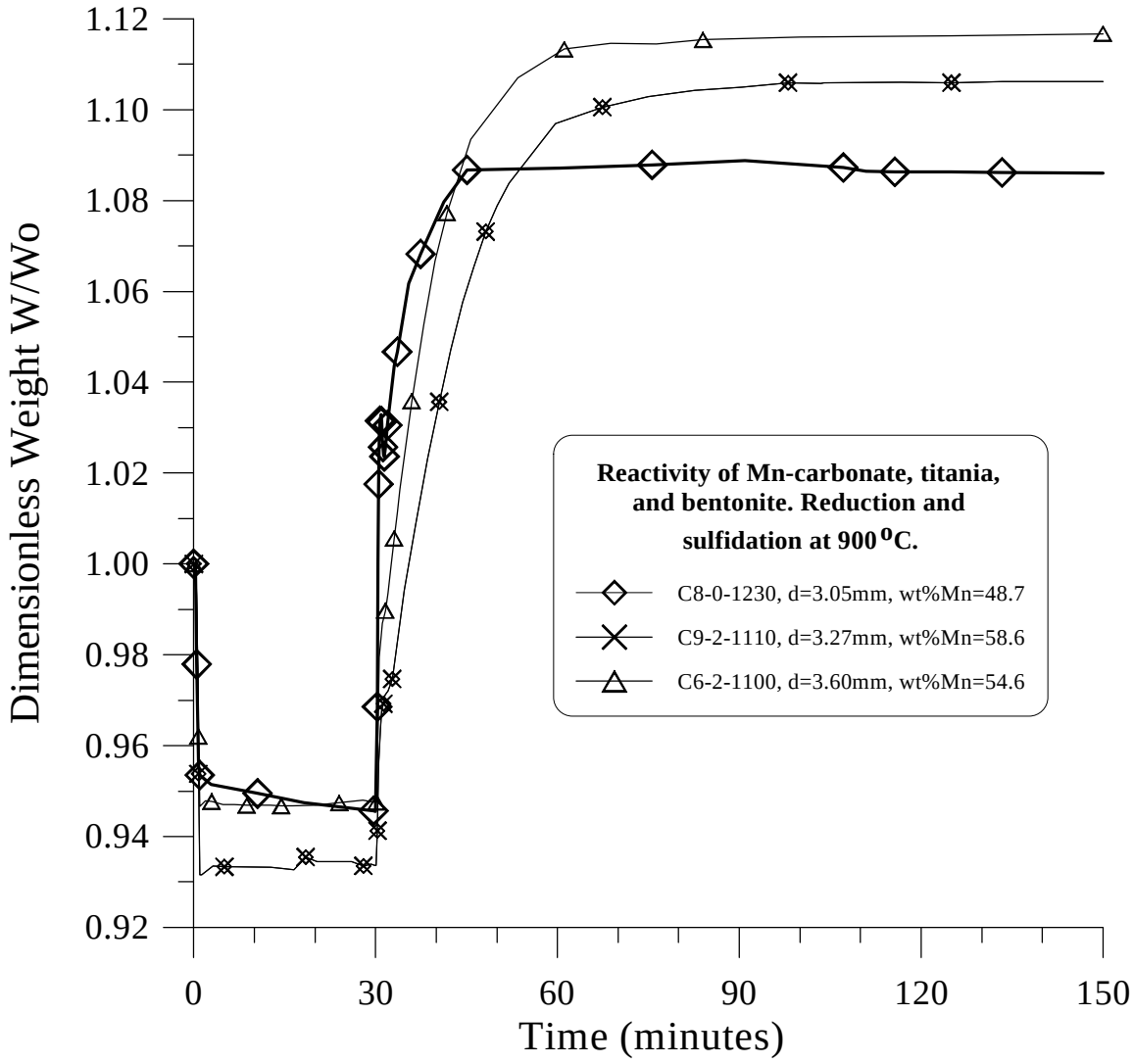

Figure 6.1. $MnCO_3/TiO_2$ reactivity at 900°C.

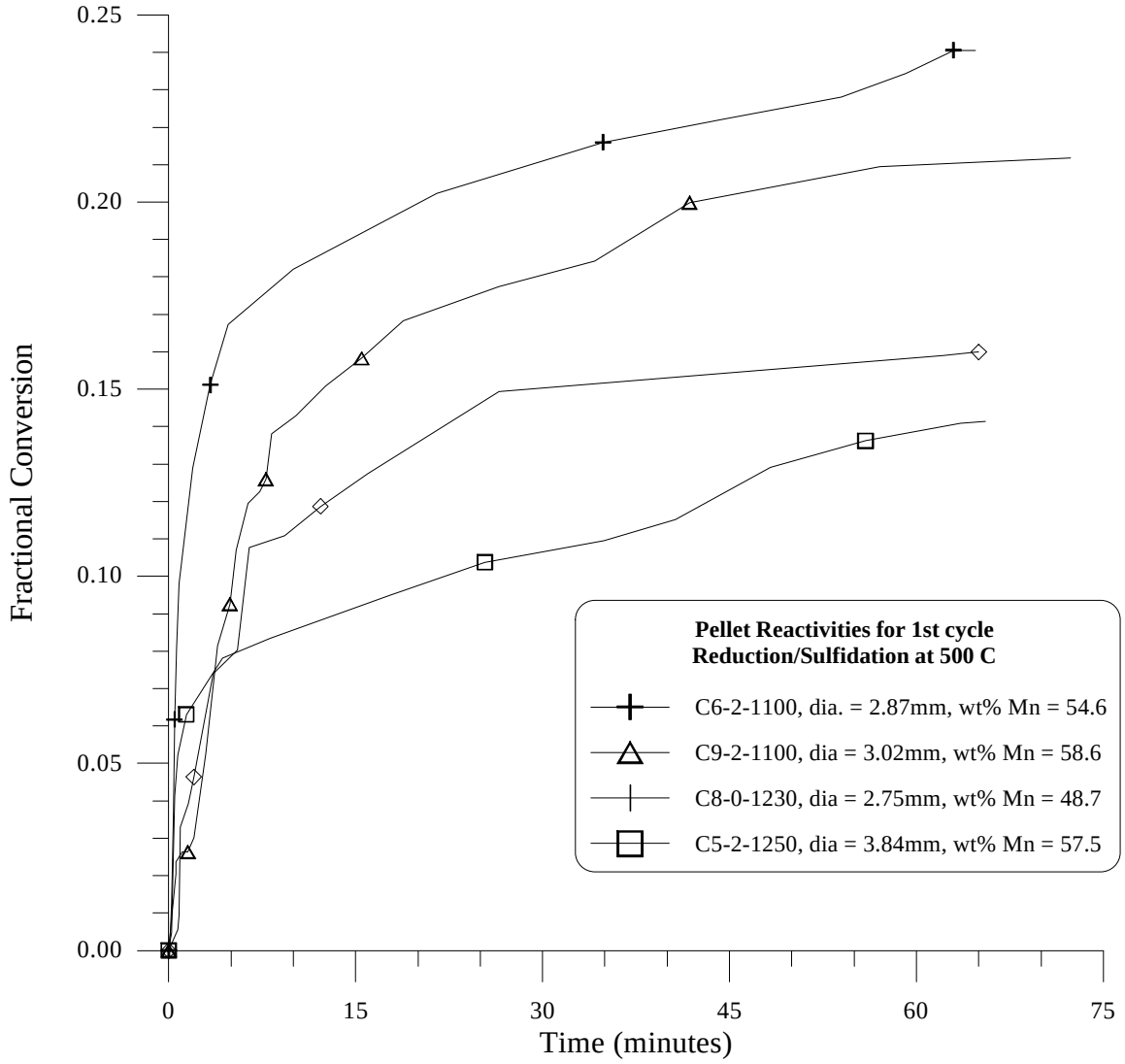

Figure 6.2. Mn-based formulation reactivity at 500^{o}C.

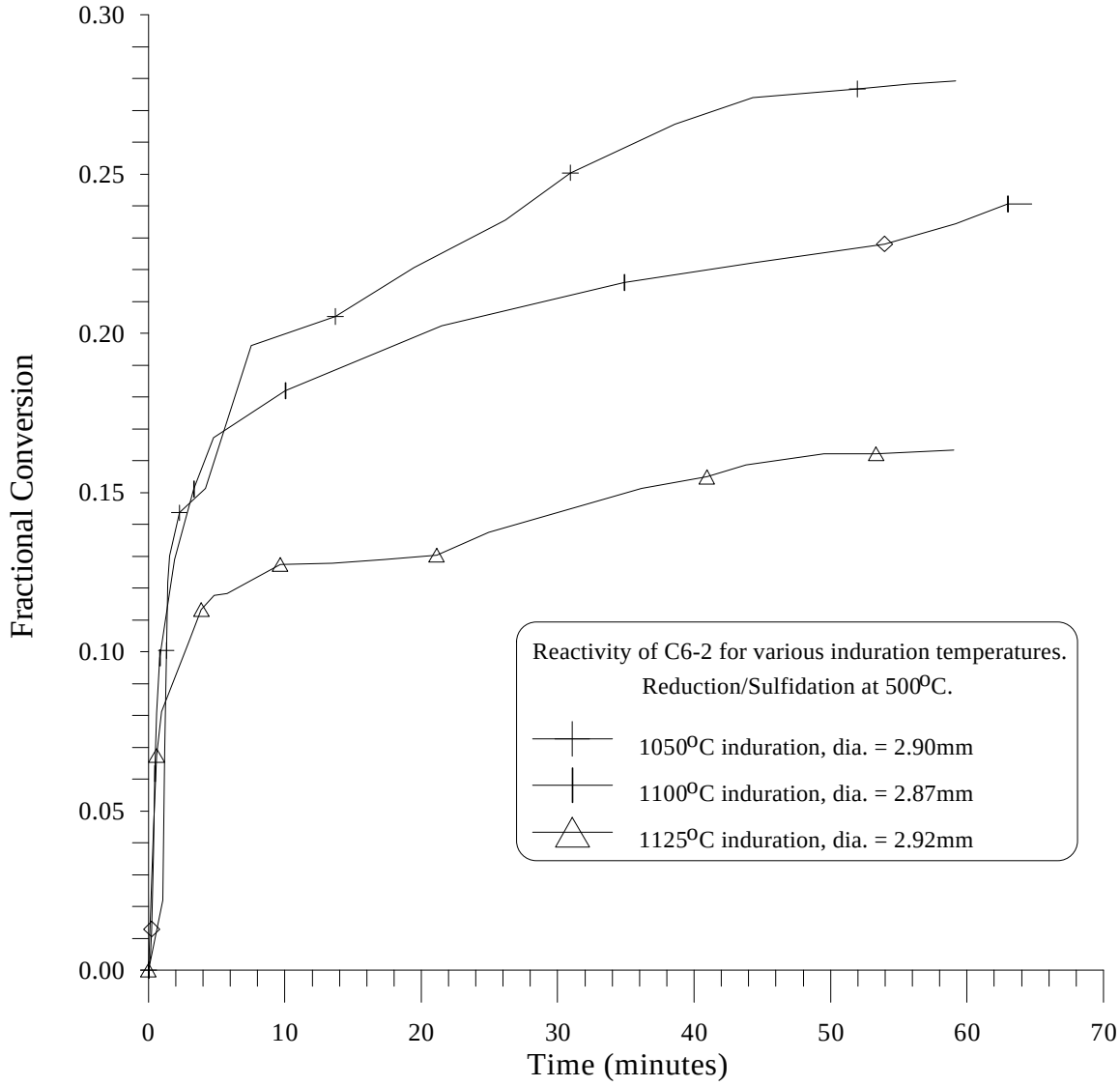

Figure 6.3. Effect of preparation temperature on reactivity for C6-2-1100.

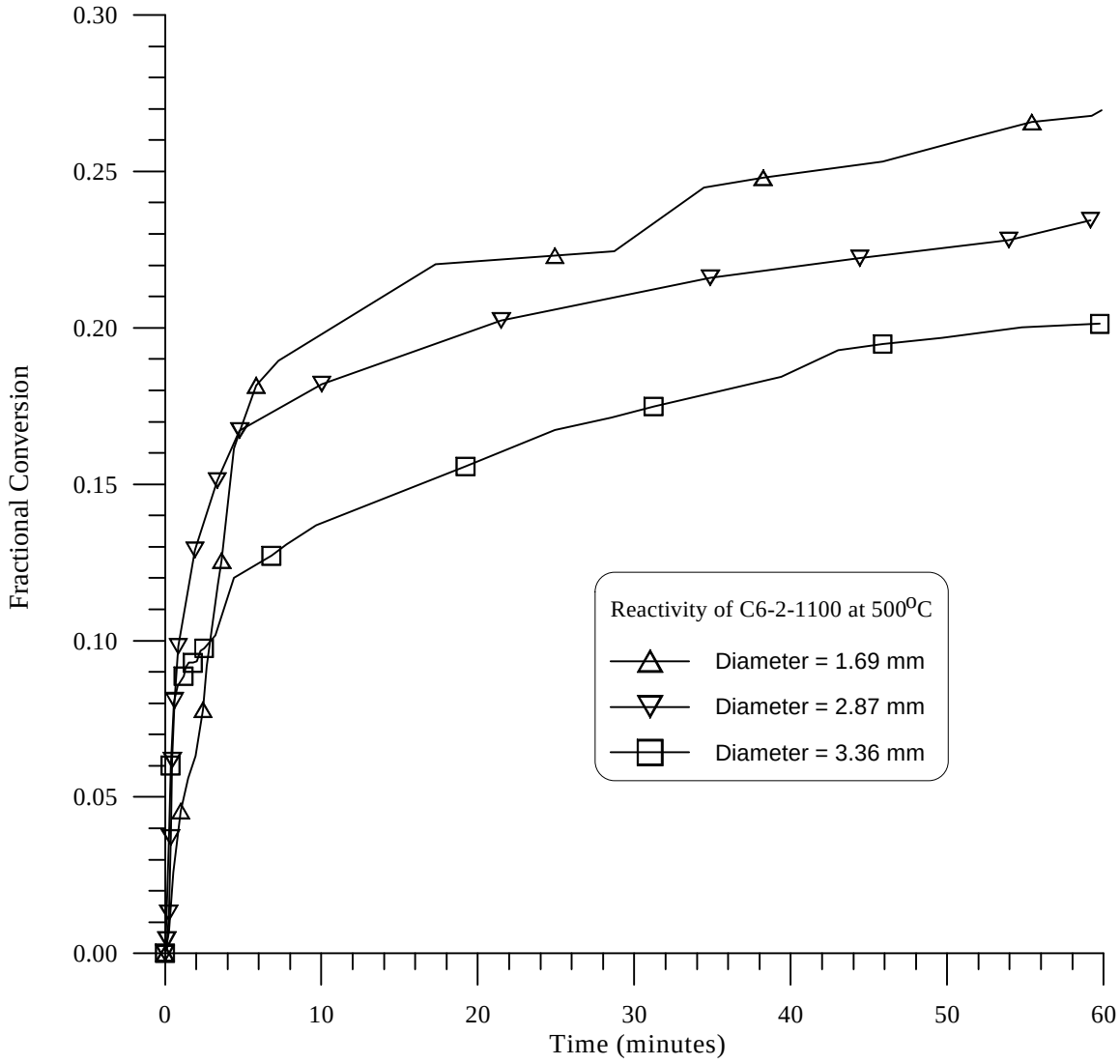

Figure 6.4. Effect of pellet diameter on reactivity for C6-2-1100.

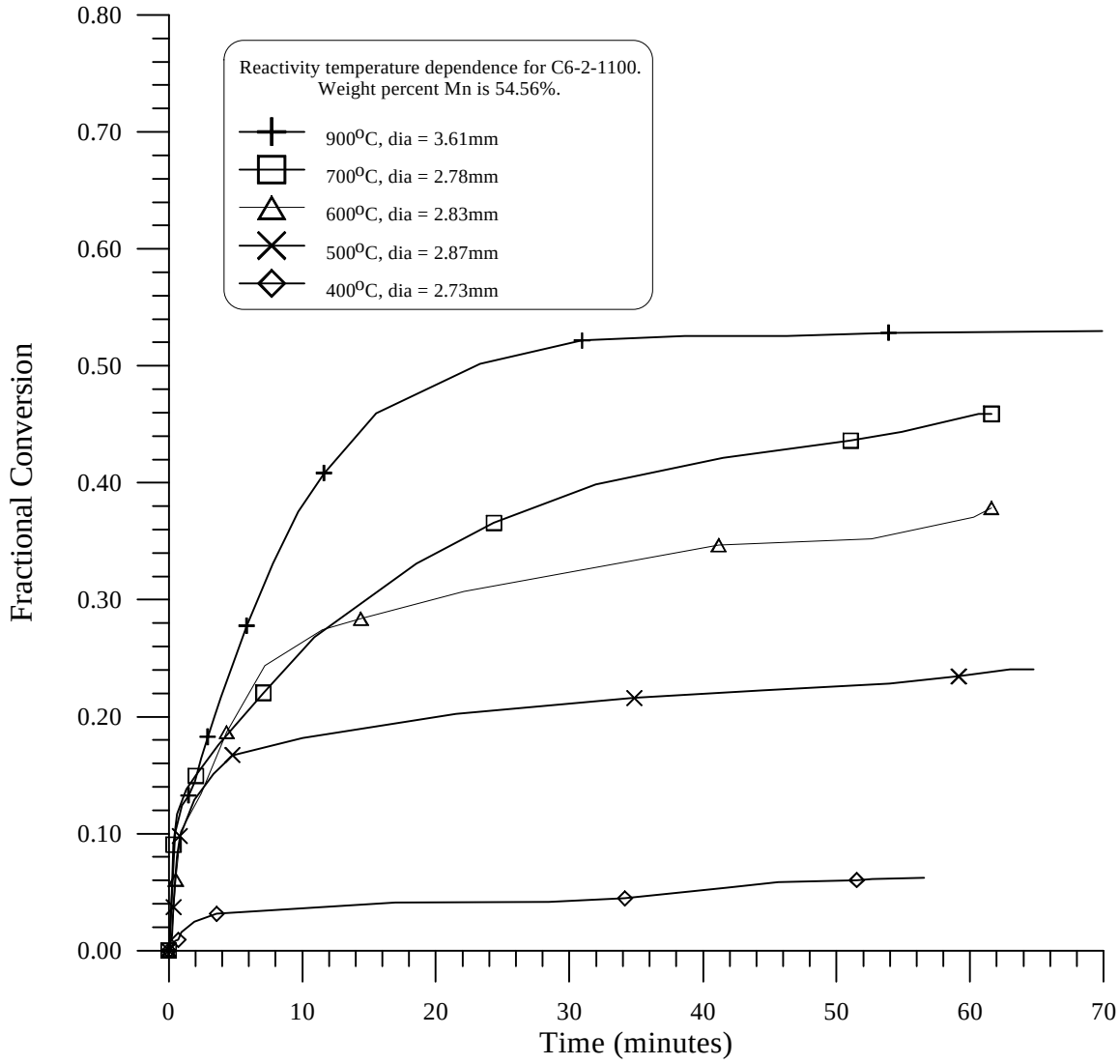

Figure 6.5. Effect of sulfidation temperature on reactivity for C6-2-1100.

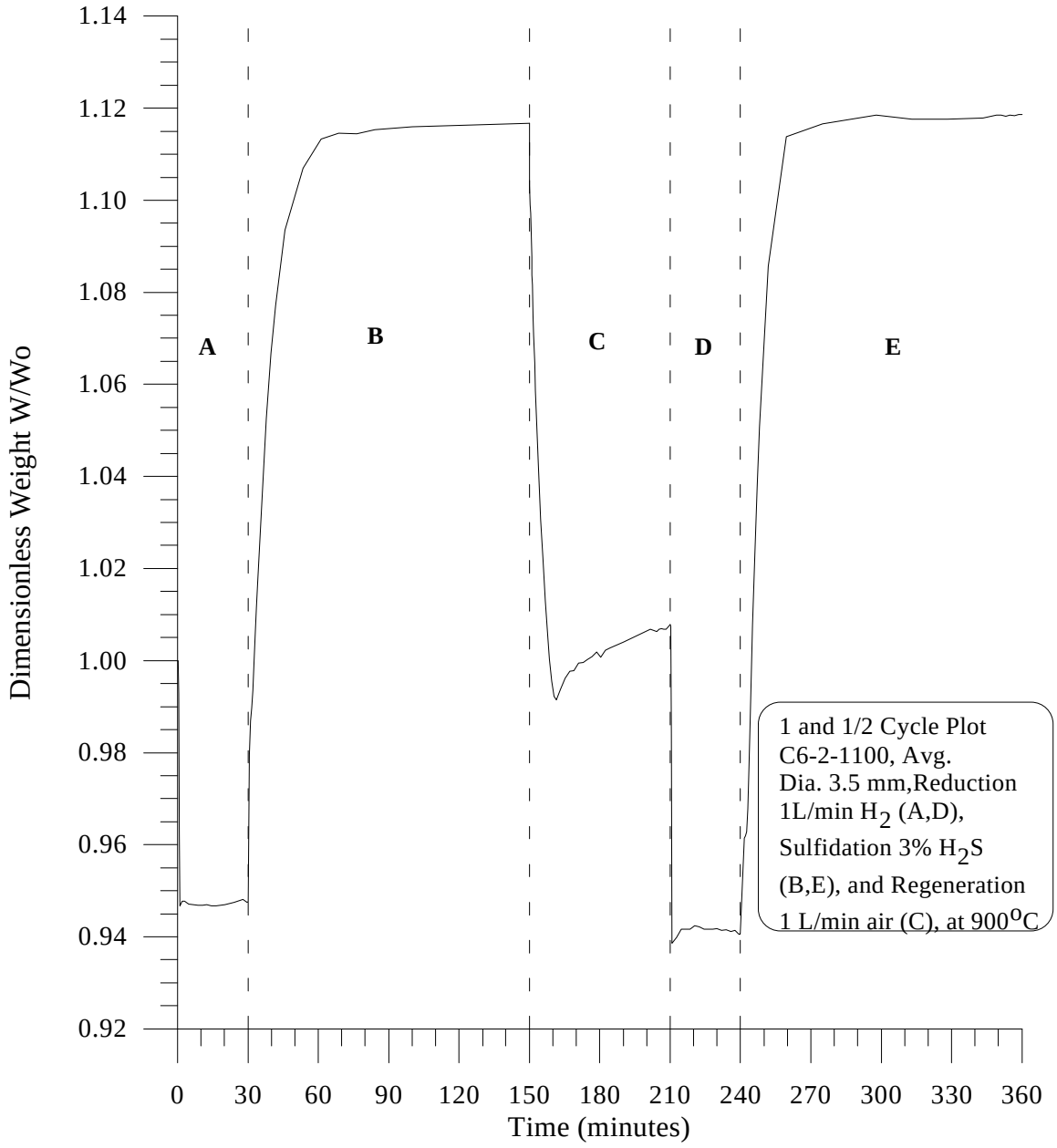

Figure 6.6. 1 and 1/2 cycle plot for C6-2-1100.

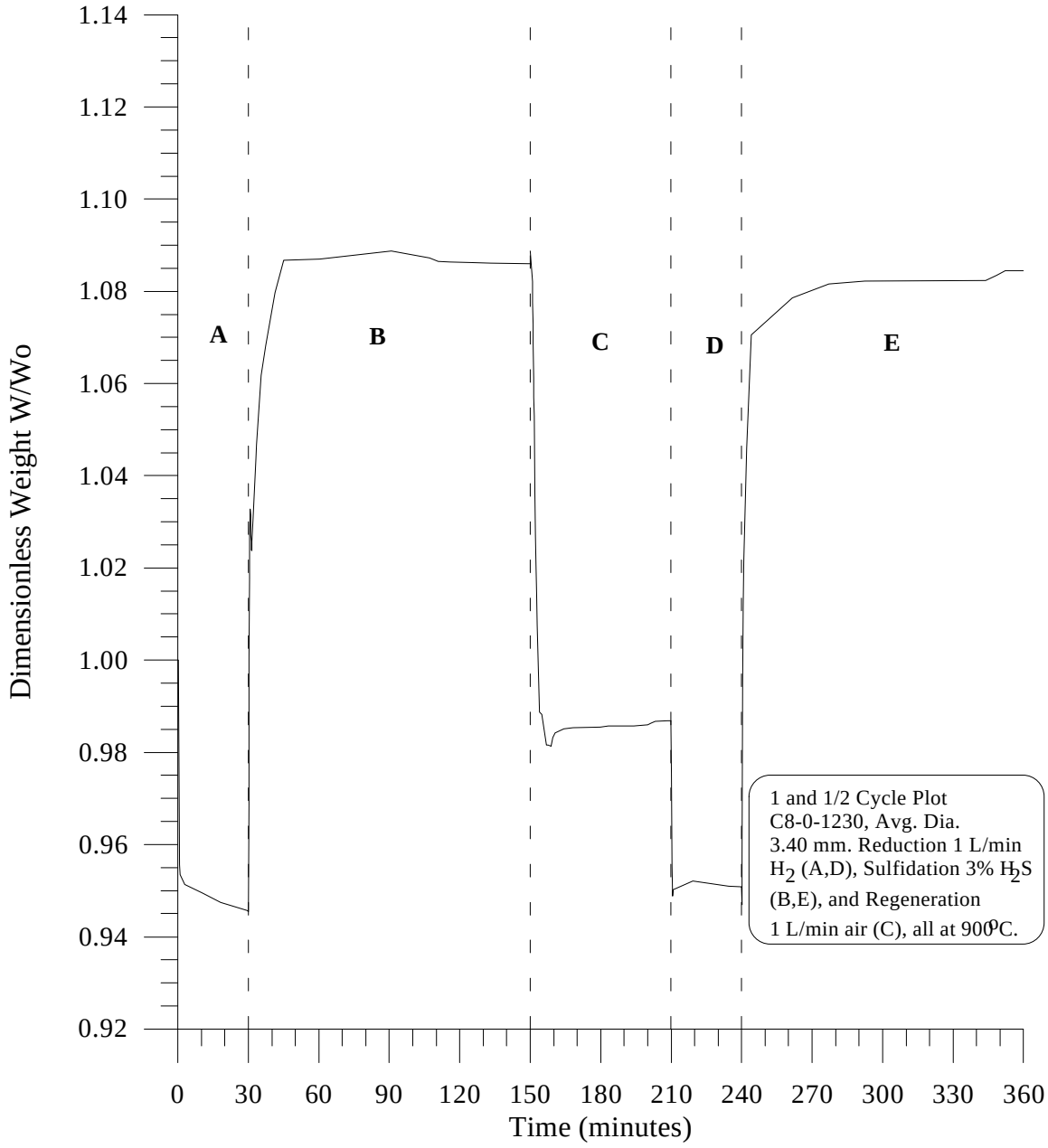

Figure 6.7. 1 and 1/2 cycle plot for C8-0-1230.

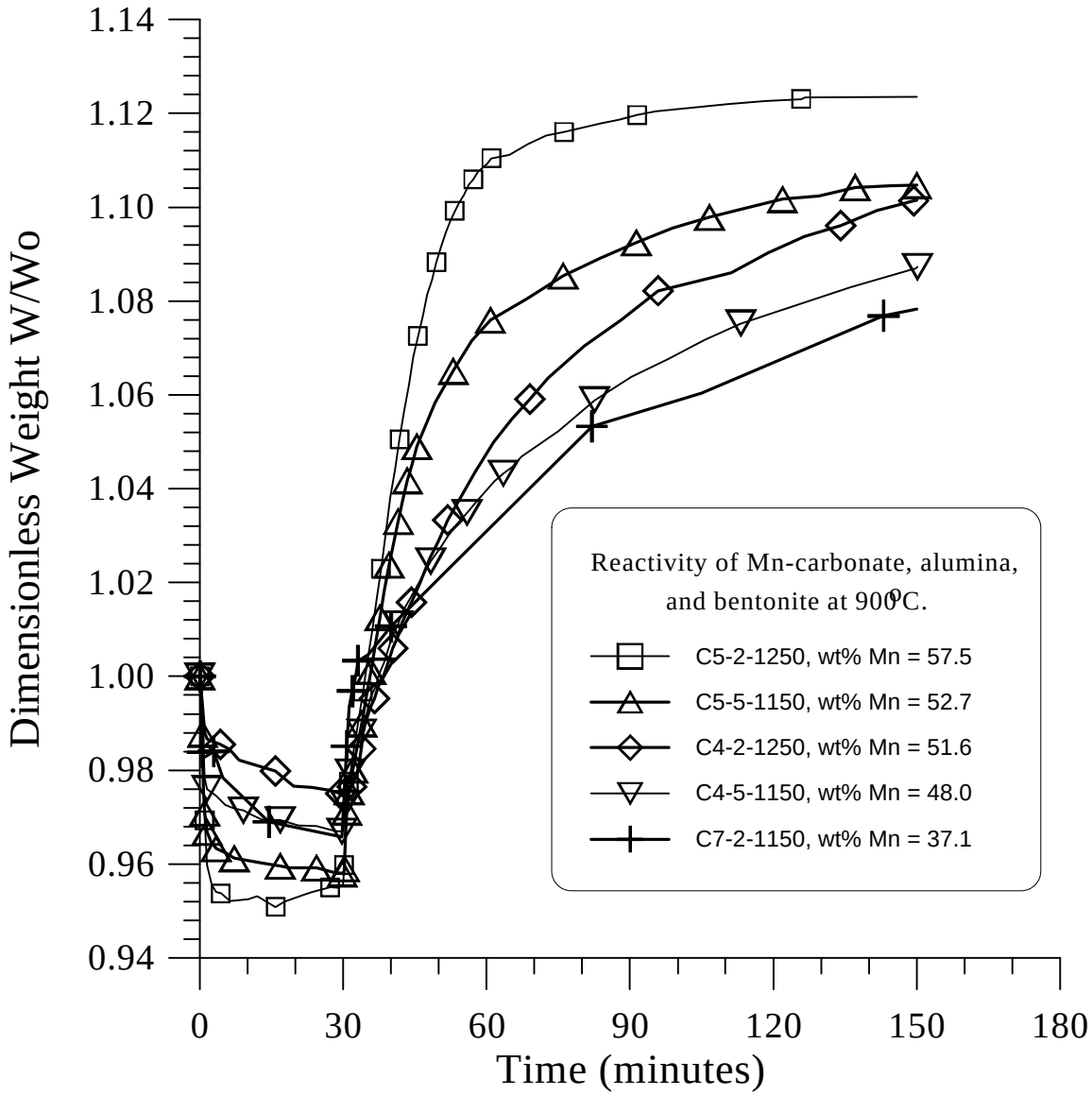

Figure 6.8. $MnCO_3/Al_2O_3$ reactivity at 900°C.

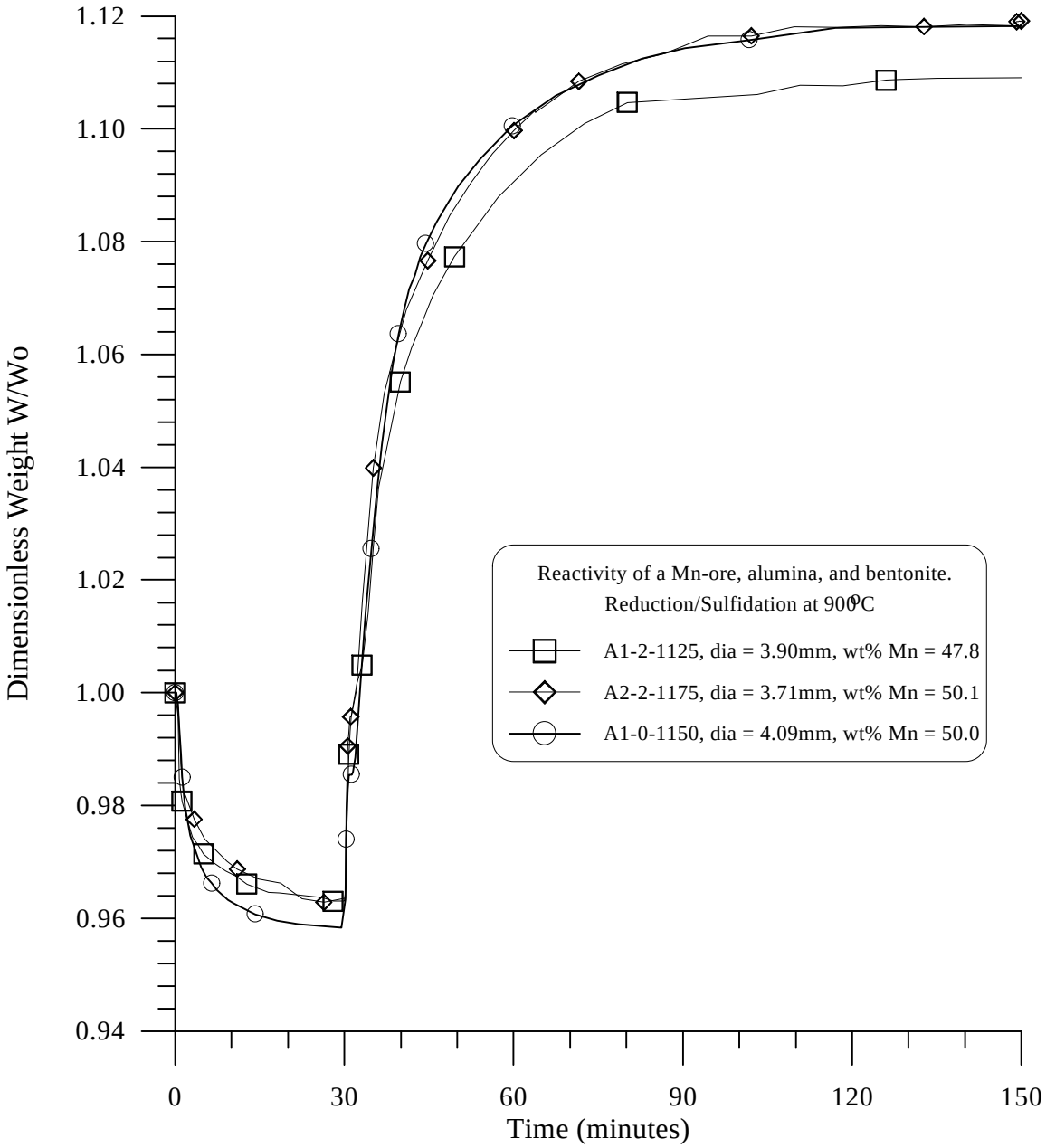

Figure 6.9. Mn-ore/Al_2O_3 reactivity at 900°C.

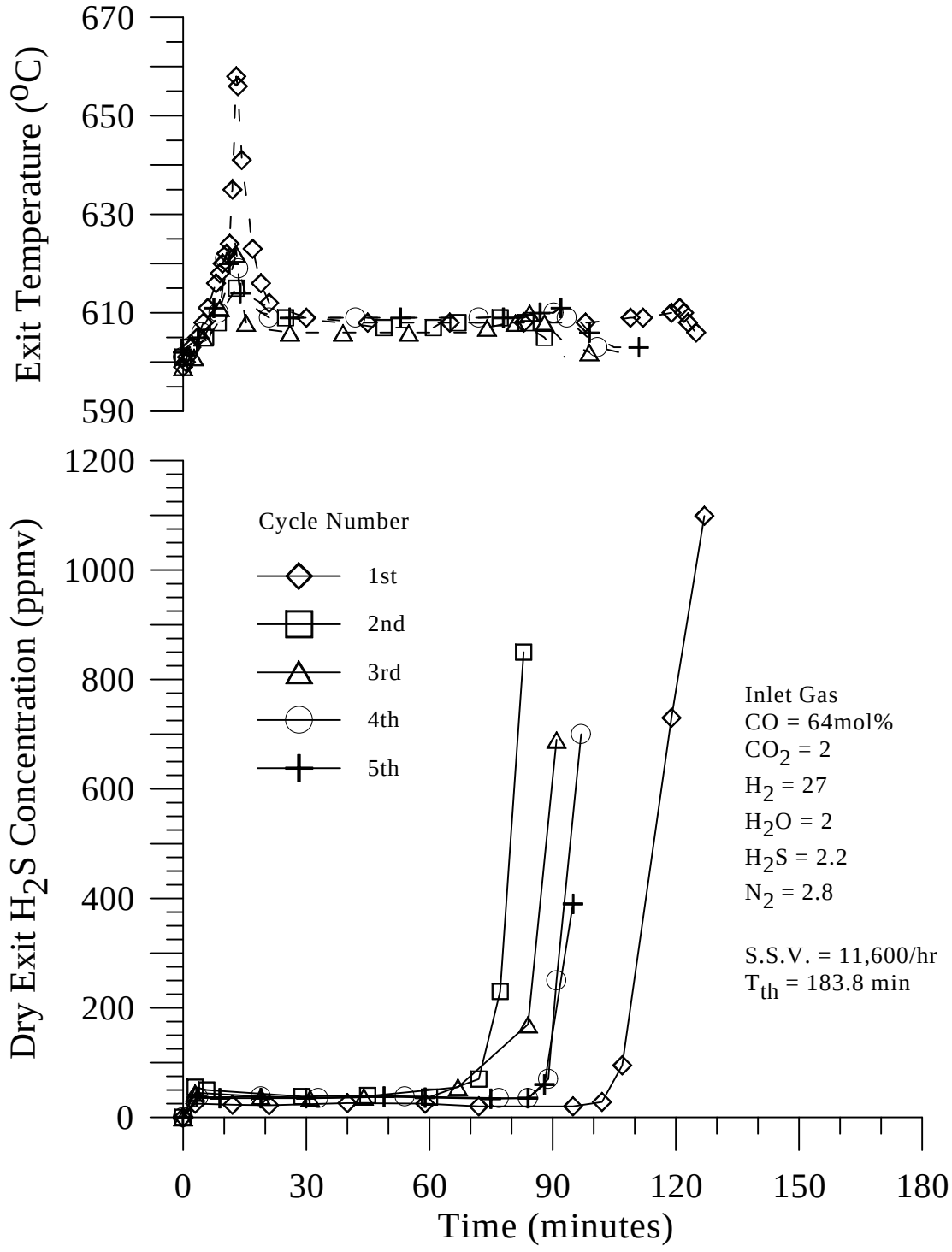

Figure 6.10. Sulfidation breakthrough curves for test 1FB using C6-2-1100 sorbent, with regeneration at 900°C in 1000 cc/min air (STP). T_{th} is the theoretical time to breakthrough.

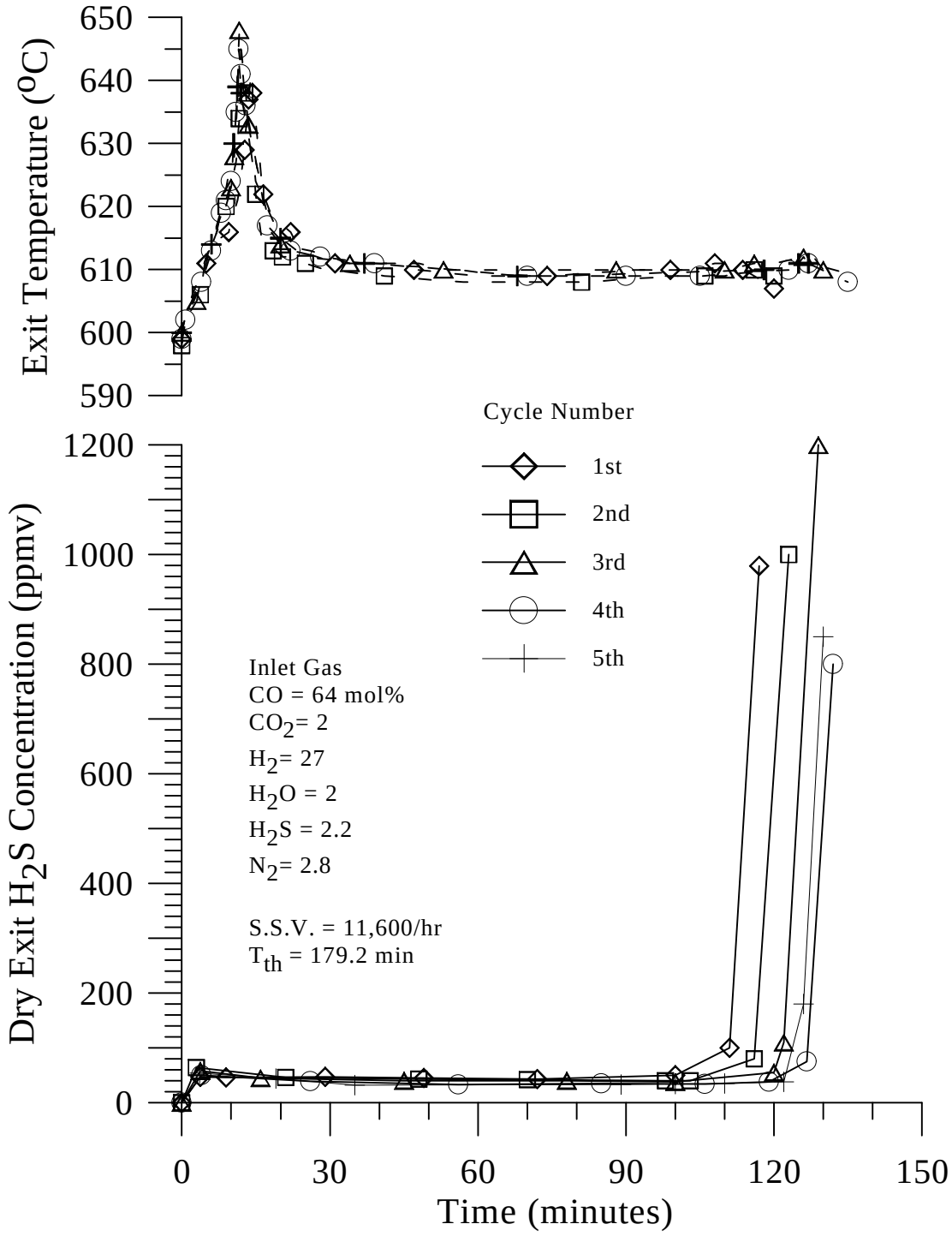

Figure 6.11. Sulfidation breakthrough curves for test 2FB using C6-2-1100 sorbent, with regeneration at 750°C in 100 cc/min O_2 and 900 cc/min N_2 (STP). T_{th} is the theoretical time to breakthrough.

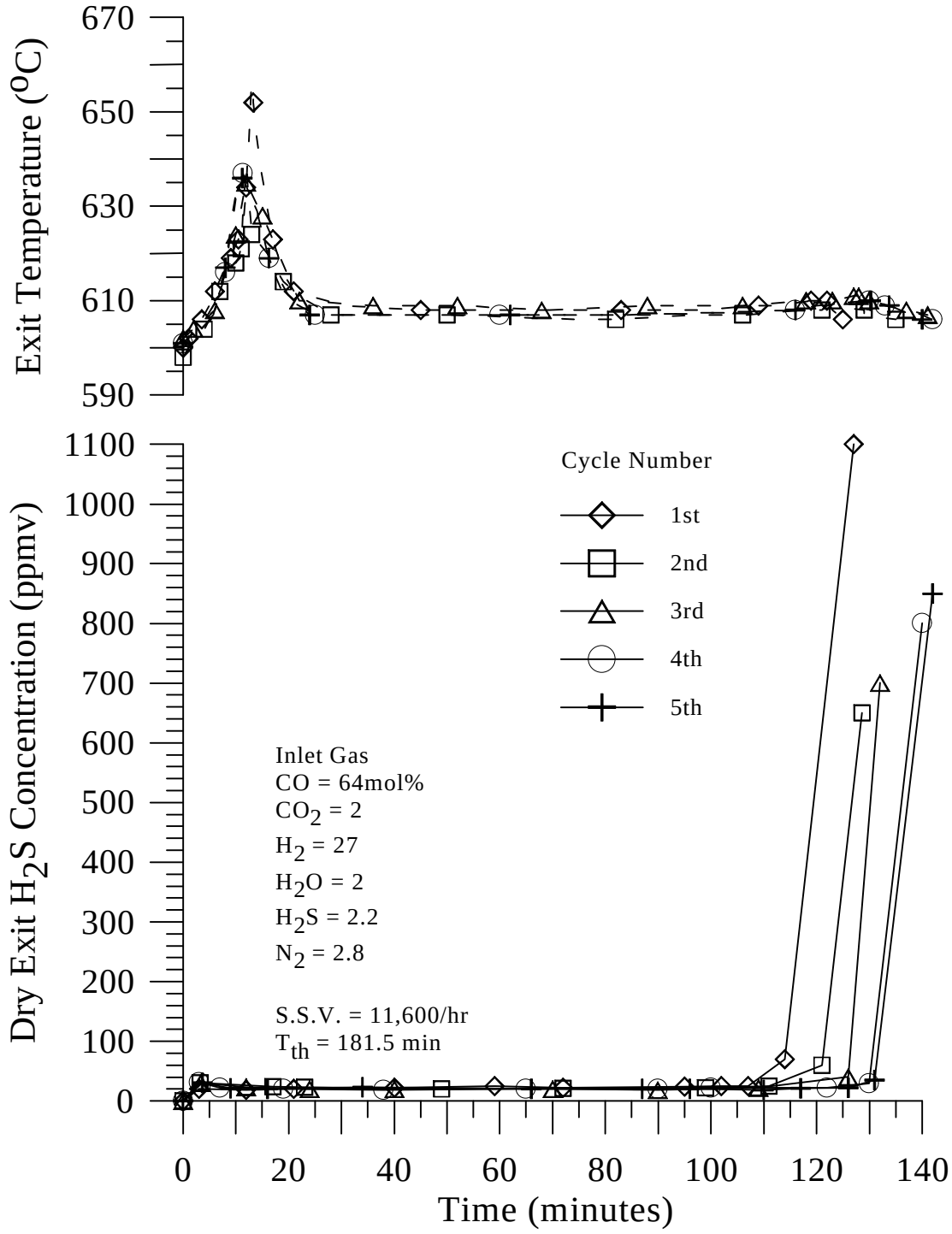

Figure 6.12. Sulfidation breakthrough curves for test 3FB using C6-2-1100 sorbent, with regeneration at 750°C in 50 cc/min O_2 and 950 cc/min N_2 (STP). T_{th} is the theoretical time to breakthrough.

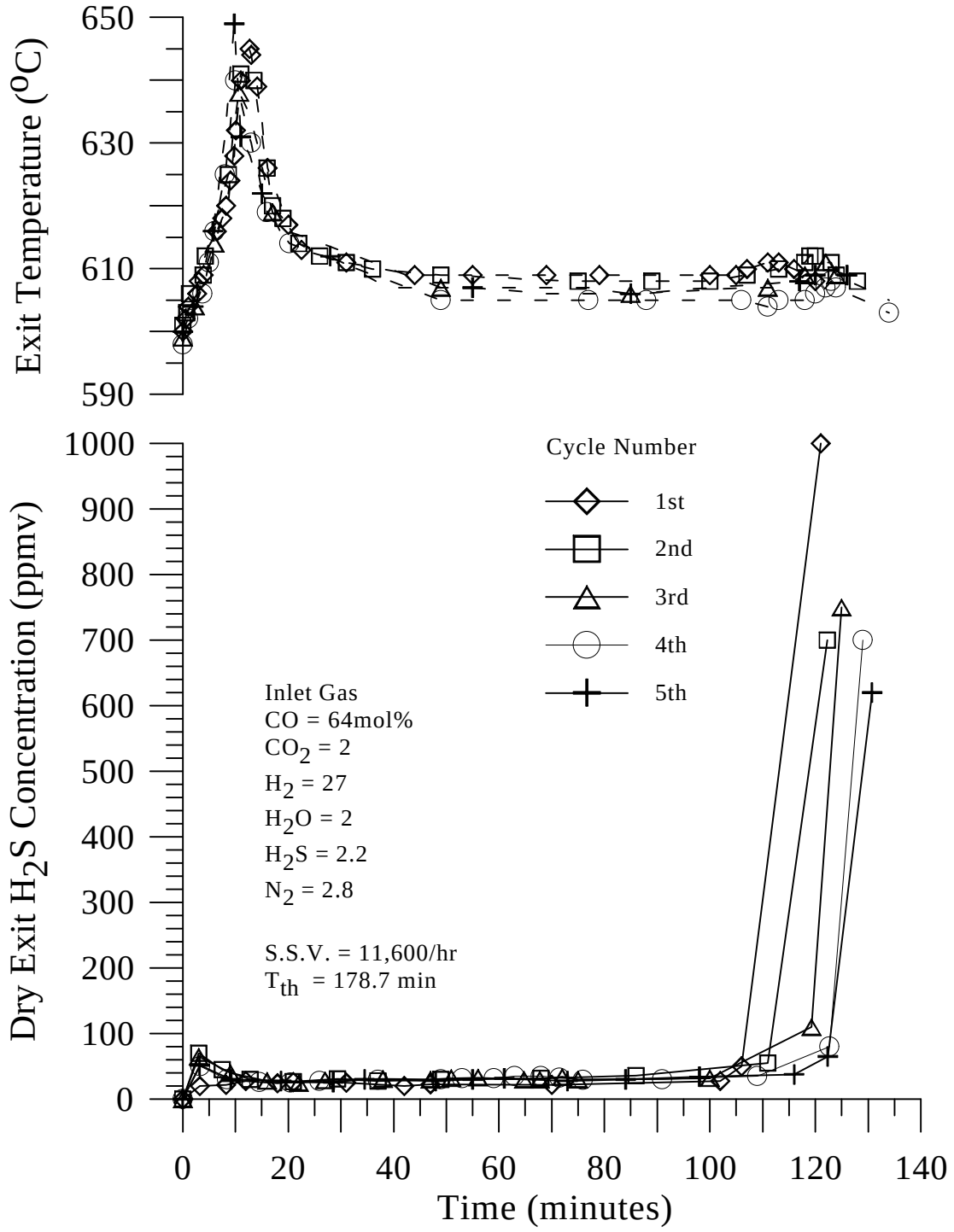

Figure 6.13. Sulfidation breakthrough curves for test 7FB using C6-2-1100 sorbent, with regeneration at 750°C in 400 cc/min steam and 600 cc/min air (STP). T_{th} is the theoretical time to breakthrough.

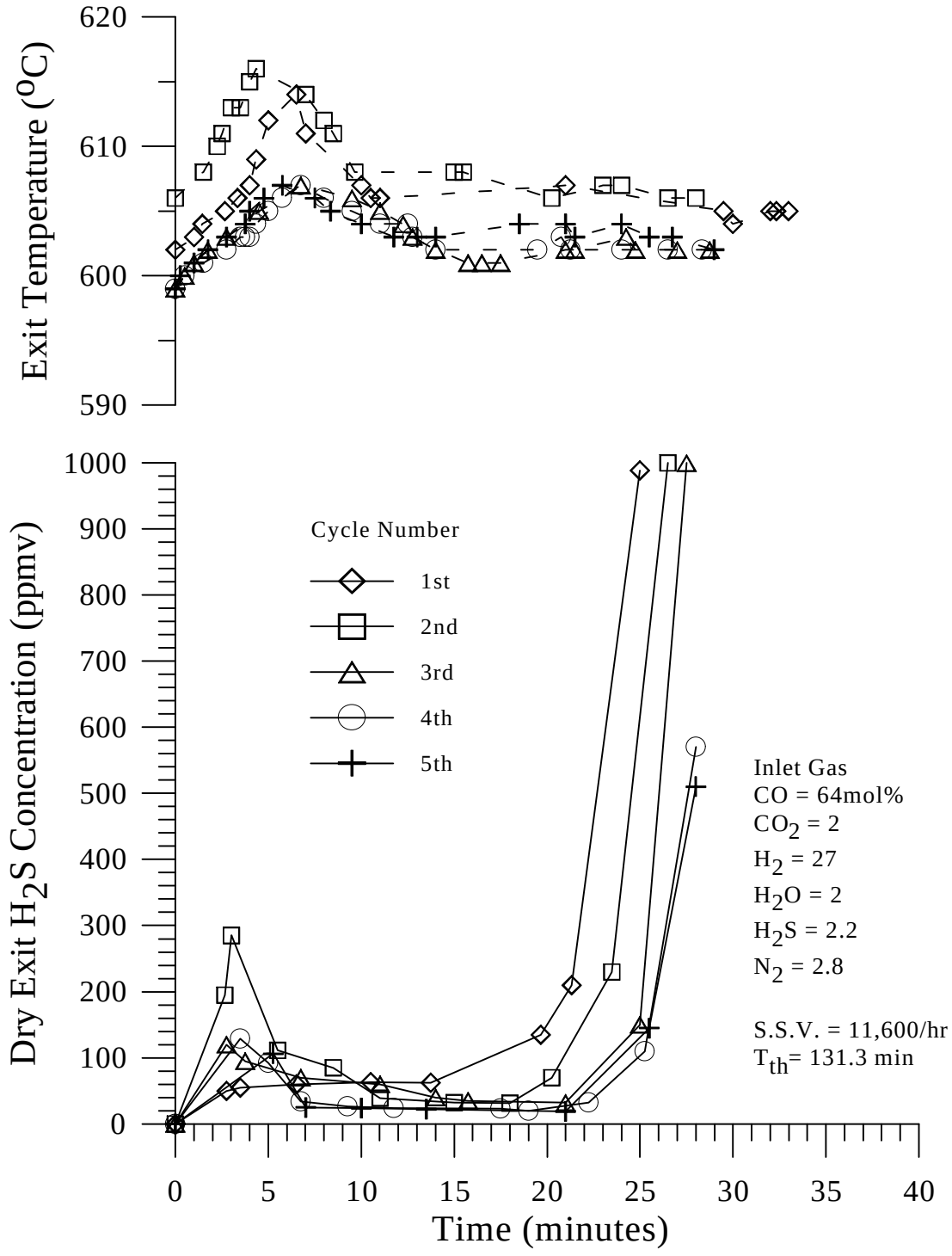

Figure 6.14. Sulfidation breakthrough curves for test 5FB using C8-0-1200 sorbent, with regeneration at 750°C in 400 cc/min steam and 600 cc/min air (STP). T_{th} is the theoretical time to breakthrough.

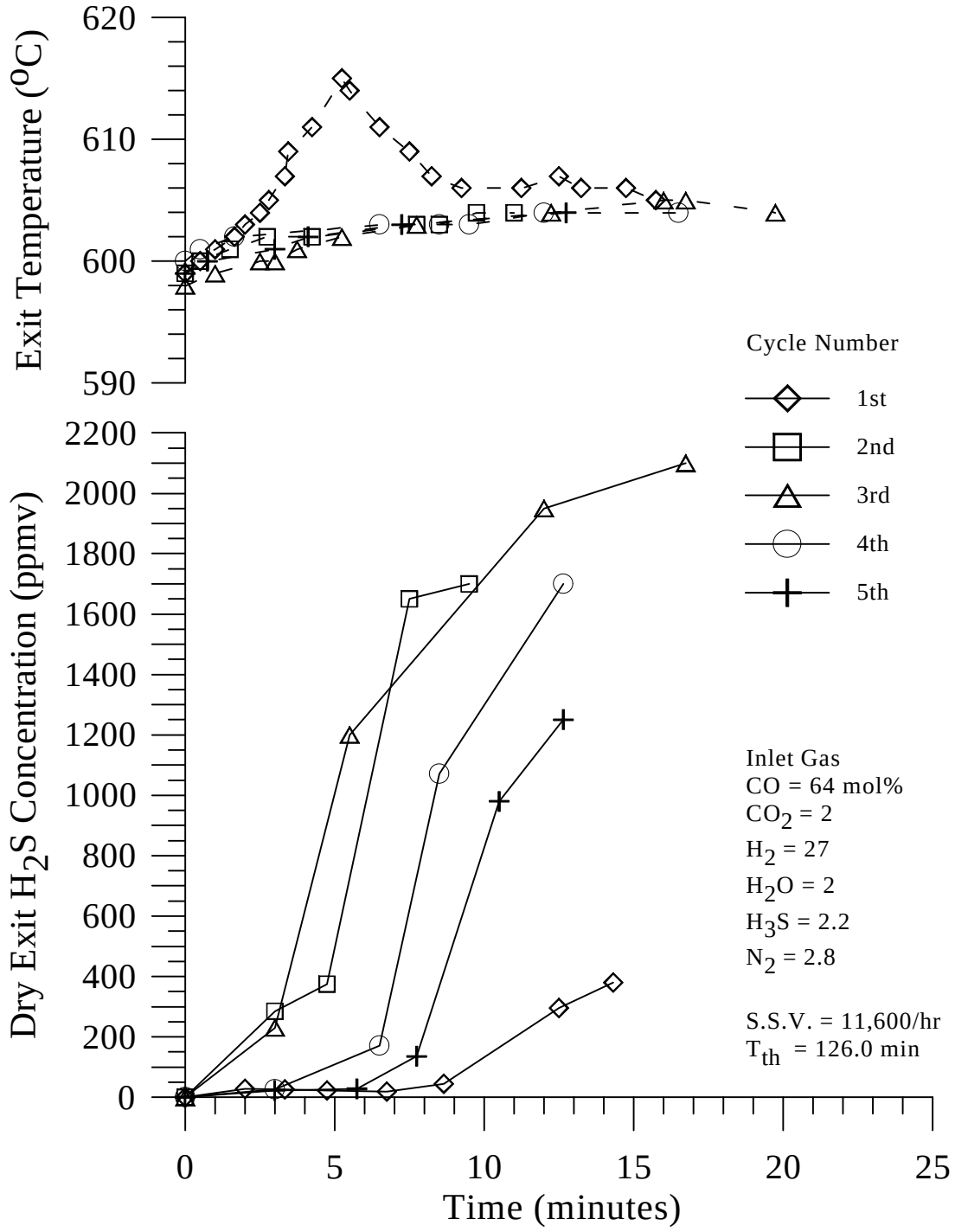

Figure 6.15. Sulfidation breakthrough curves for test 6FB using C8-0-1200 sorbent, with regeneration at 750°C in 800 cc/min steam and 200 cc/min N_2 (STP). T_{th} is the theoretical time to breakthrough.

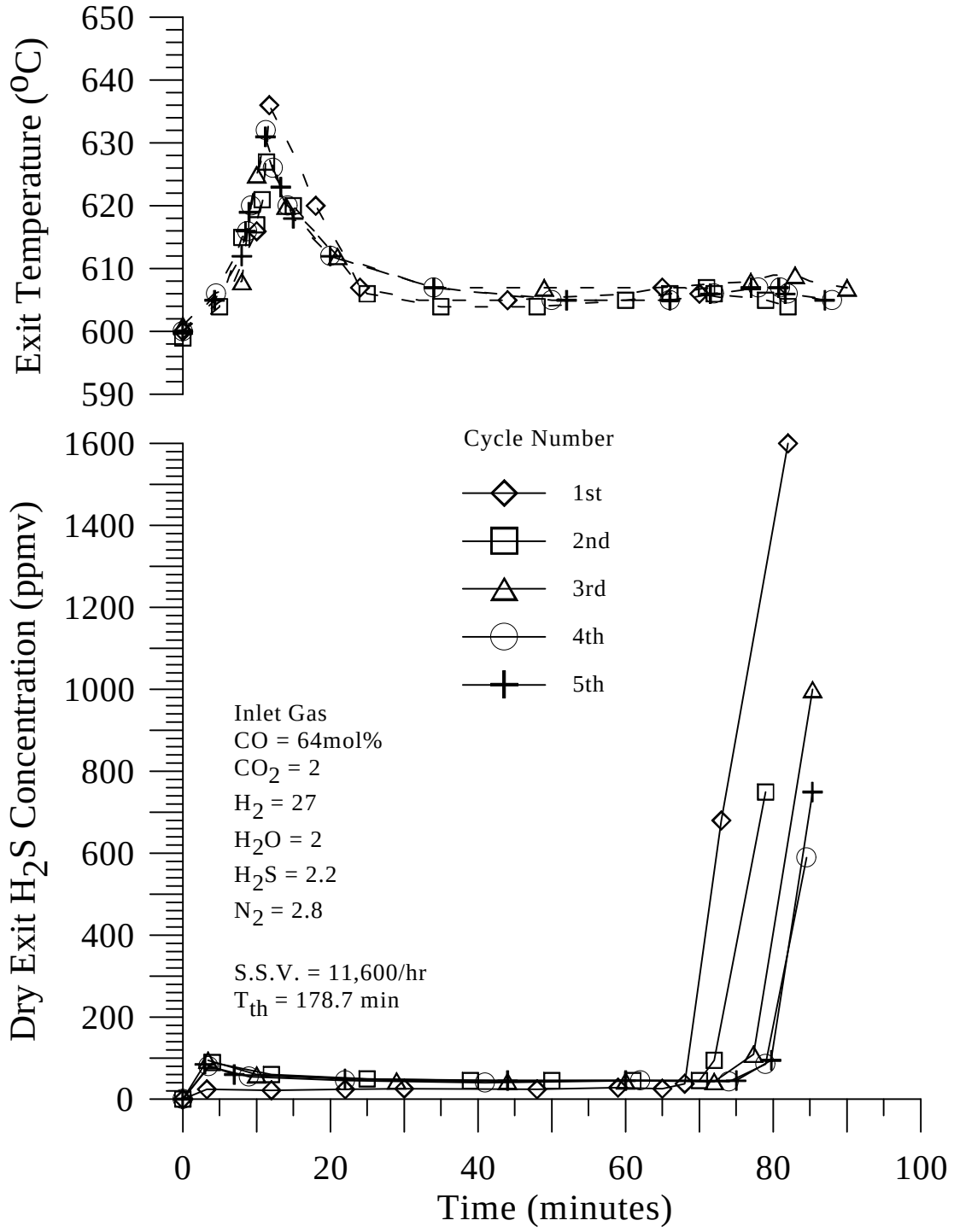

Figure 6.16. Sulfidation breakthrough curves for test 4FB using C4-2-1175 sorbent, with regeneration at 750°C in 400 cc/min steam and 600 cc/min air (STP). T_{th} is the theoretical time to breakthrough.

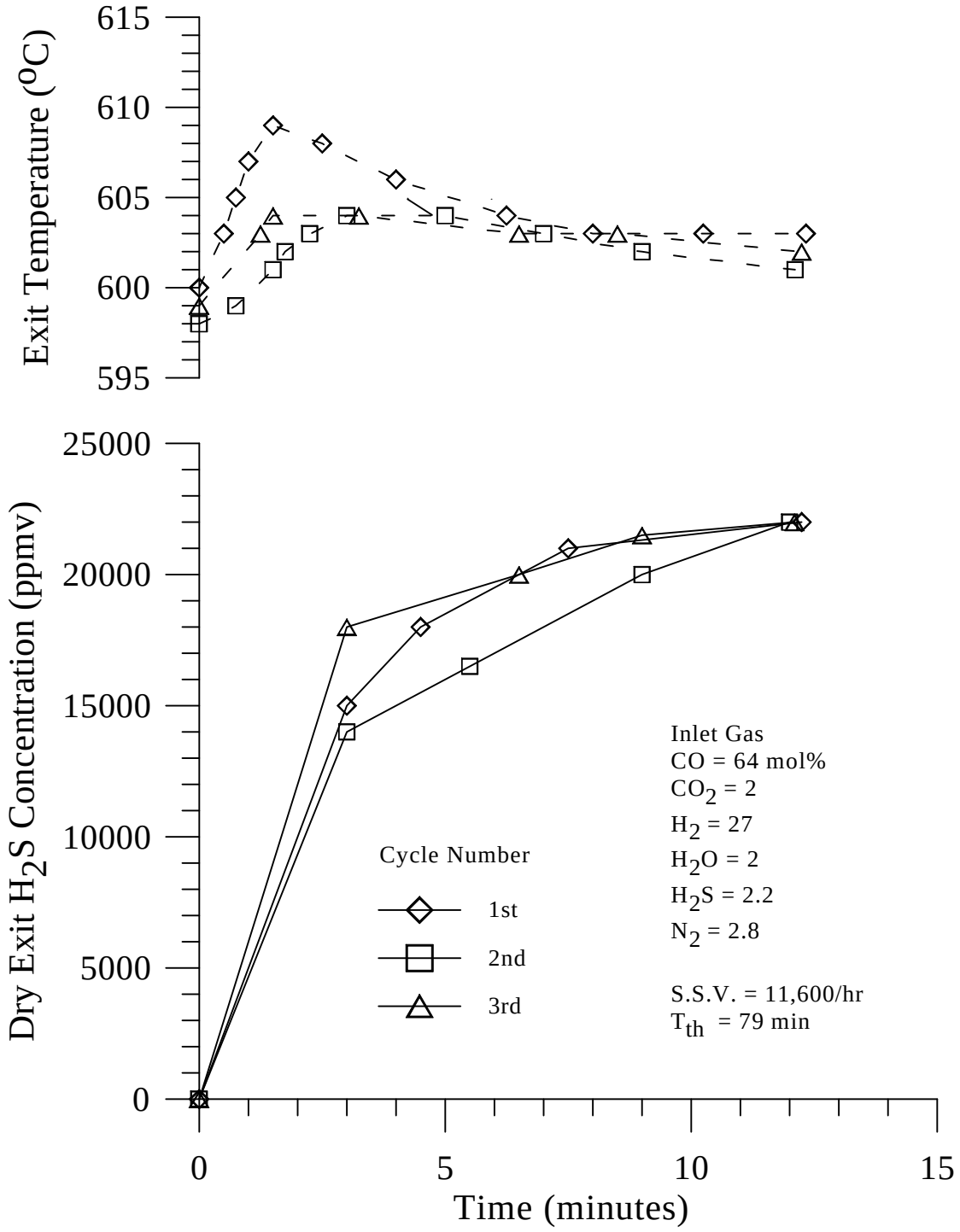

Figure 6.17. Sulfidation breakthrough curves for test 8FB using C11-0-1160 sorbent, with regeneration at 750°C in 800 cc/min steam and 200 cc/min N_2 (STP). T_{th} is the theoretical time to breakthrough.

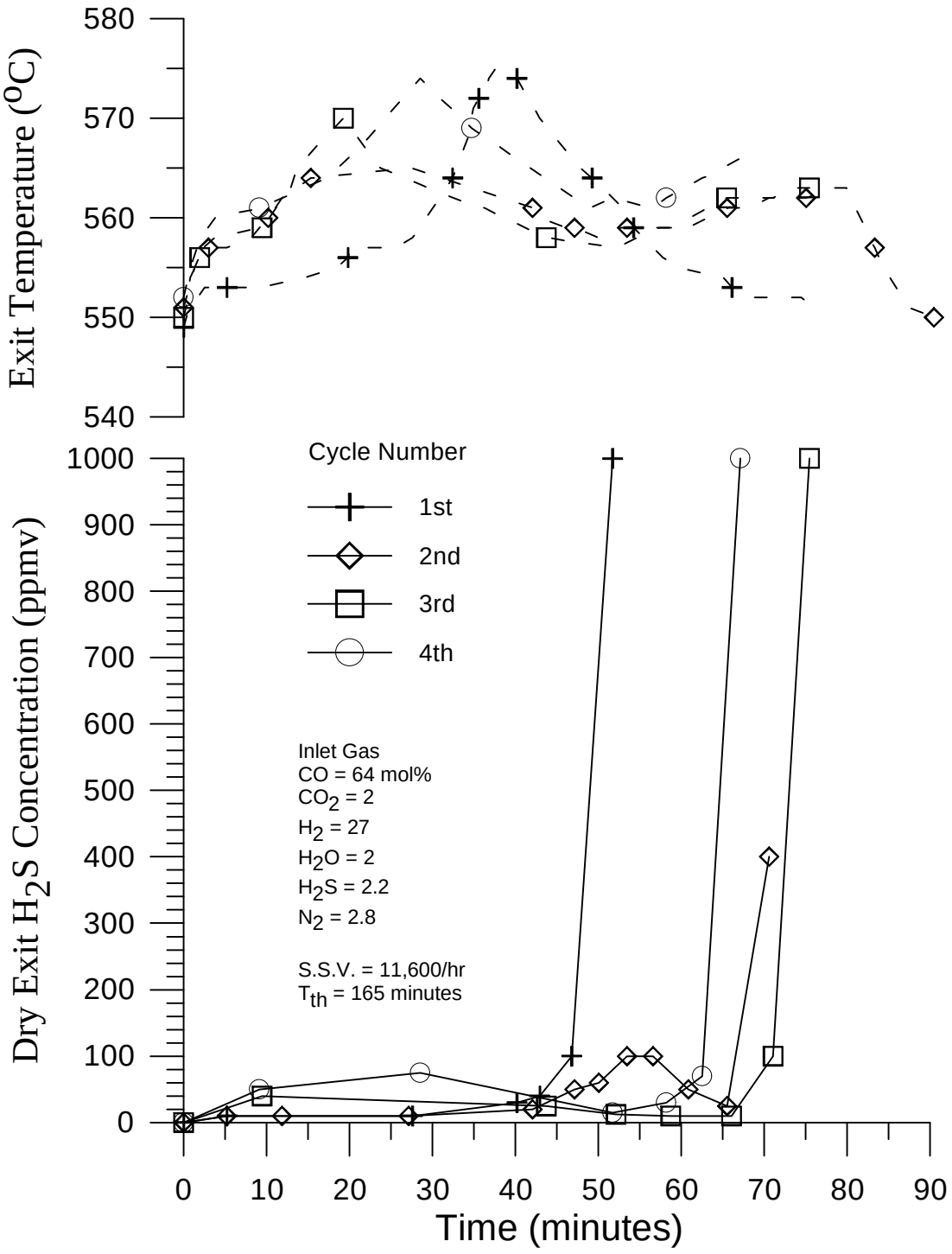

Figure 6.18. Sulfidation breakthrough curves for test FB1A using C6-2-1100 sorbent. T_{th} is the theoretical time to breakthrough.

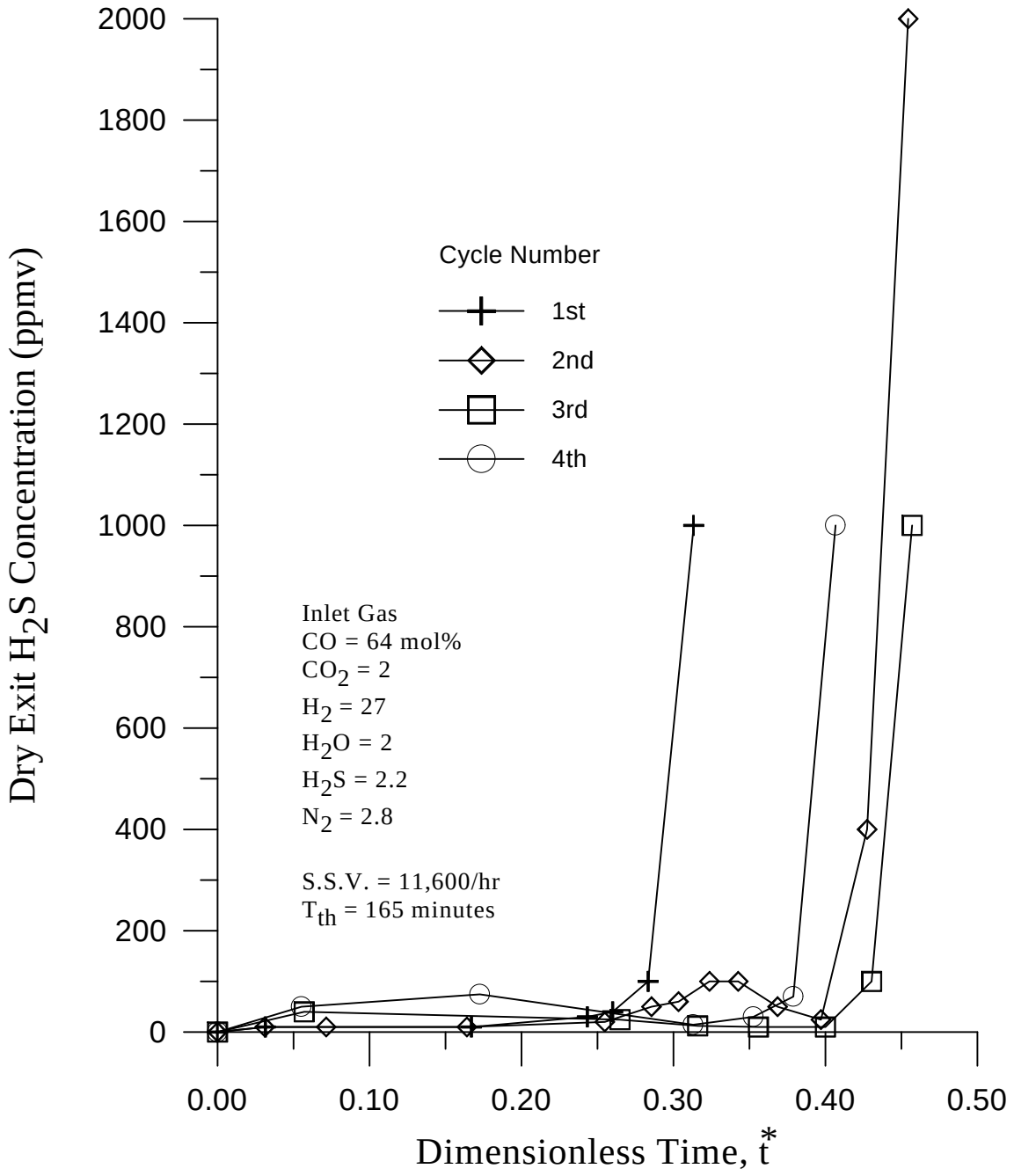

Figure 6.19. Sulfidation breakthrough curves for test FB1A using sorbent C6-2-1100 at 550^{o}C, plotted as H_2S concentration versus dimensionless time.

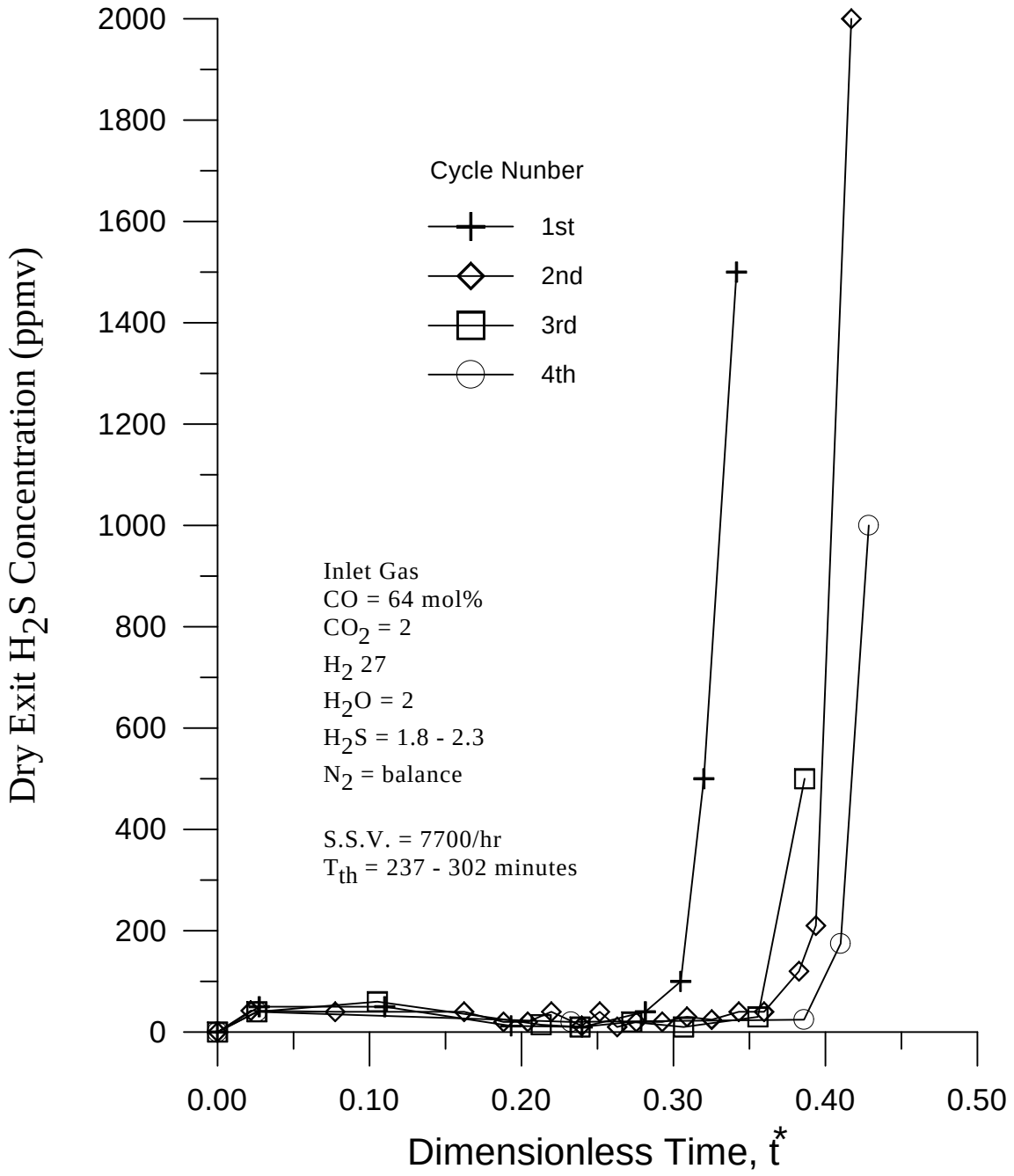

Figure 6.20. Sulfidation breakthrough curves for test FB2A using sorbent C6-2-1100 at 550^{o}C, plotted as H_2S concentration versus dimensionless time.

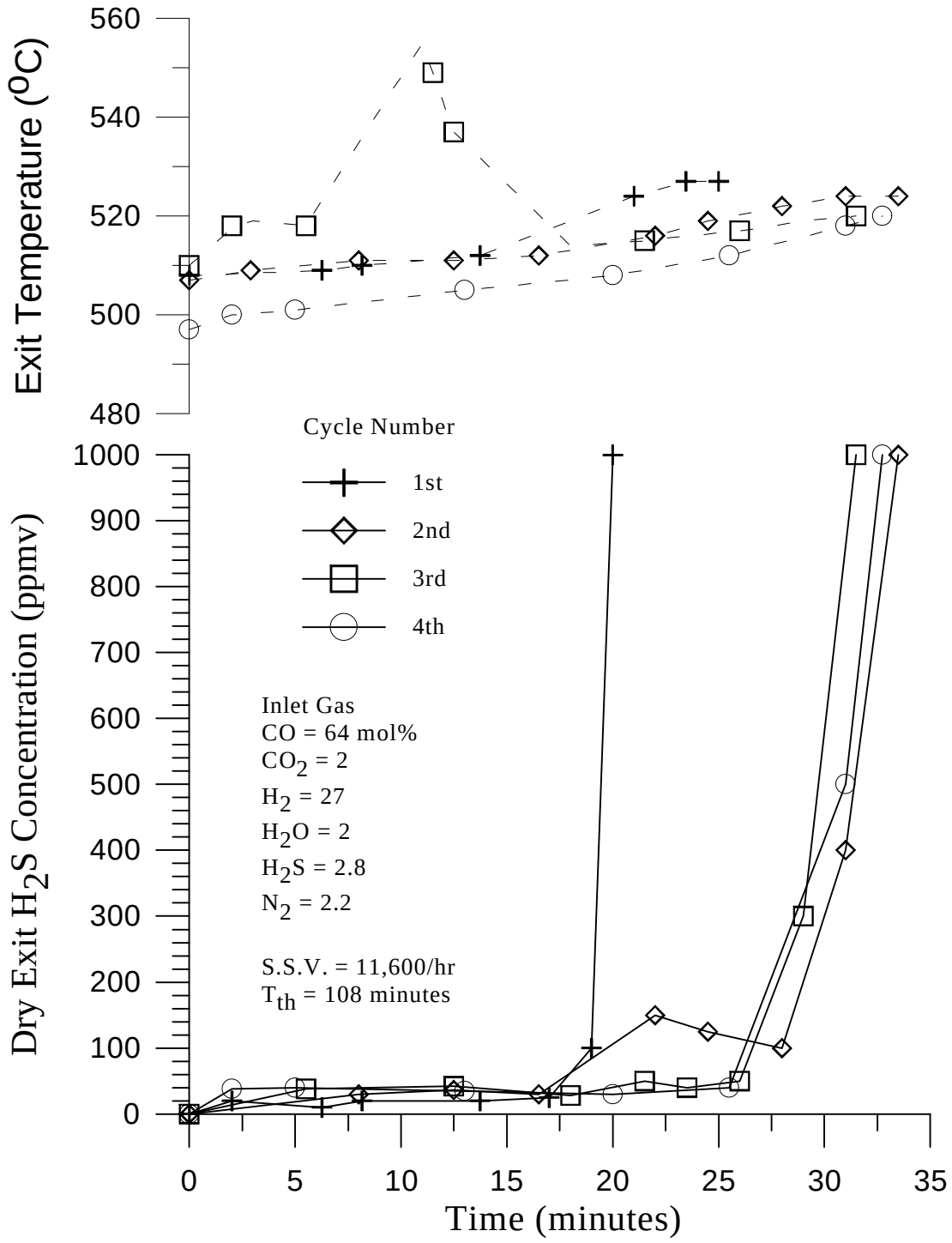

Figure 6.21. Sulfidation breakthrough curves for test FB3A using C6-2-1100 sorbent. T_{th} is the theoretical time to breakthrough.

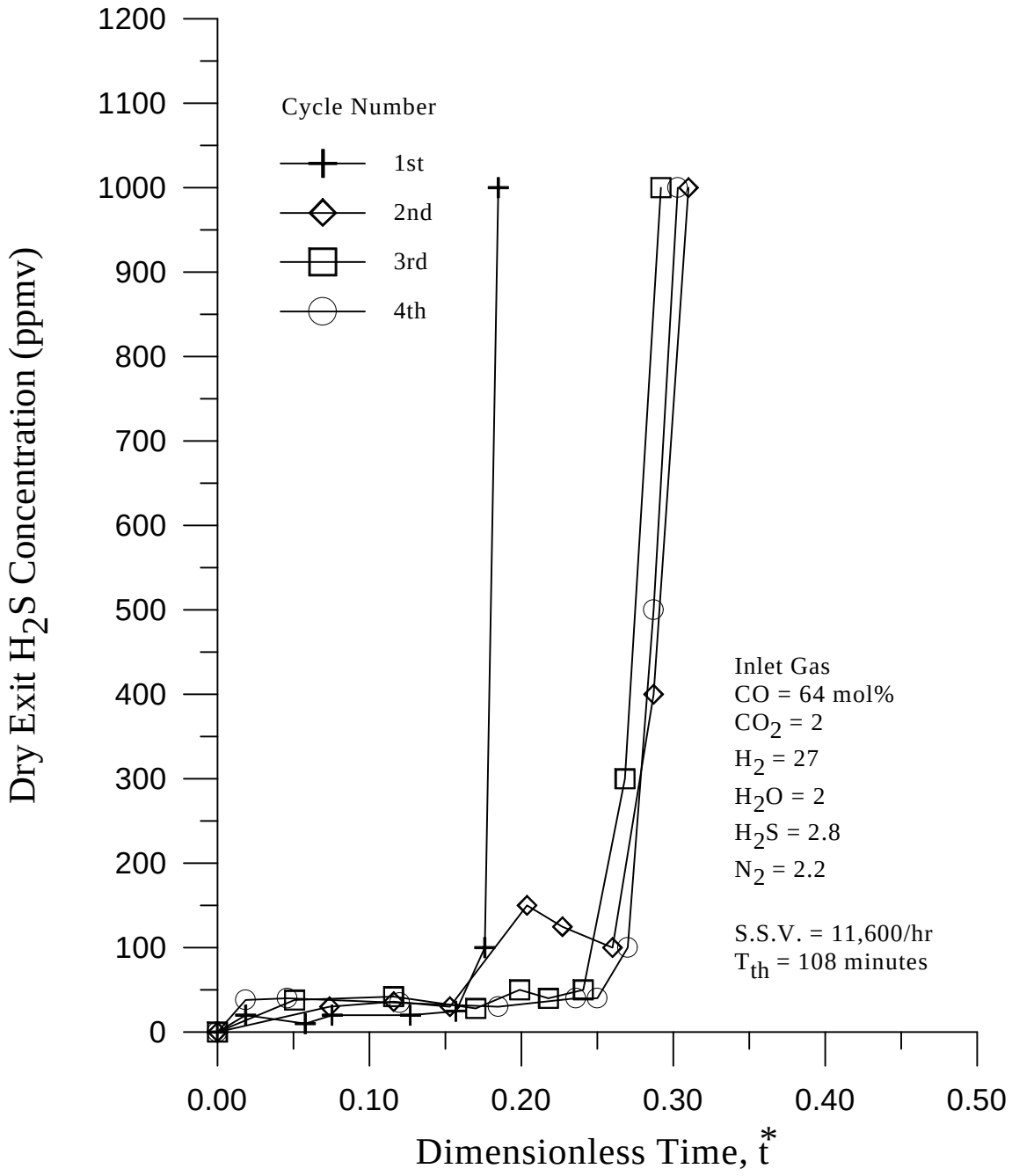

Figure 6.22. Sulfidation breakthrough curves for test FB3A using sorbent C6-2-1100 at 500^{o}C, plotted as H_2S concentration versus dimensionless time.

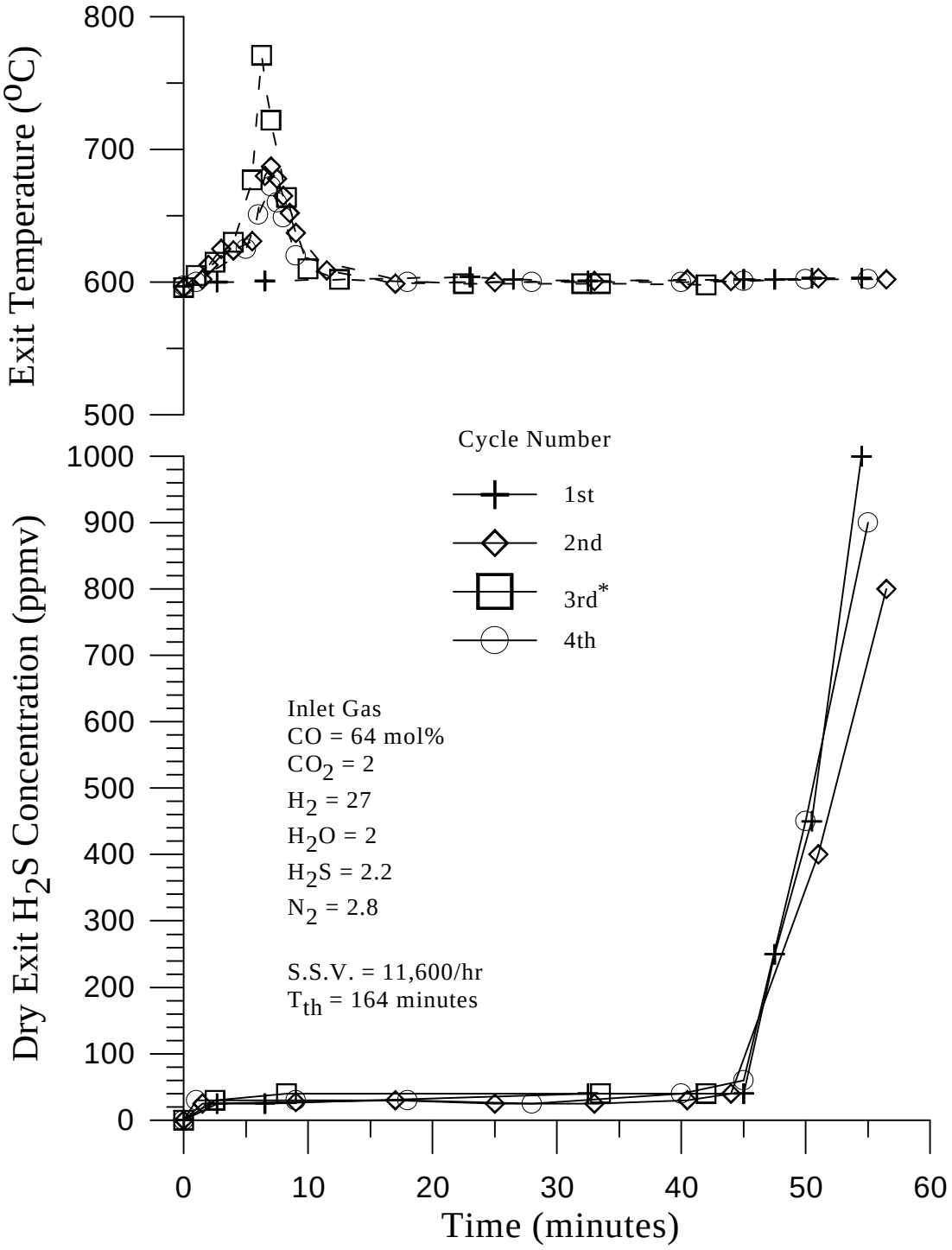

Figure 6.23. Sulfidation breakthrough curves for test FB4A using C6-2-1115 sorbent. T_{th} is the theoretical time to breakthrough. *H_2S tank ran out at 44 minutes, cycle terminated.

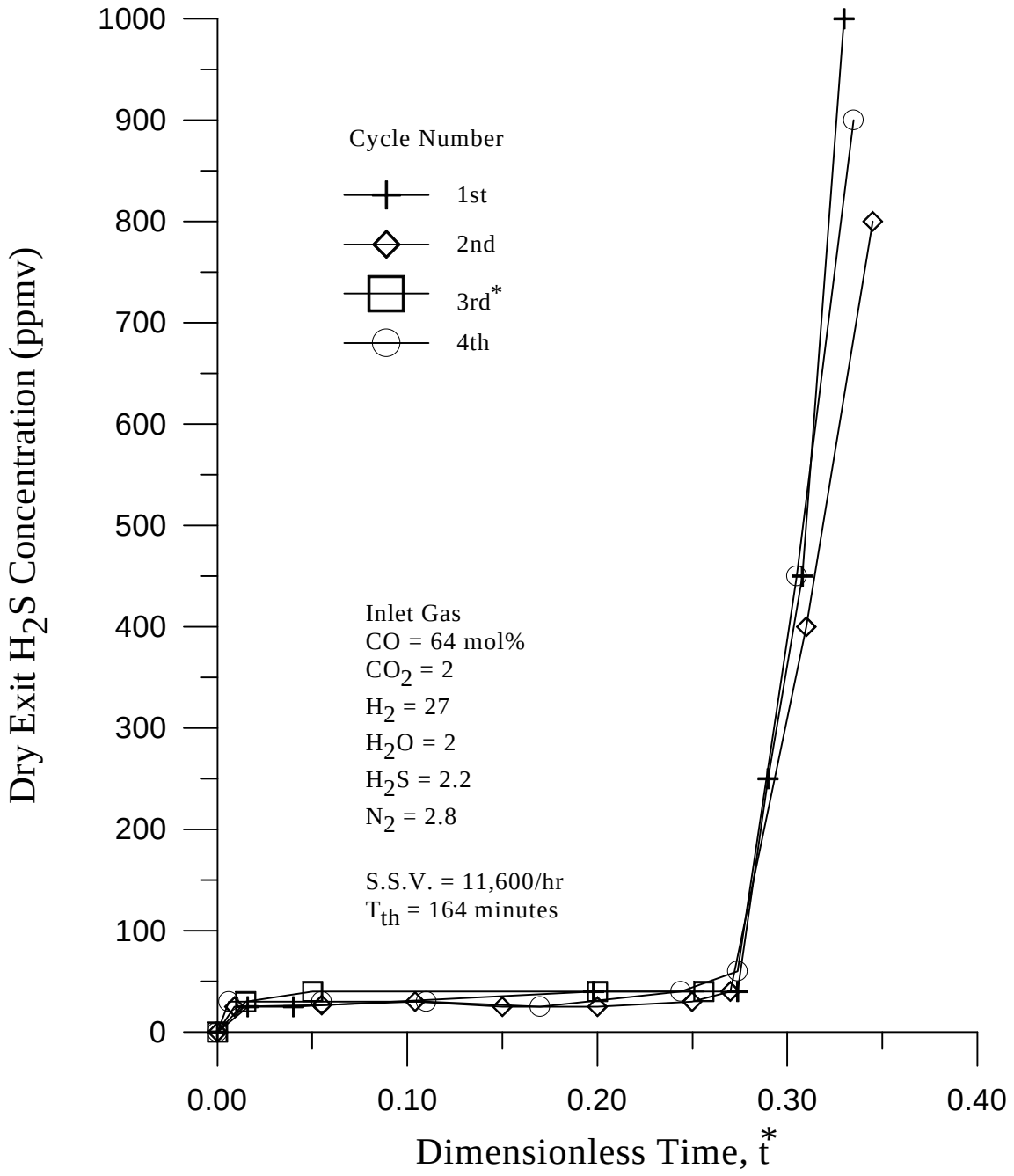

Figure 6.24. Sulfidation breakthrough curves for test FB4A using sorbent C6-2-1115 at 600^{o}C, plotted as H_2S concentration versus dimensionless time. *H_2S tank ran out at 44 minutes, cycle terminated.

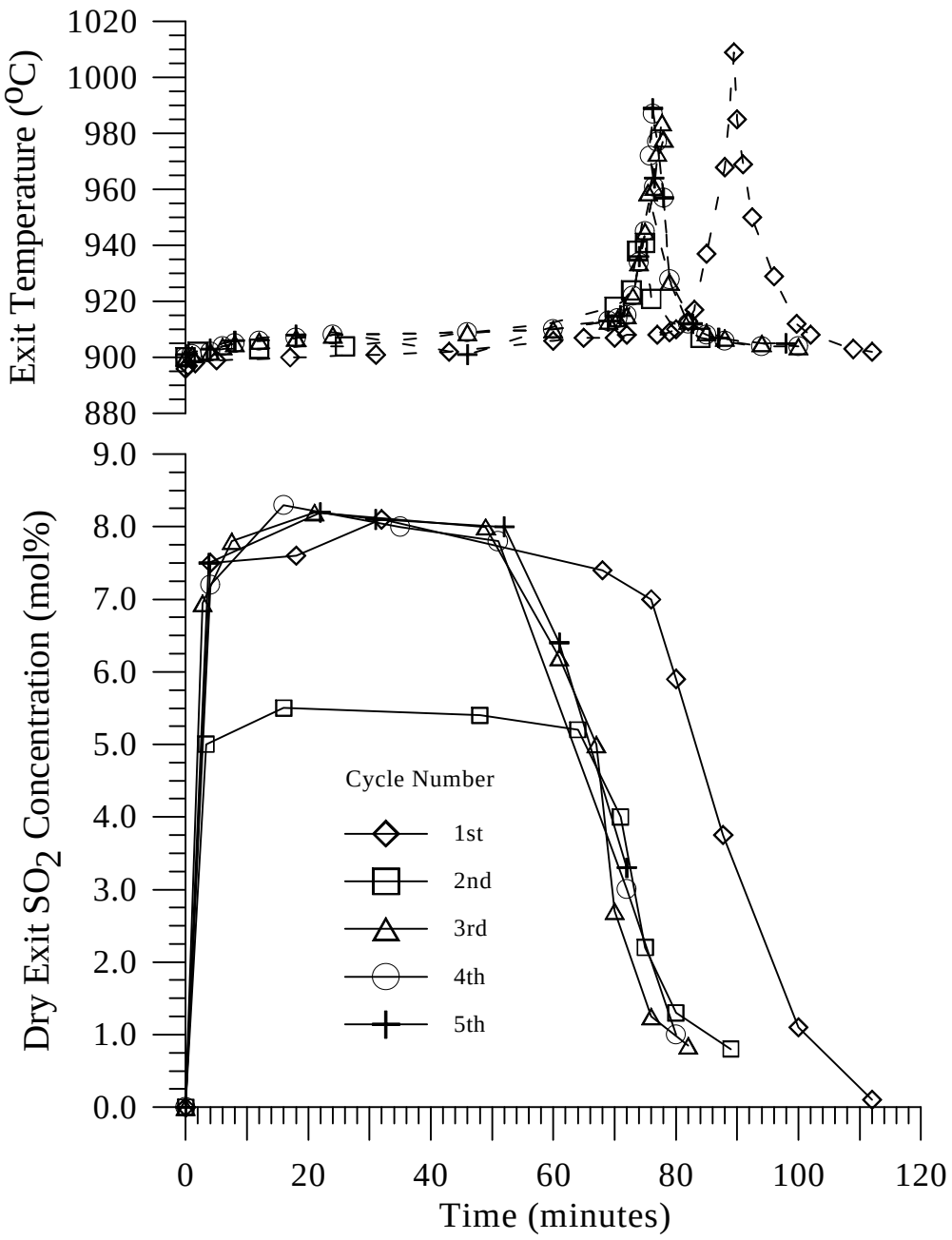

Figure 6.25. Regeneration curves for C6-2-1100. Regeneration in air with a standard space velocity of 3900/hr.

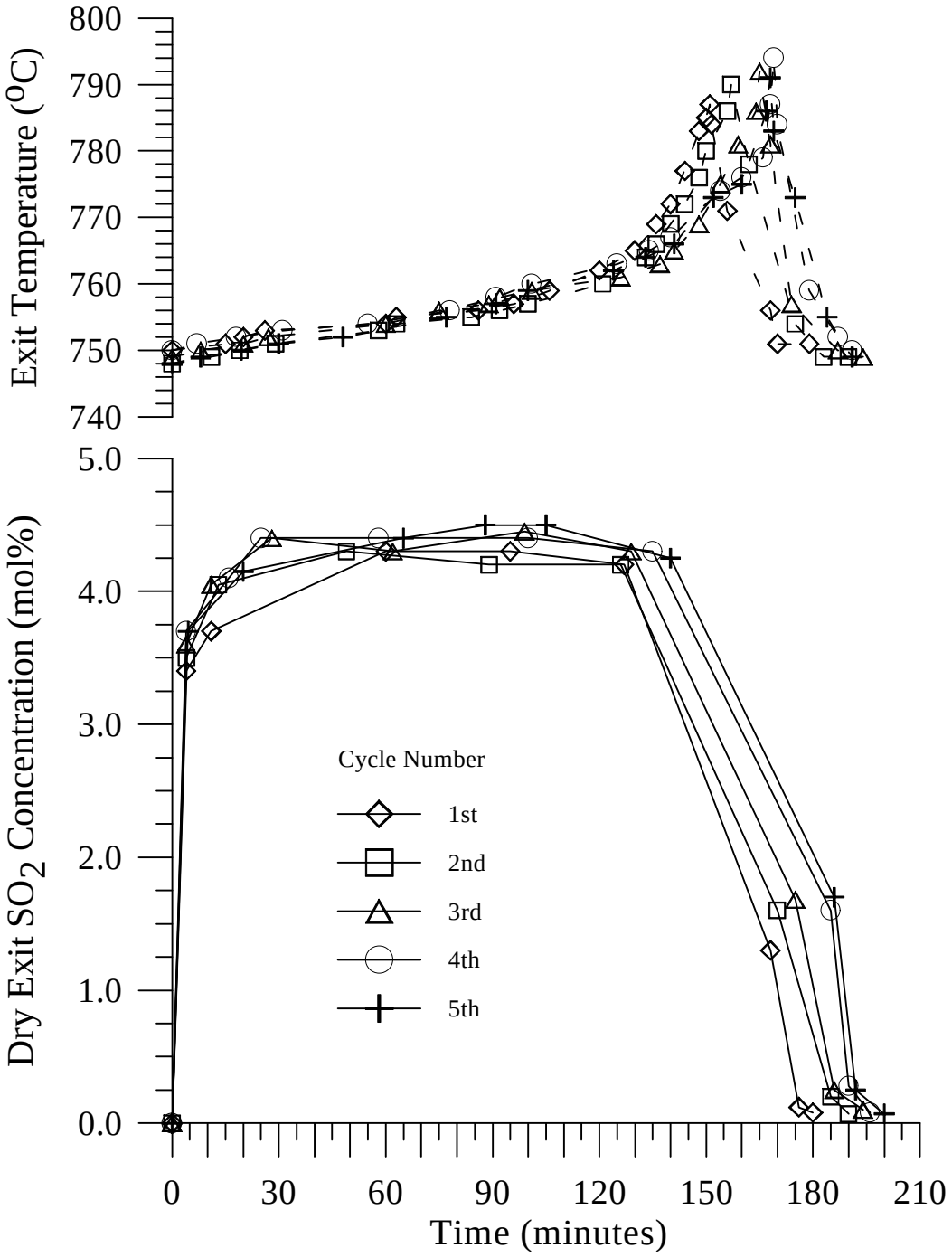

Figure 6.26. Regeneration curves for C6-2-1100. Regeneration in 90% N_2 and 10% O_2, with a standard space velocity of 3900/hr.

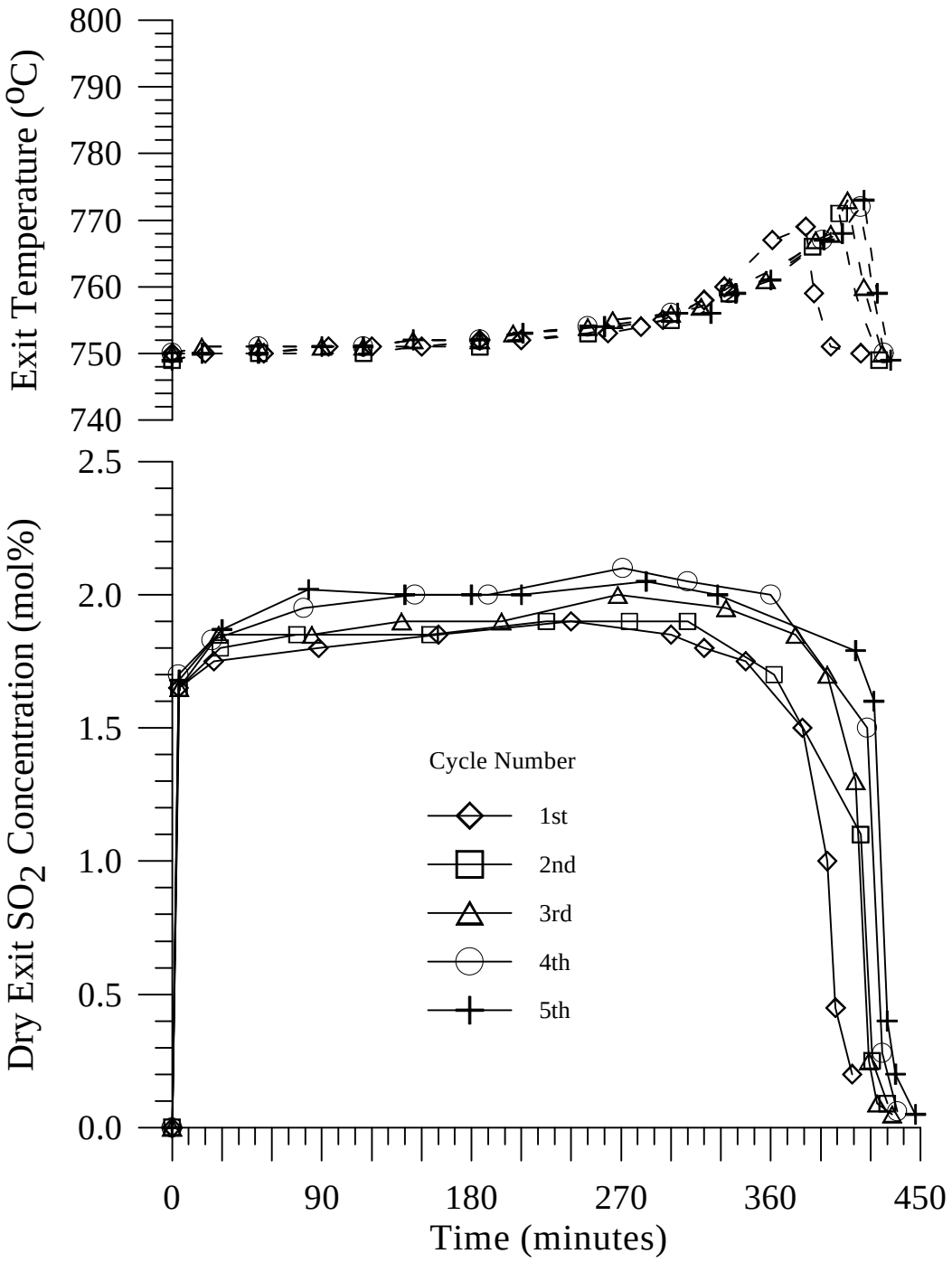

Figure 6.27. Regeneration curves for C6-2-1100. Regeneration in 95% N_2 and 5% O_2, with a standard space velocity of 3900/hr.

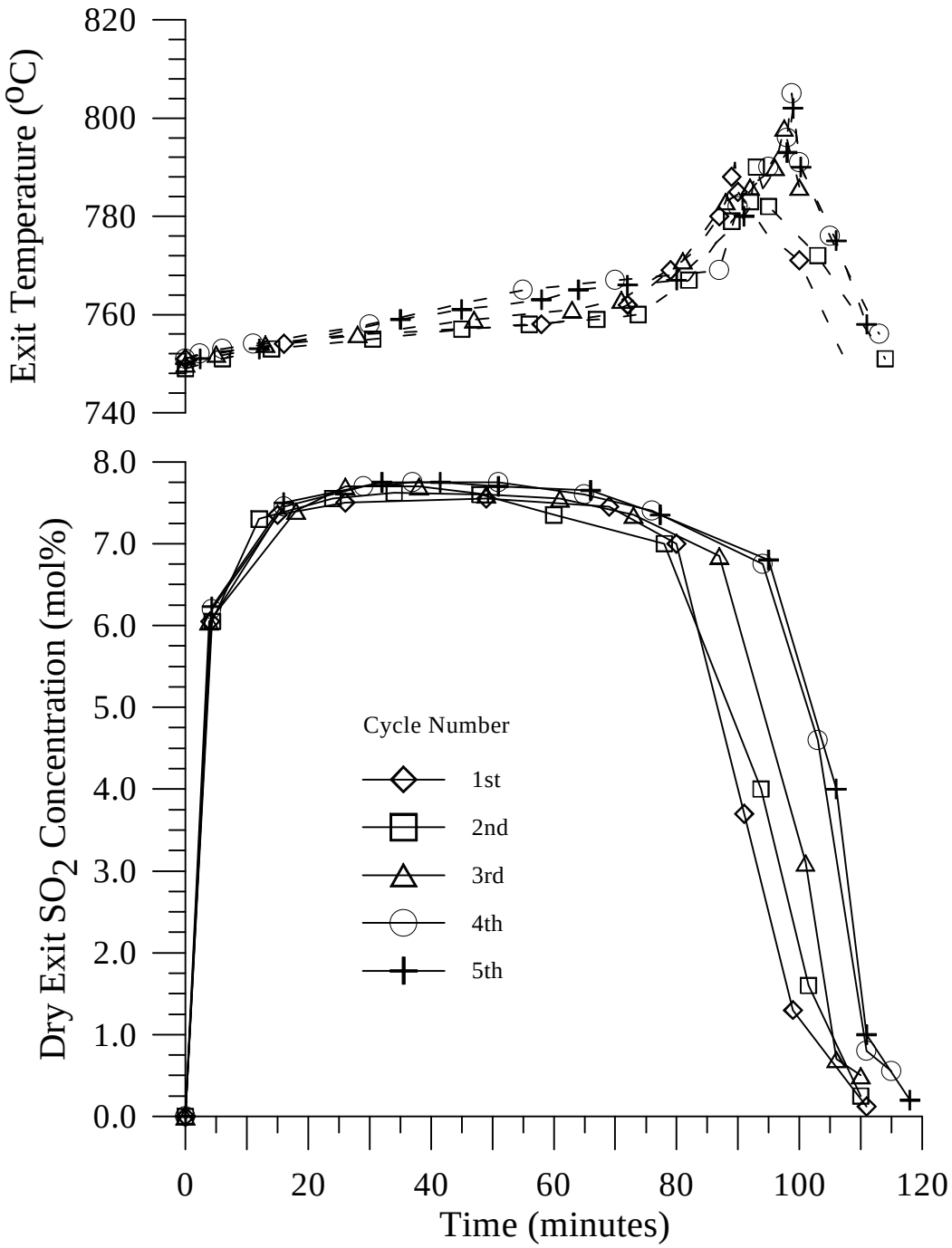

Figure 6.28. Regeneration curves for C6-2-1100. Regeneration in 47.4 mol% N_2, 12.6% O_2 and 40% H_20, with a standard space velocity of 3900/hr.

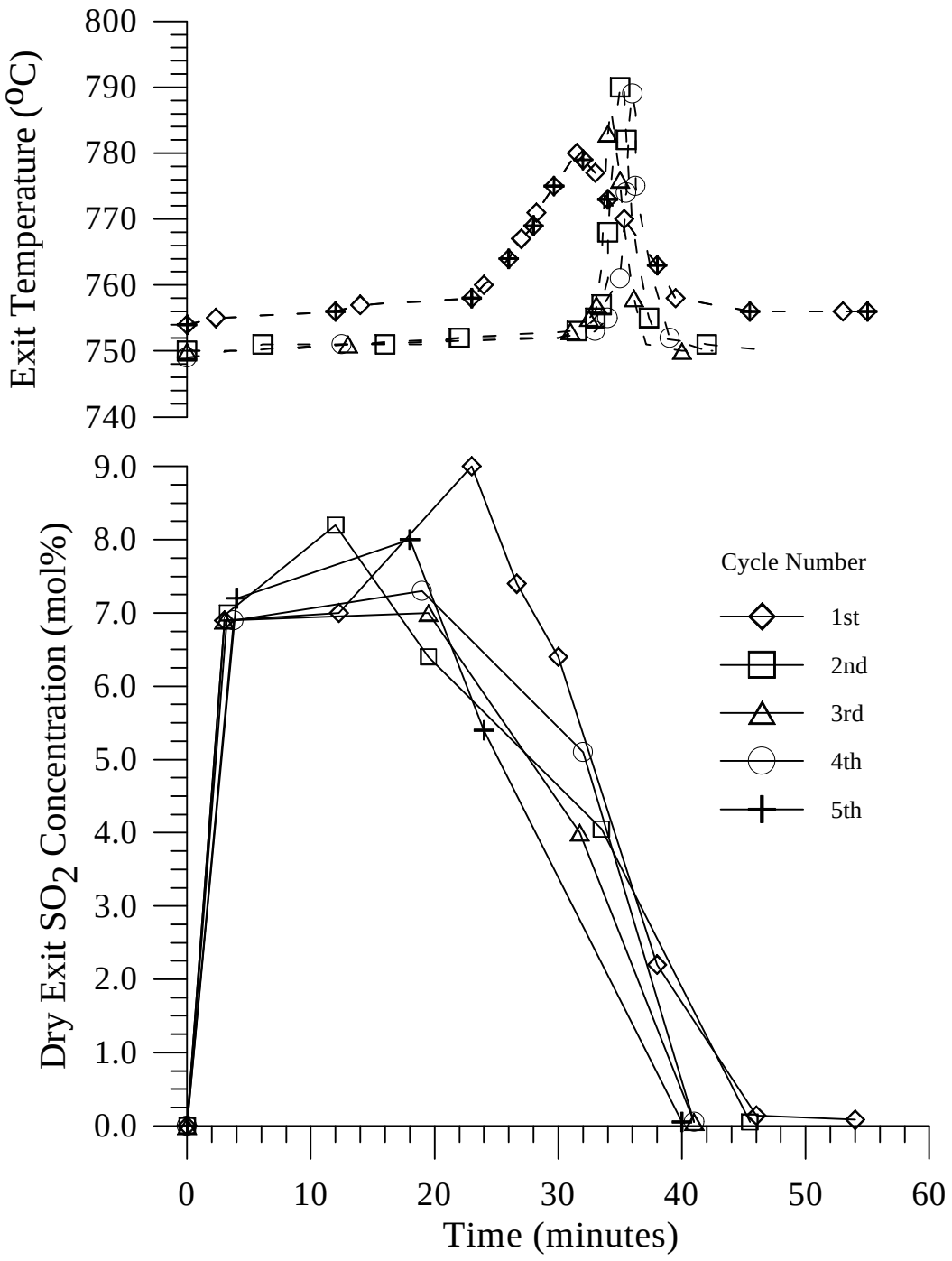

Figure 6.29. Regeneration curves for C8-0-1200. Regeneration in 47.4 mol% N_2, 12.6% O_2 and 40% H_2O, with a standard space velocity of 3900/hr.

Regeneration Breakthrough for C8-0-1200

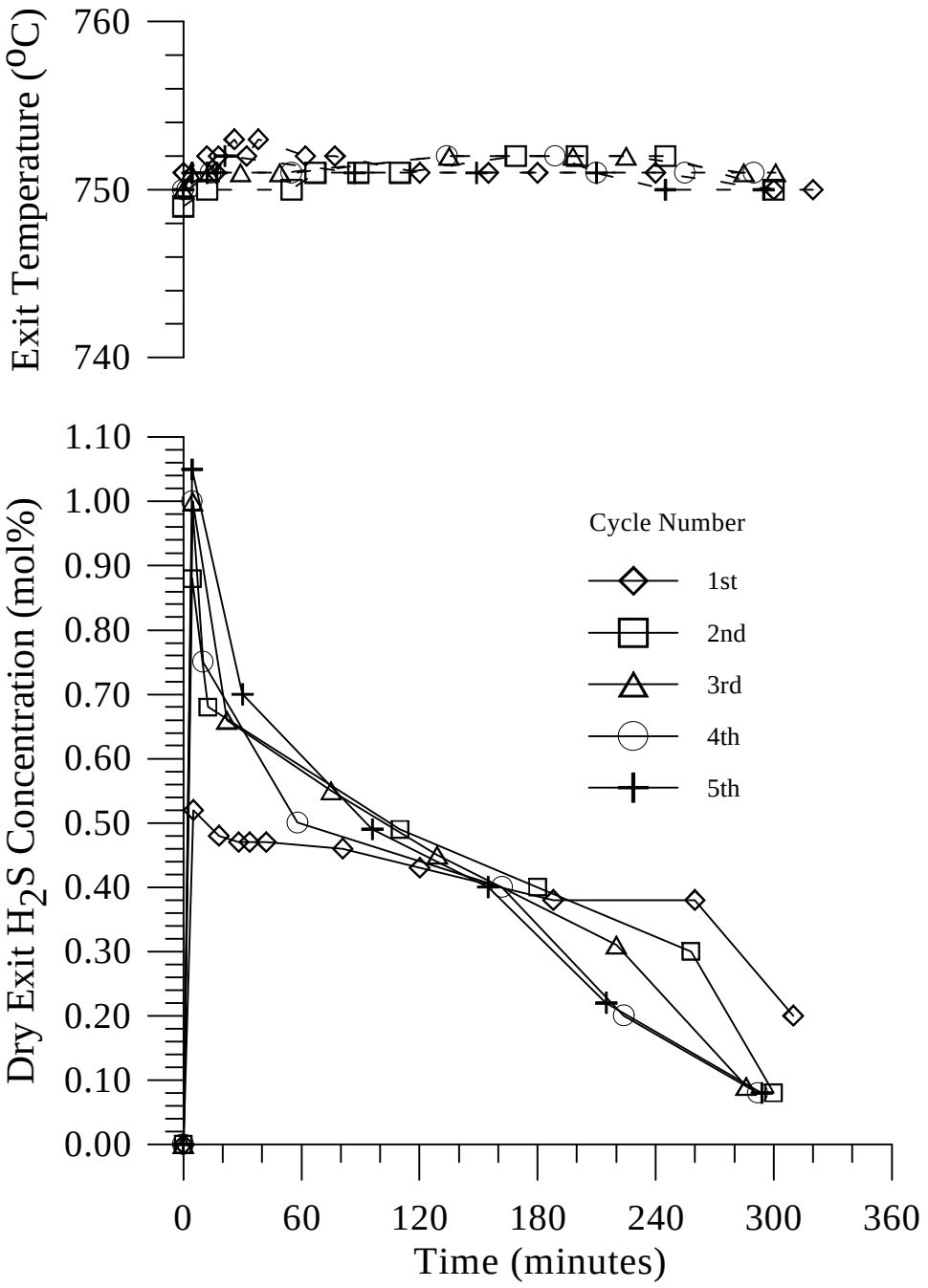

Figure 6.30. Regeneration curves for C8-0-1200. Regeneration in 80 mol% H_2O and 20% N_2, with a standard space velocity of 3900/hr.

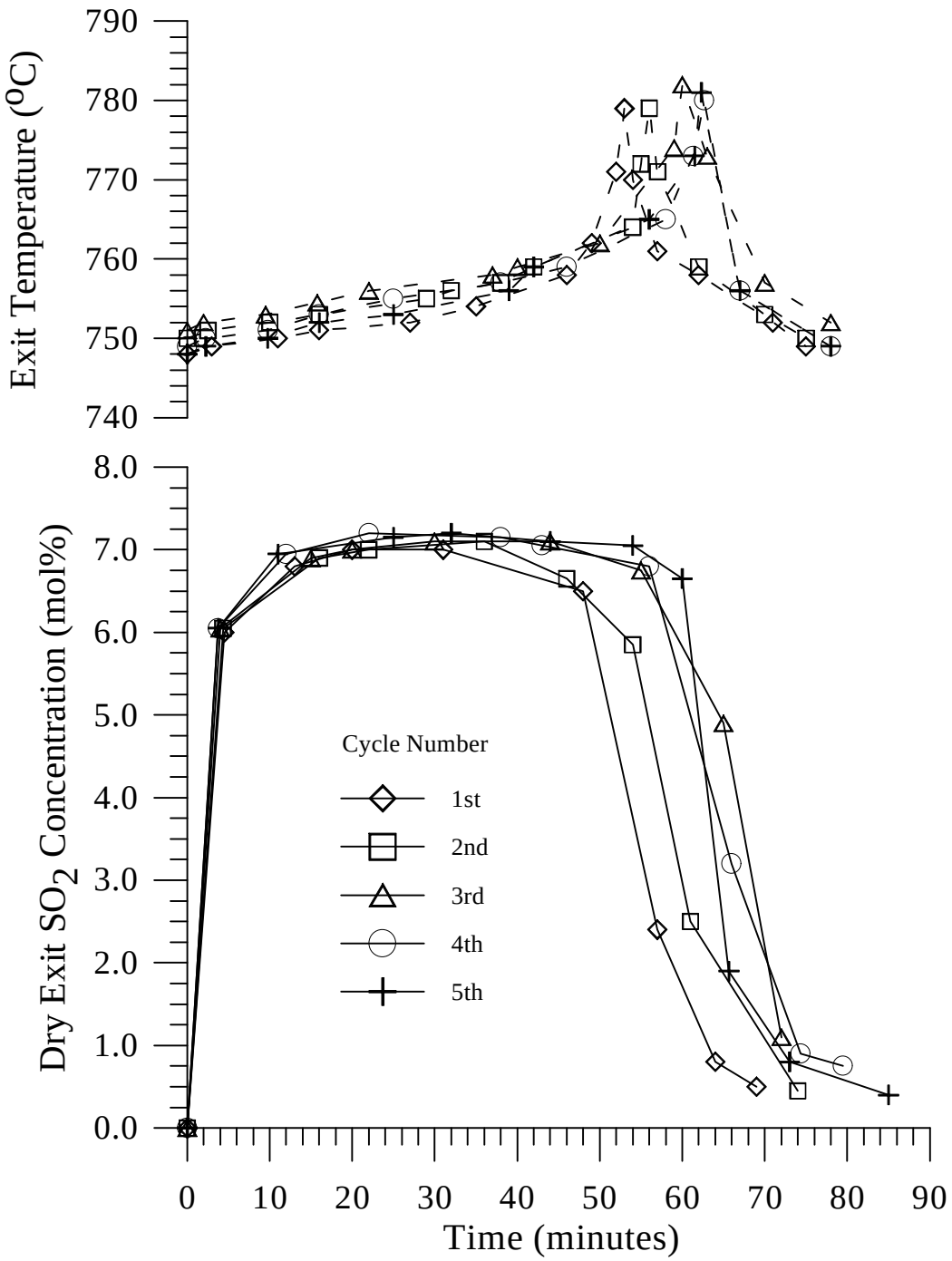

Figure 6.31. Regeneration curves for C4-2-1175. Regeneration in 47.4 mol% N_2, 12.6% O_2 and 40% H_2O, with a standard space velocity of 3900/hr.

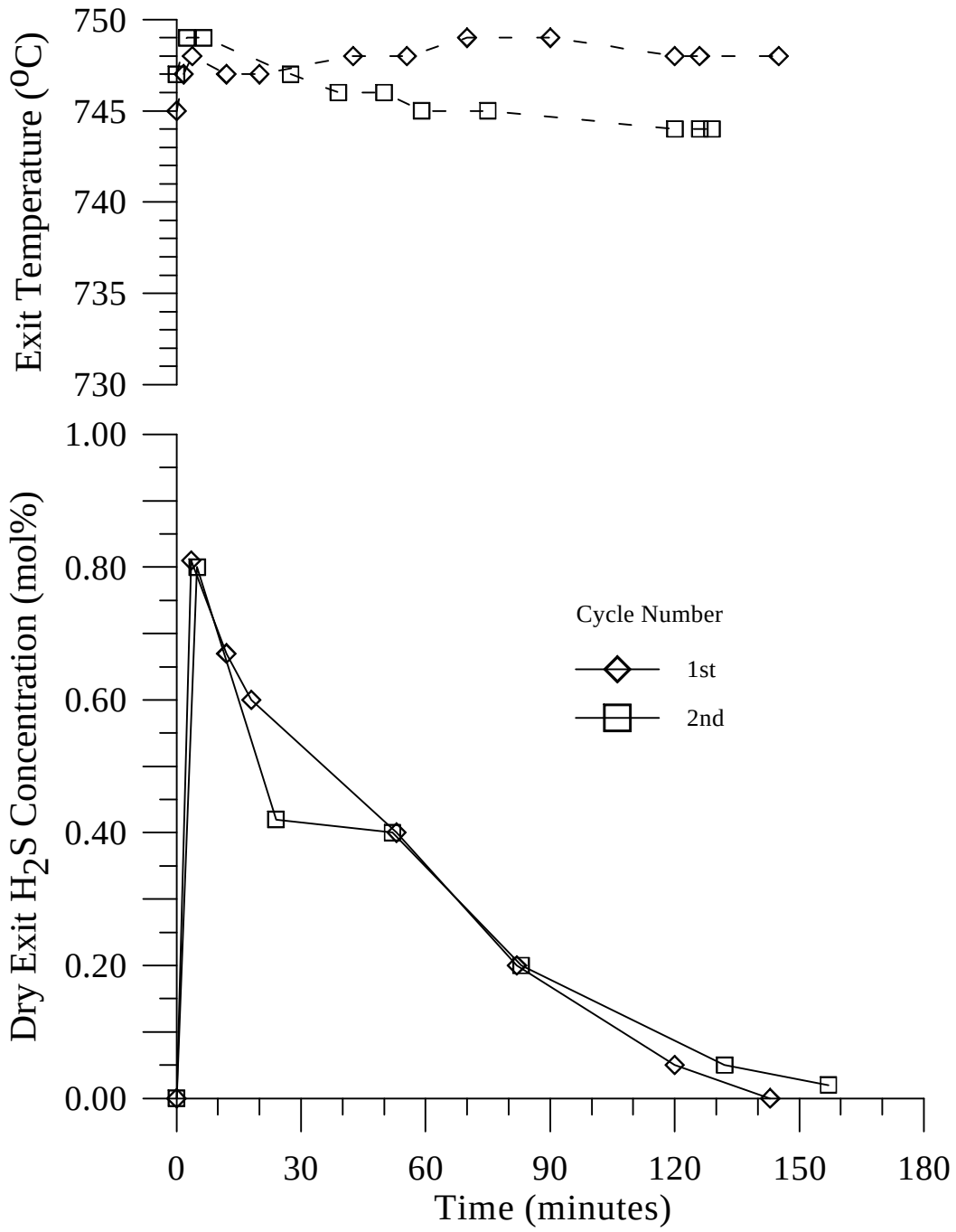

Figure 6.32. Regeneration curves for C8-0-1600. regeneration in 80 mol% H_2O and 20% N_2, with a standard space velocity of 3900/hr.

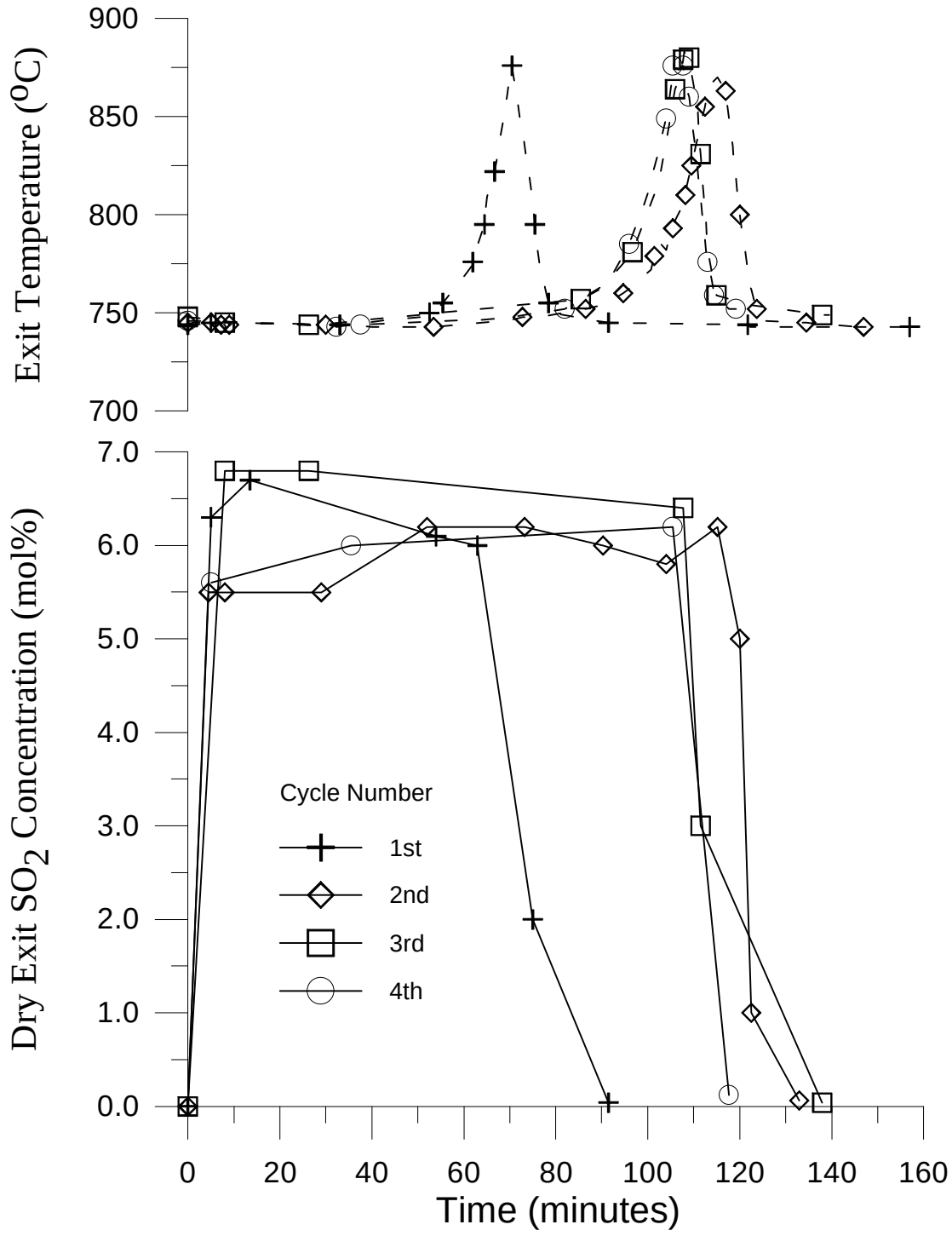

Figure 6.33 Regeneration curves for test FB1A using C6-2-1100 sorbent. Regeneration in 50 mol% air and 50 mol% H_2O, with a standard space velocity of 3900/hr at 750^{o}C.

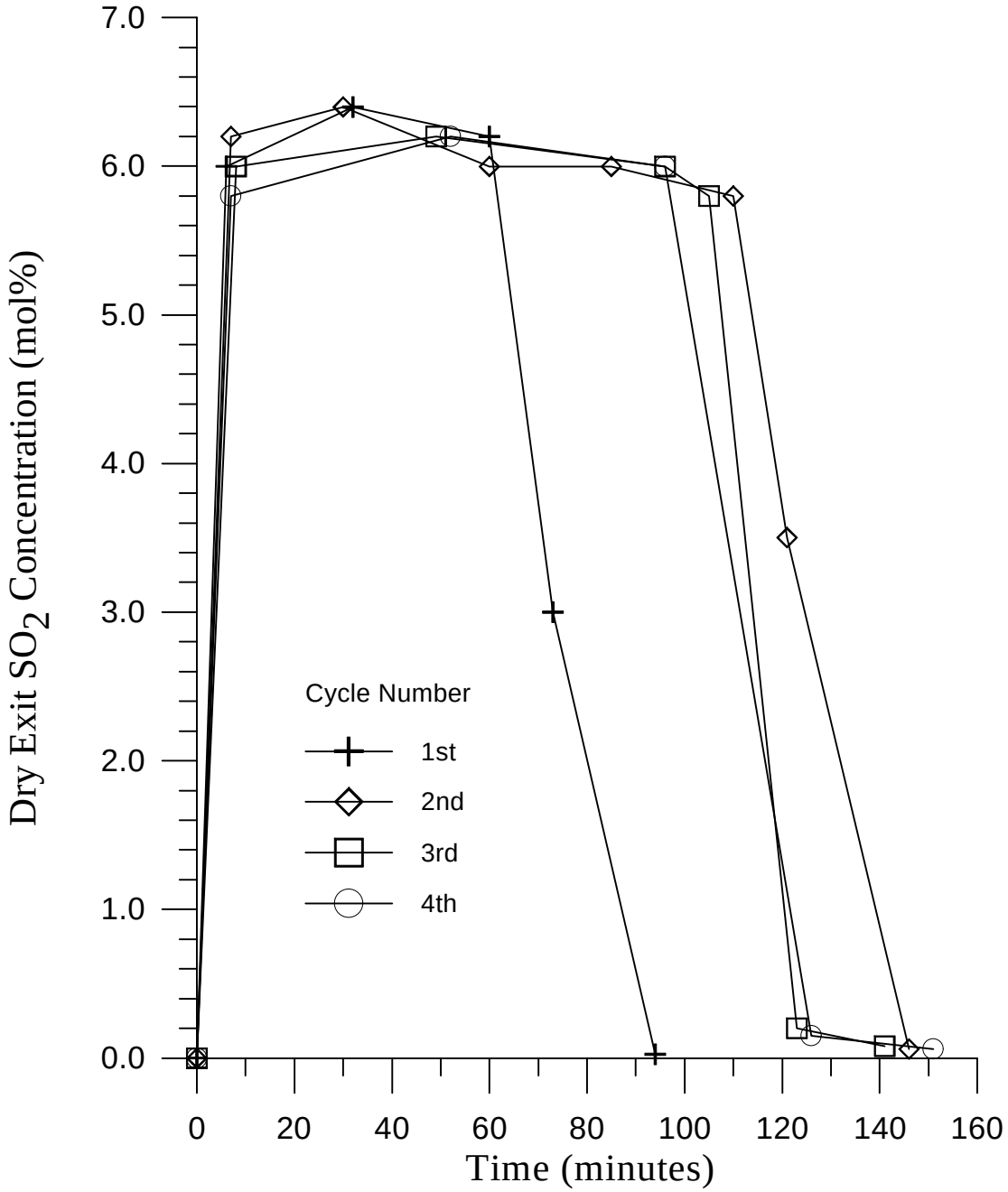

Figure 6.34 Regeneration curves for test FB2A using C6-2-1100 sorbent. Regeneration in 50 mol% air and 50 mol% H_2O, with a standard space velocity of 3900/hr at 750^{o}C.

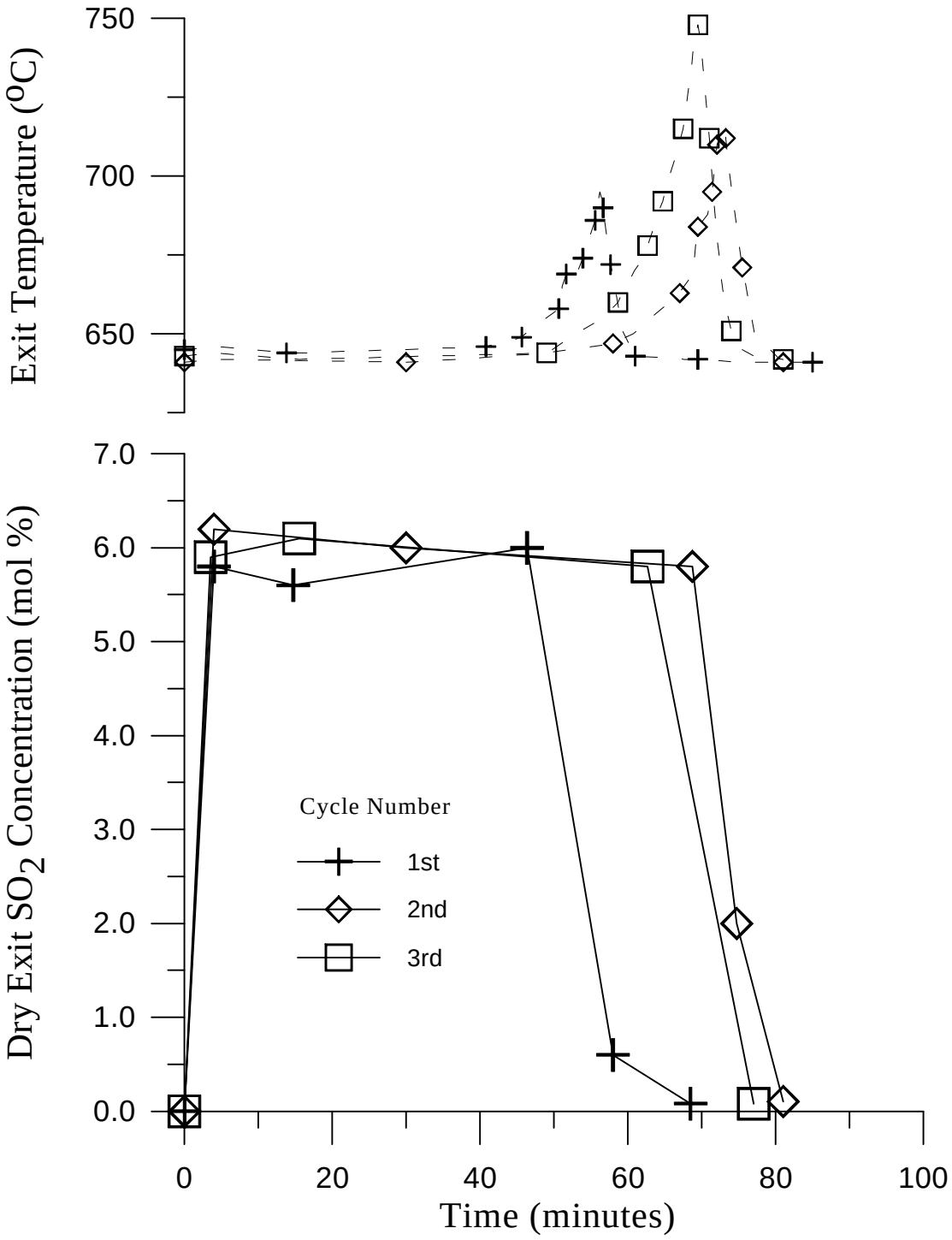

Figure 6.35. Regeneration curves for test FB3A using C6-2-1100 sorbent. Regeneration in 40 mol% air and 60 mol% H_2O, with a standard space velocity of 4800/hr at 650°C.

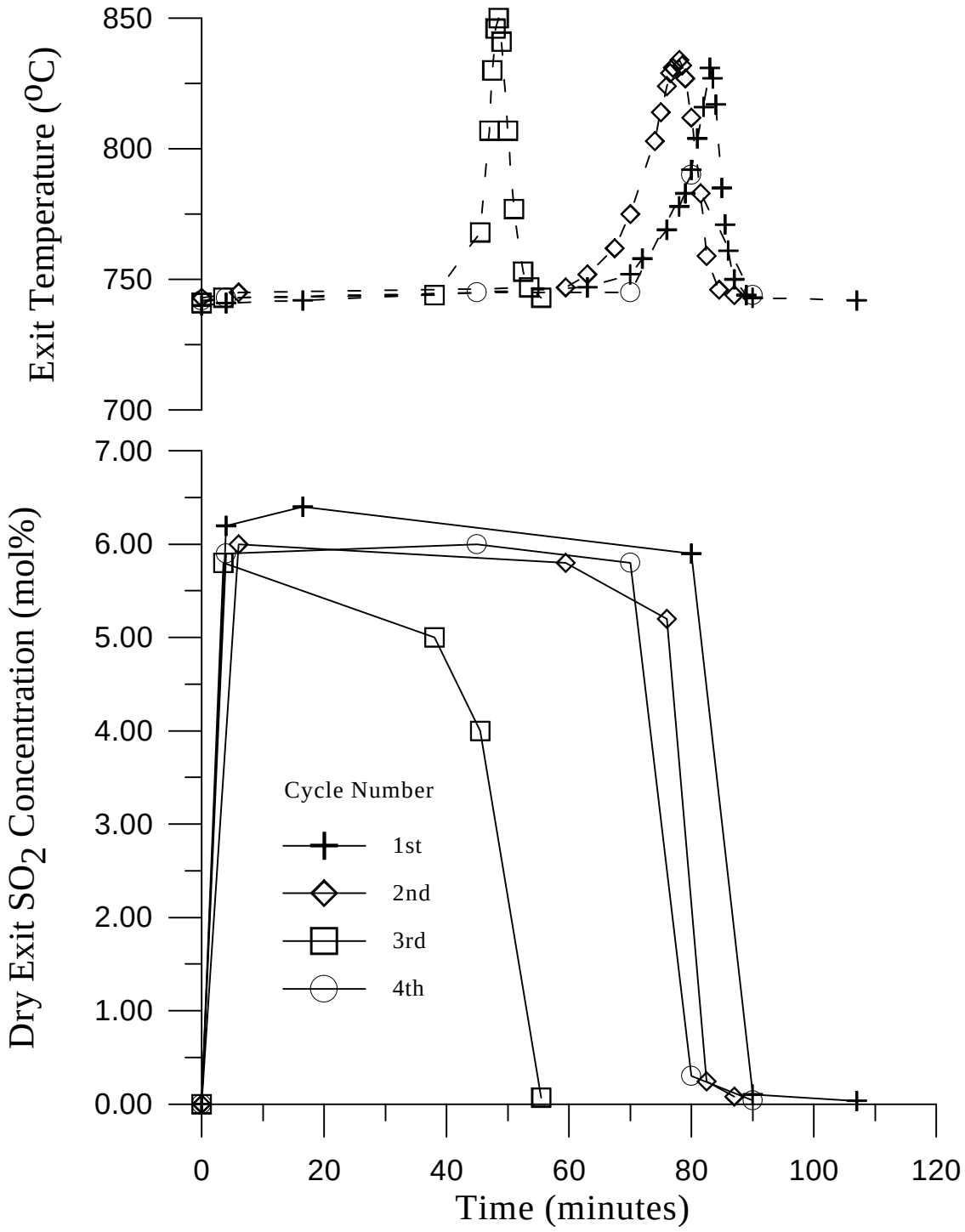

Figure 6.36. Regeneration curves for test FB4A using C6-2-1115 sorbent. Regeneration in 50 mol% air and 50 mol% H_2O, with a standard space velocity of 3900/hr at 750°C.

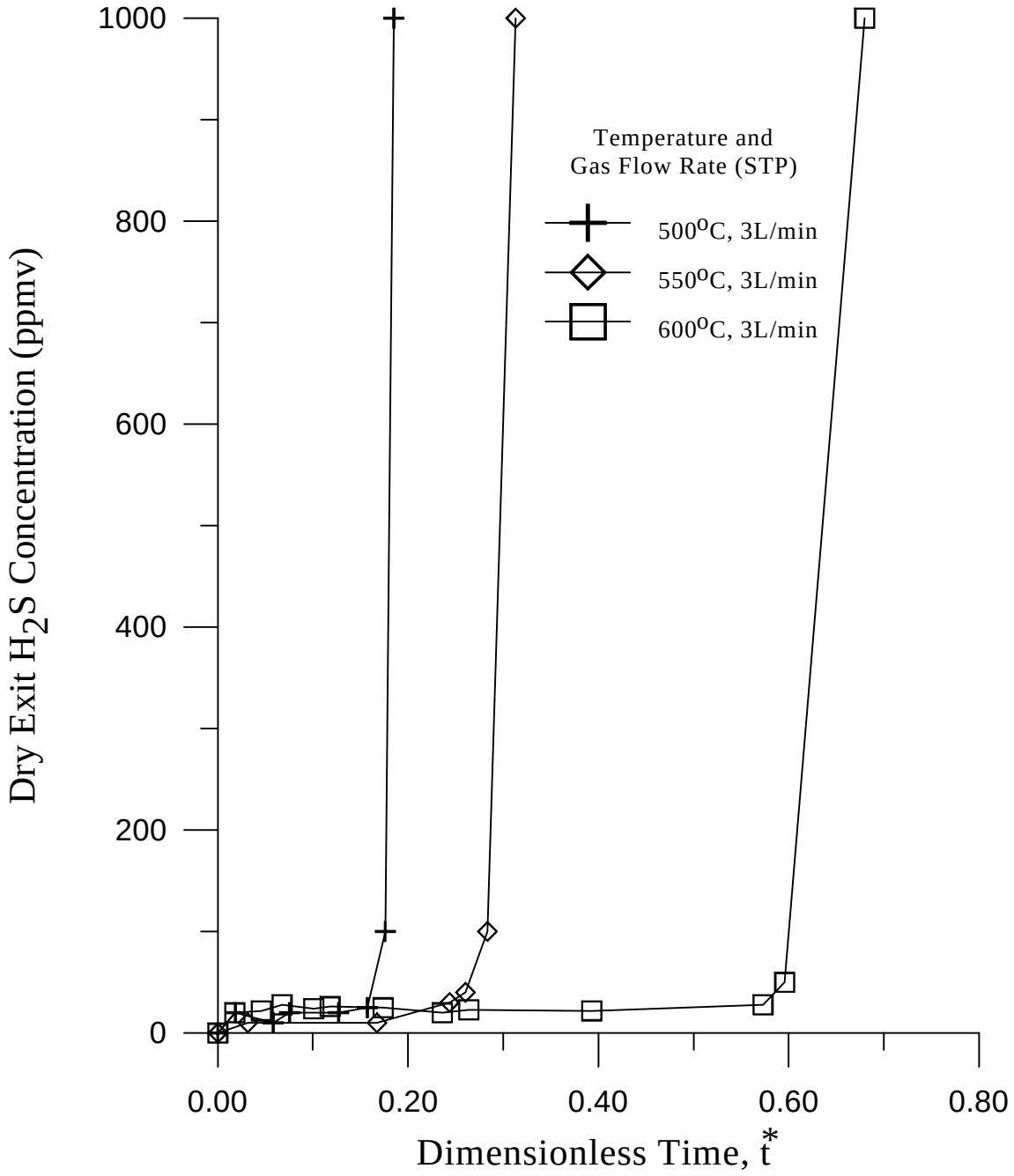

Figure 6.37. Effect of sulfidation temperature on sorbent performance (C6-2-1100).

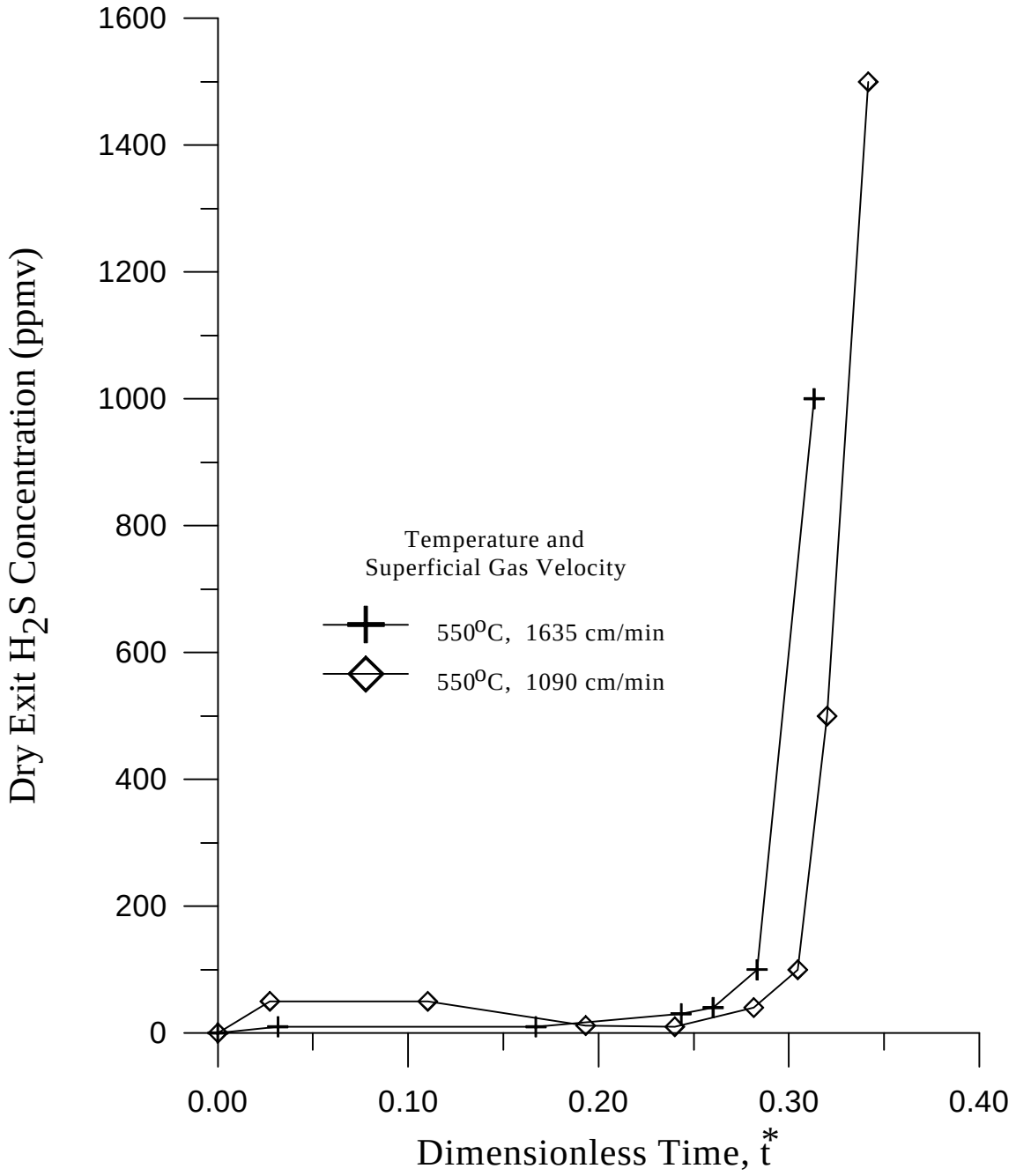

Figure 6.38 Effect of sulfidation superficial gas velocity on sorbent performance (C6-2-1100).

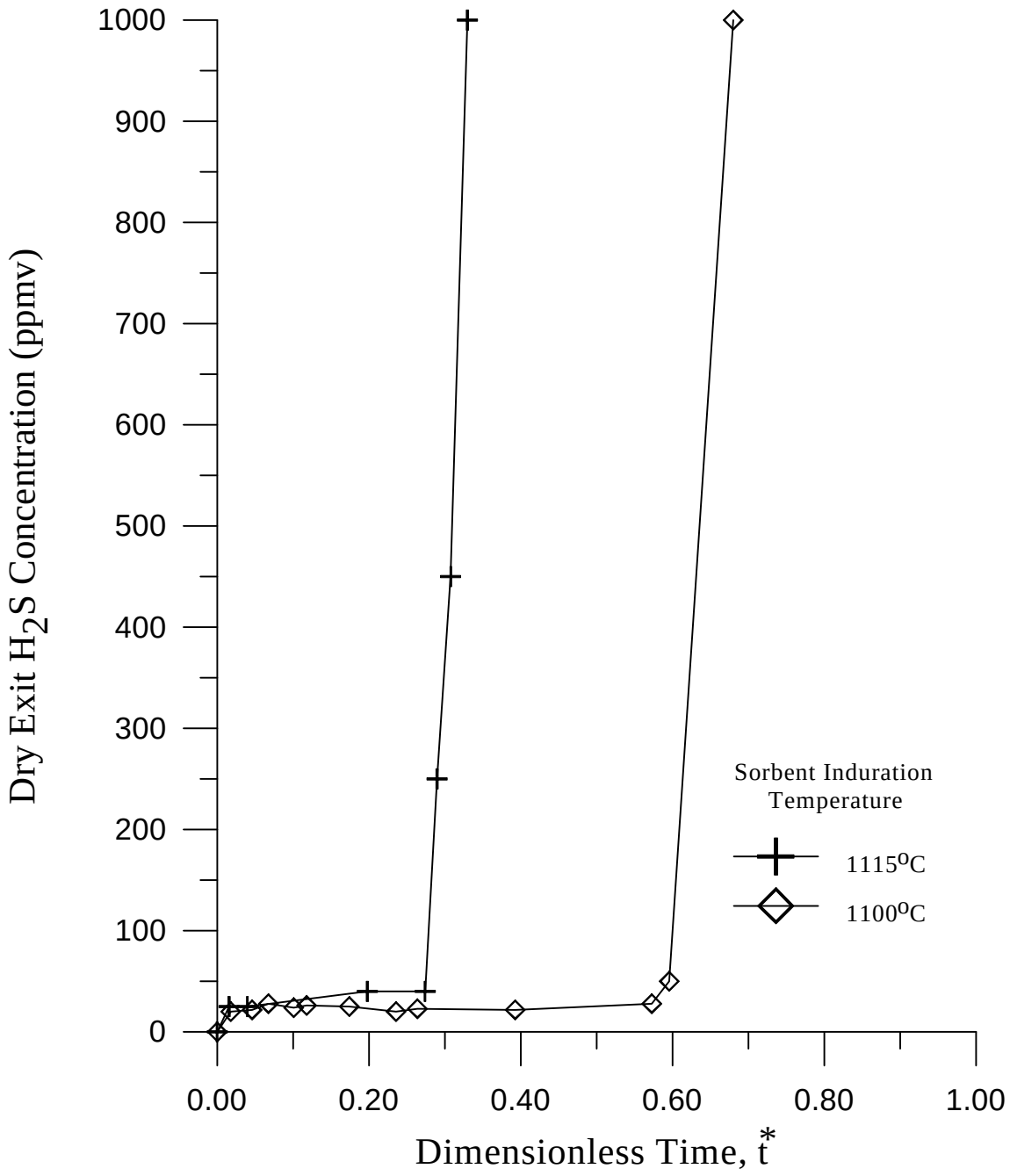

Figure 6.39 Effect of sorbent induration temperature on sulfidation breakthrough.

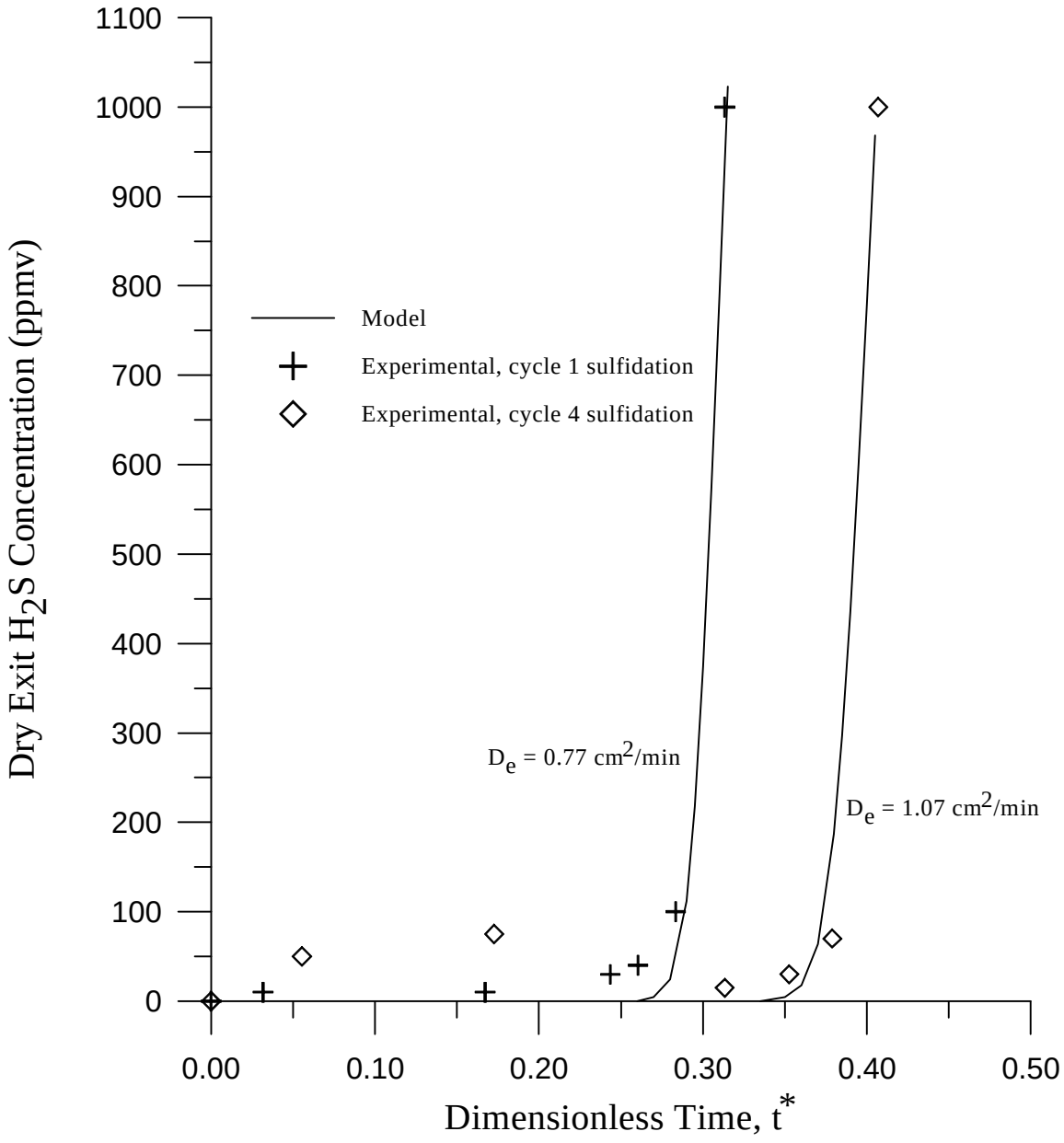

Figure 6.40. Predicted and experimental breakthrough curves for FB1A utilizing sorbent C6-2-1100.

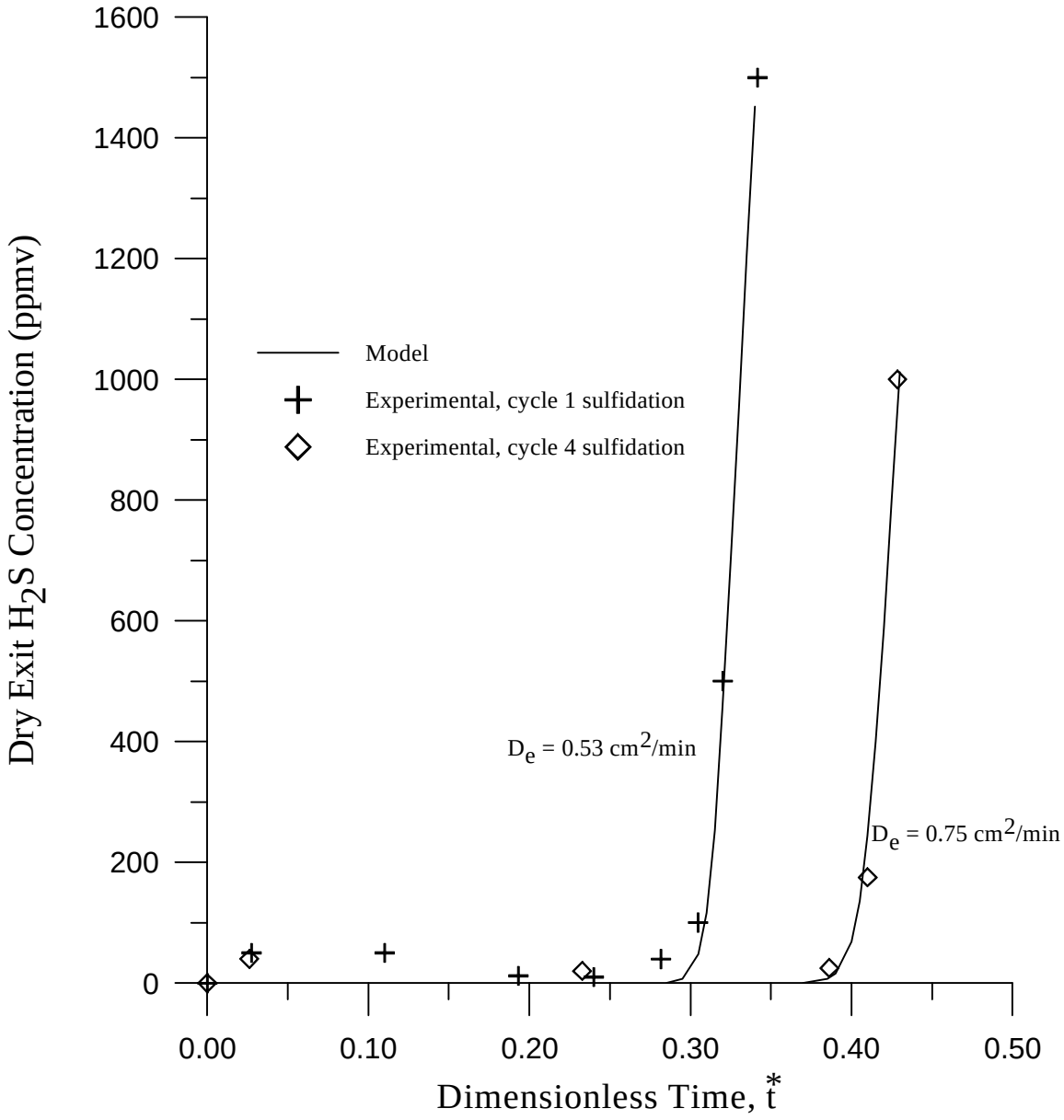

Figure 6.41 Predicted and experimental breakthrough curves for FB2A utilizing sorbent C6-2-1100.

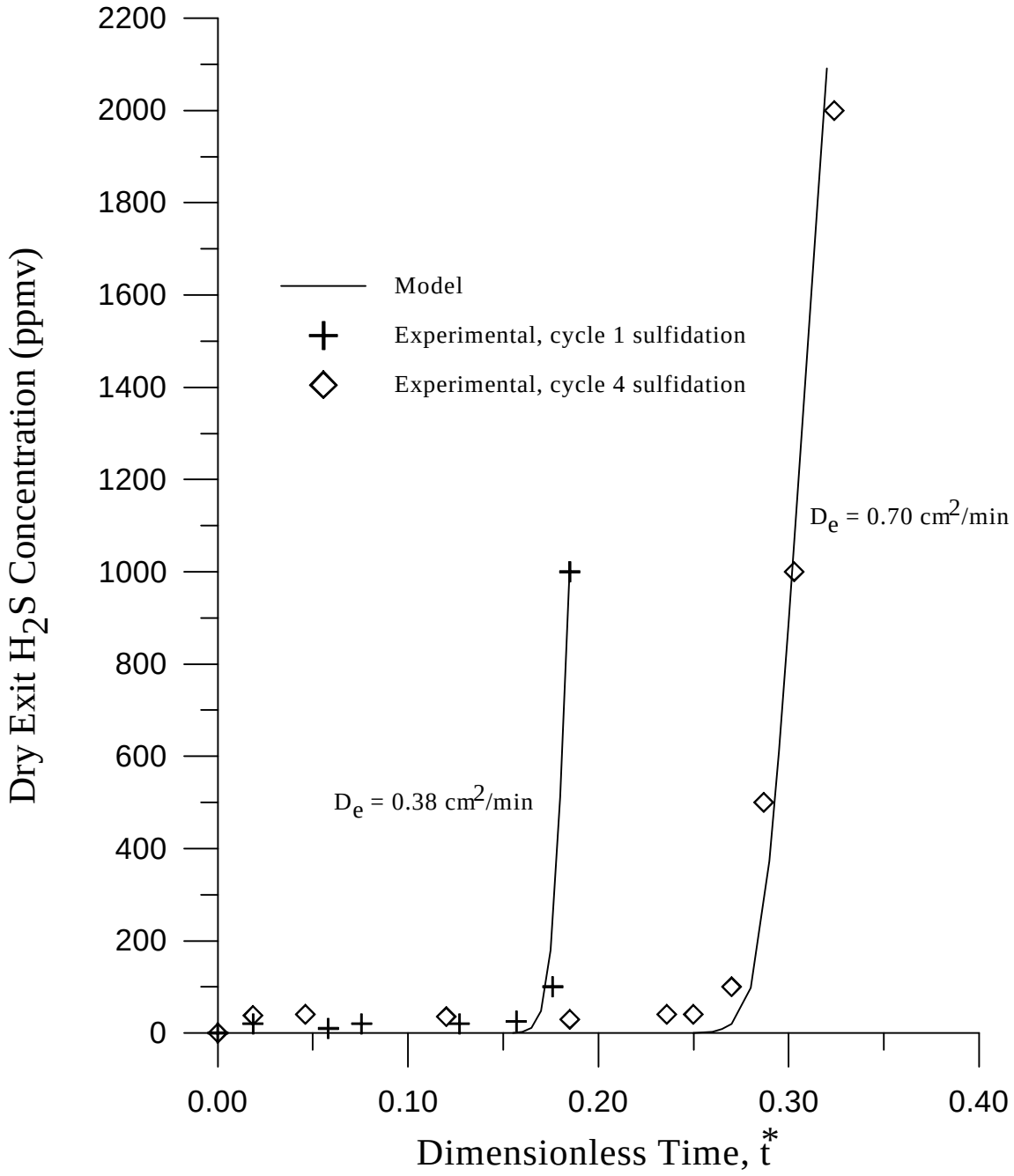

Figure 6.42. Predicted and experimental breakthrough curves for FB3A utilizing sorbent C6-2-1100.

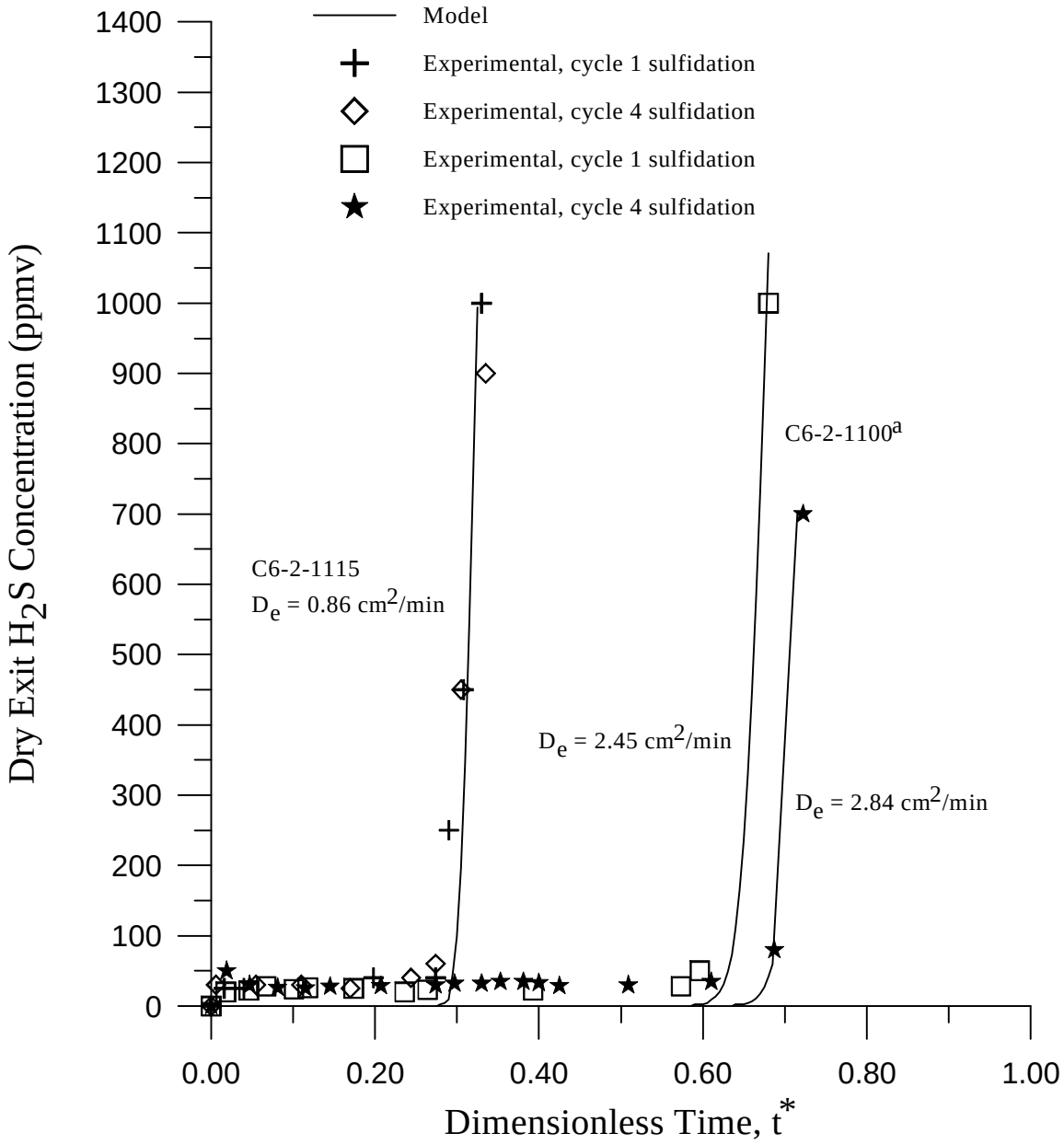

Figure 6.43. Predicted and experimental breakthrough curves for FB4A utilizing sorbent C6-2-1115 and 7FB [a] utilizing sorbent C6-2-1100. [a]Test was conducted in a previous study (reference 1).

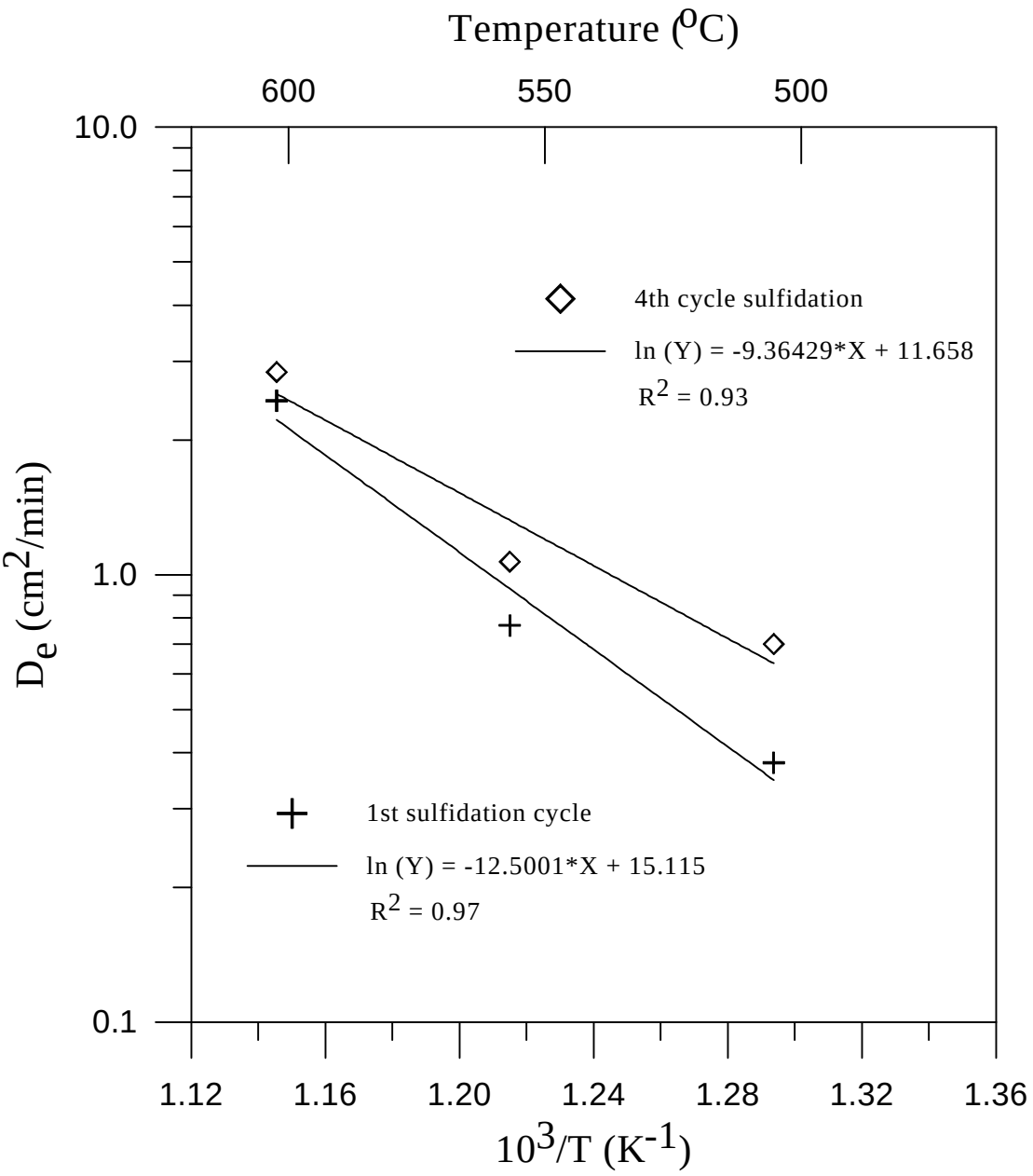

Figure 6.44. Effect of temperature on the effective diffusivity for C6-2-1100 sorbent.

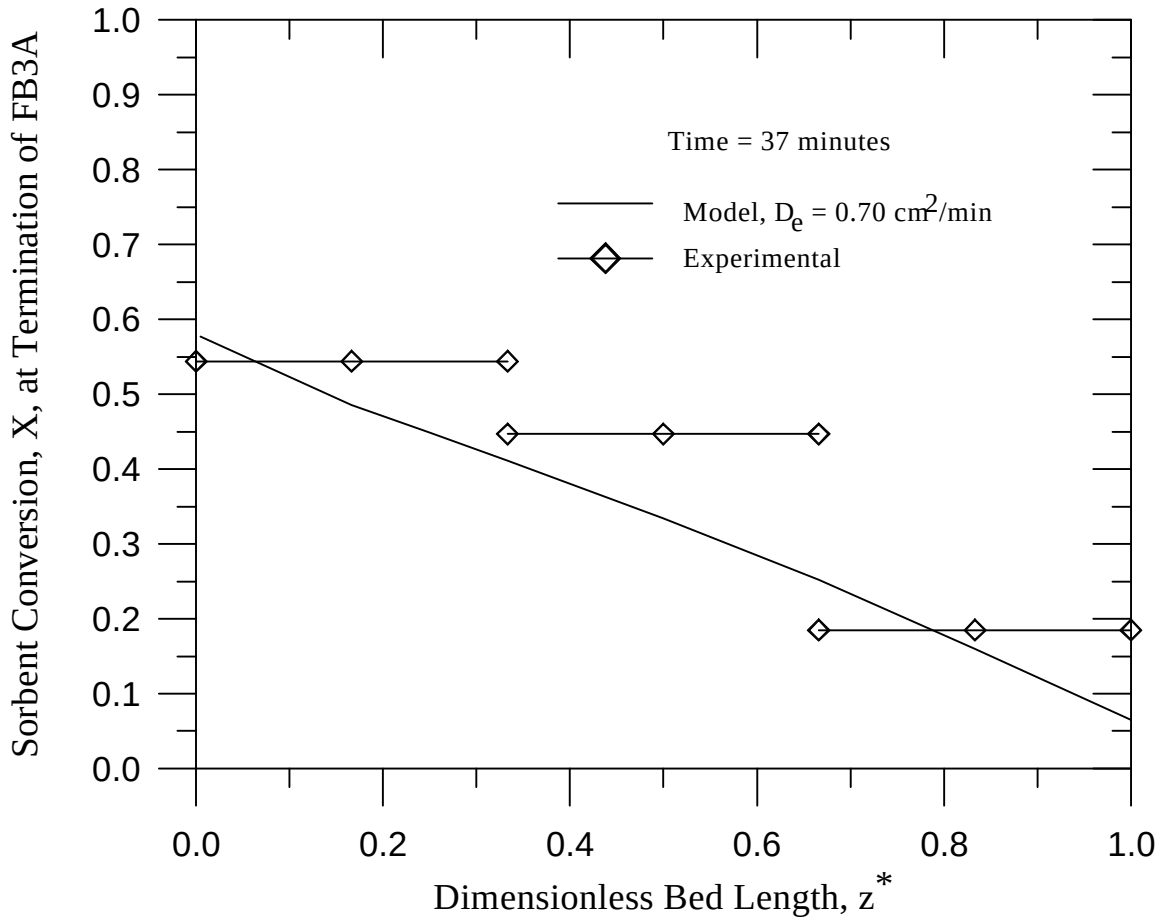

Figure 6.45. Sorbent conversion as a function of distance from the sorbent bed inlet at the termination of test FB3A.

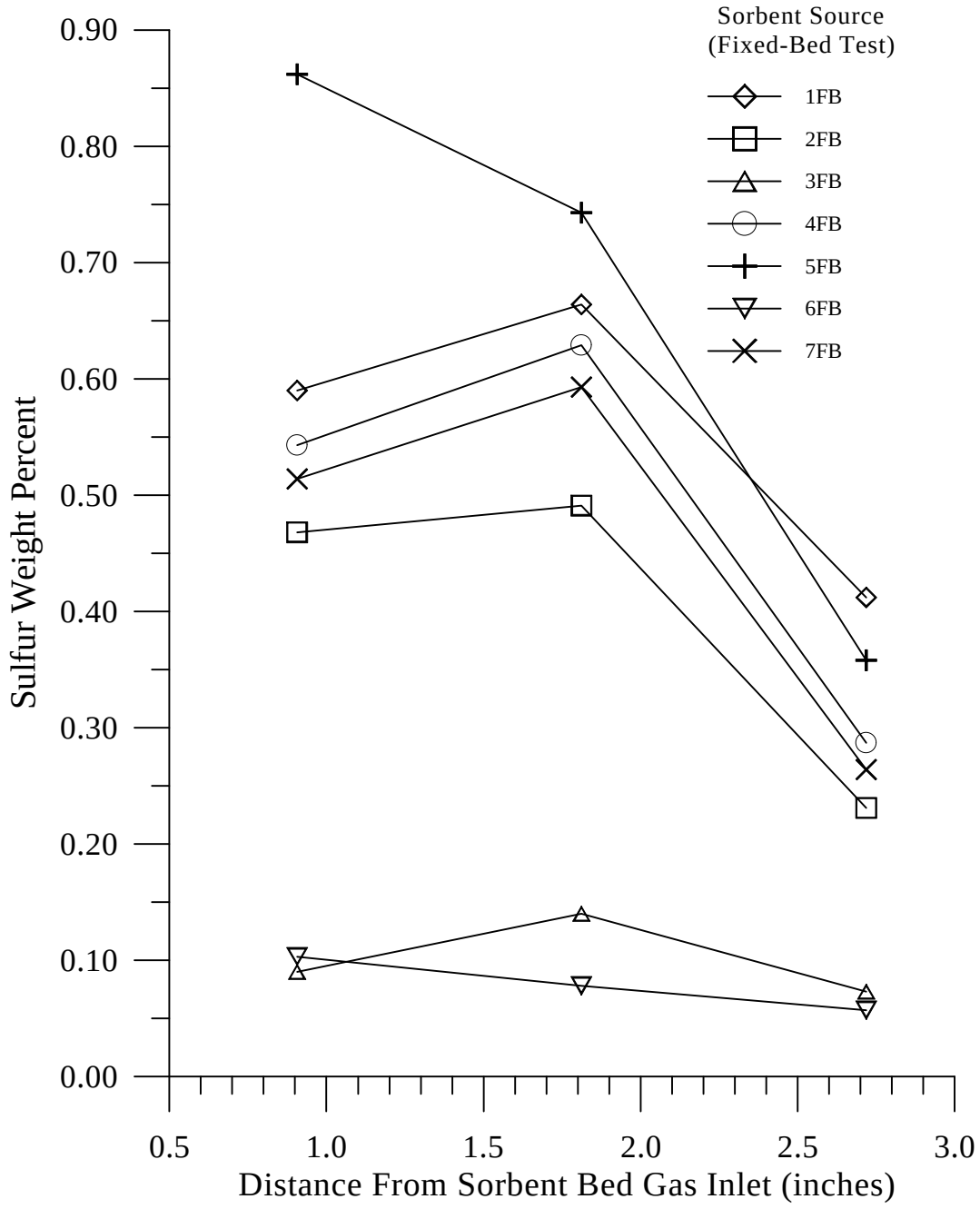

Figure 6.46. Sulfur weight percent in regenerated sorbent (after 5 cycles)

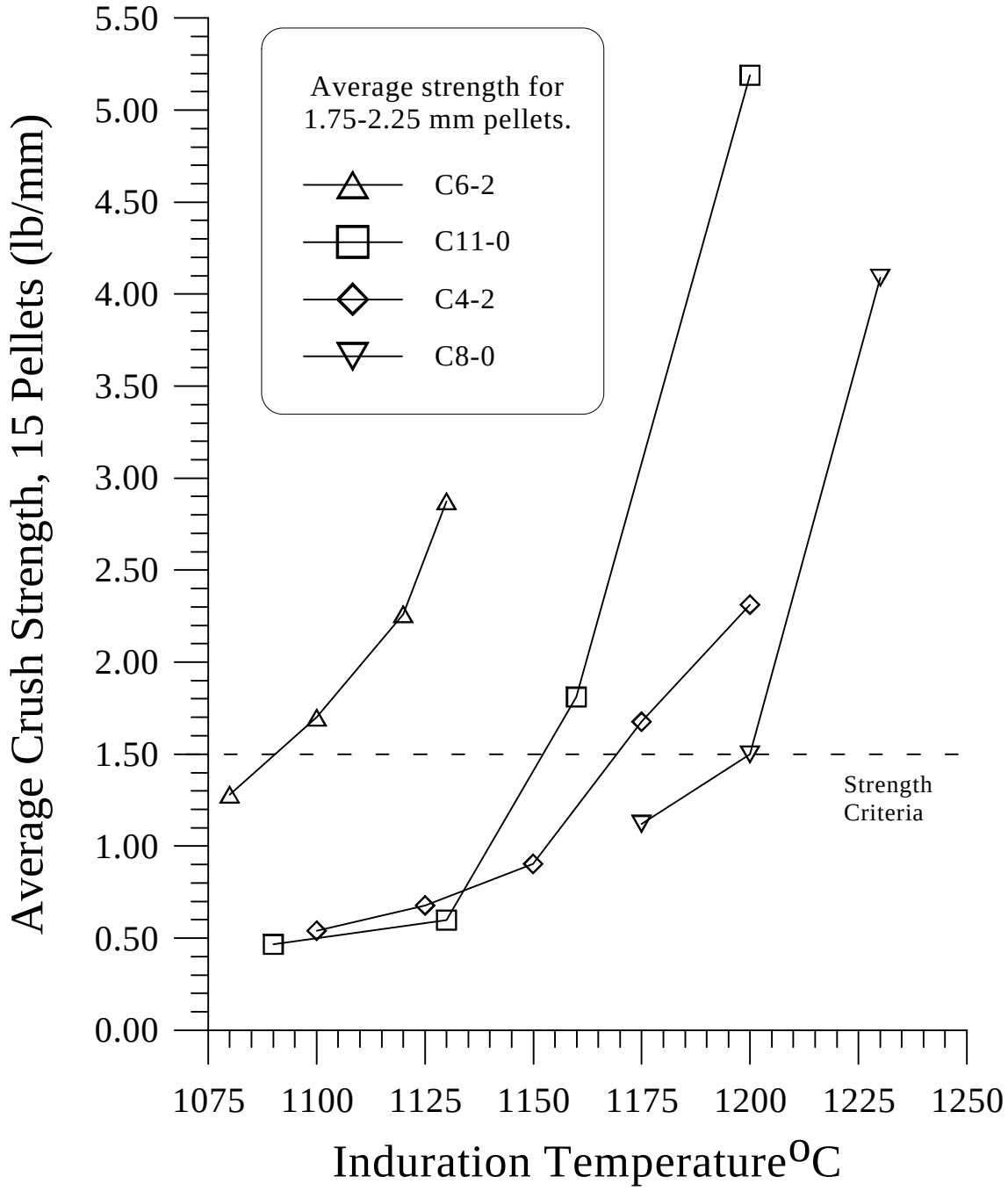

Figure 6.47. Average crush strength of fresh pellets used in fixed-bed reactor, 1.2 - 2.3 mm in diameter.

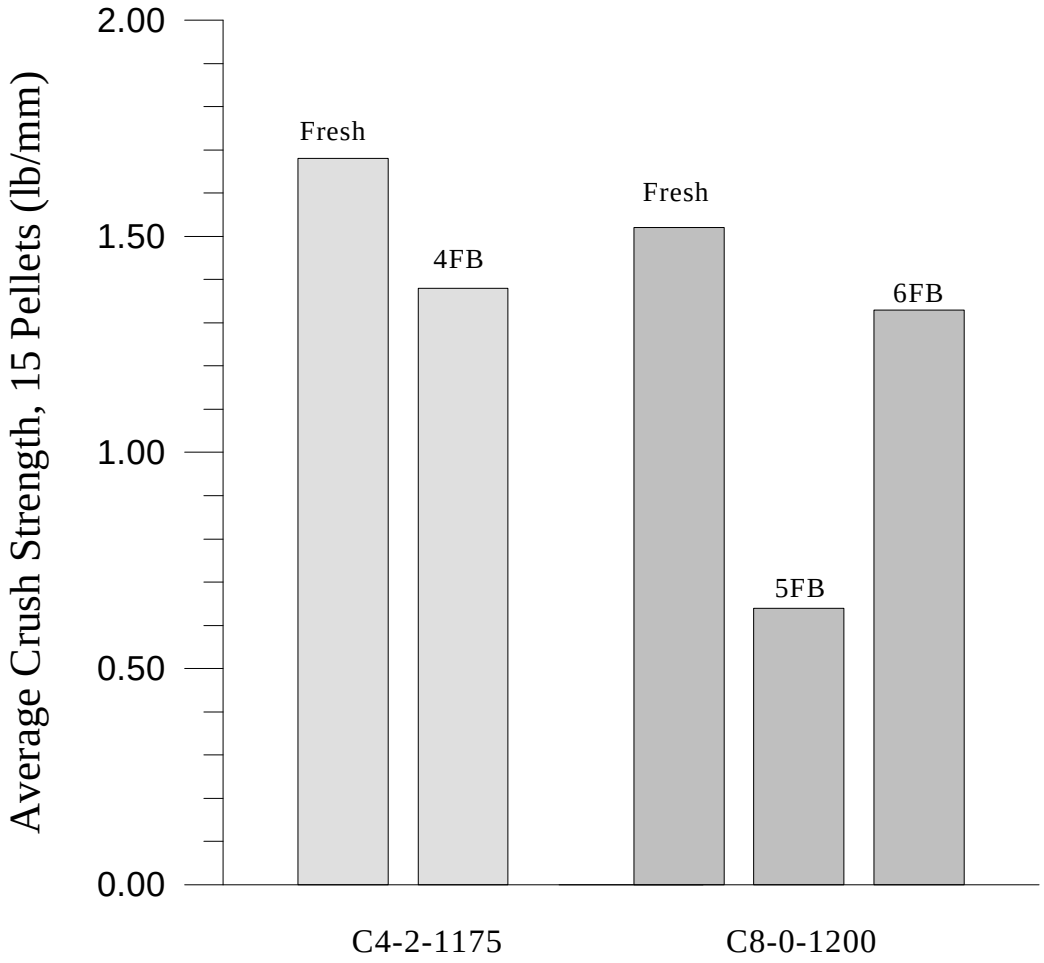

Figure 6.48. Average crush strength of fresh pellets and pellets after 5 cycles in fixed bed.

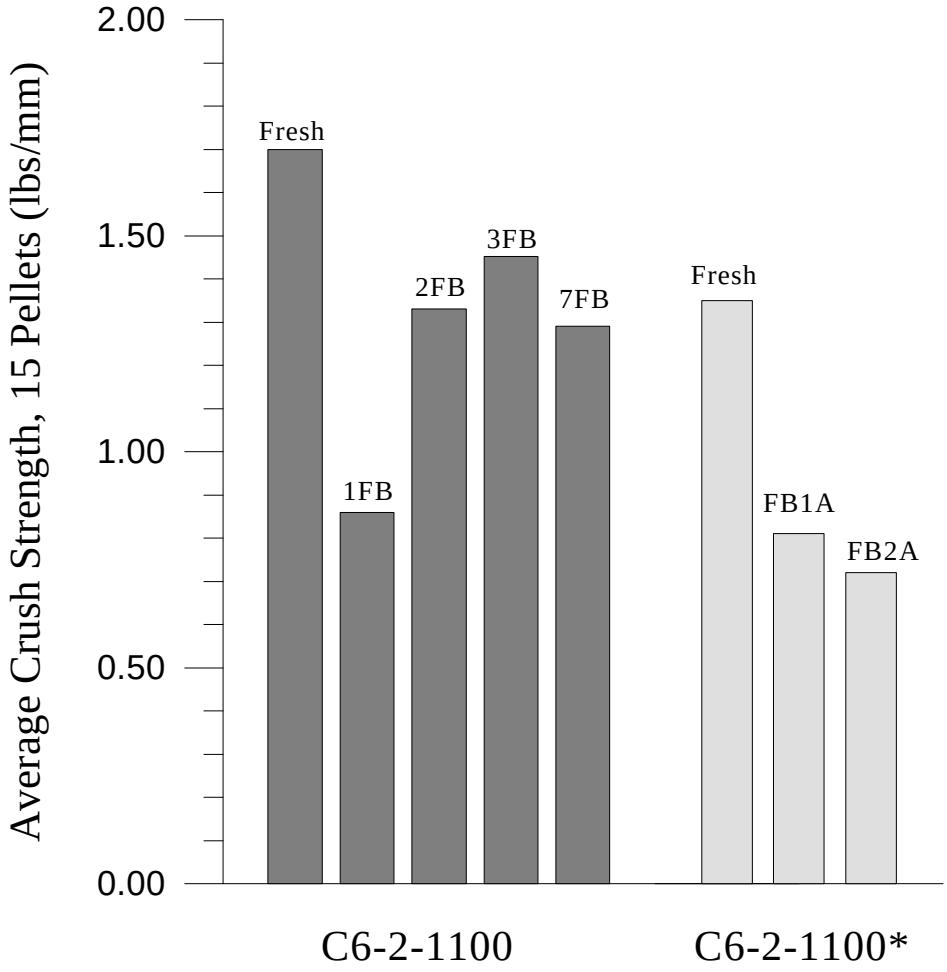

Figure 6.49. Average Crush Strength for C6-2-1100 formulations fresh and after 5 cycles in fixed bed. *A second batch of C6-2-1100 was prepared with slightly different fresh strength, 4 cycles

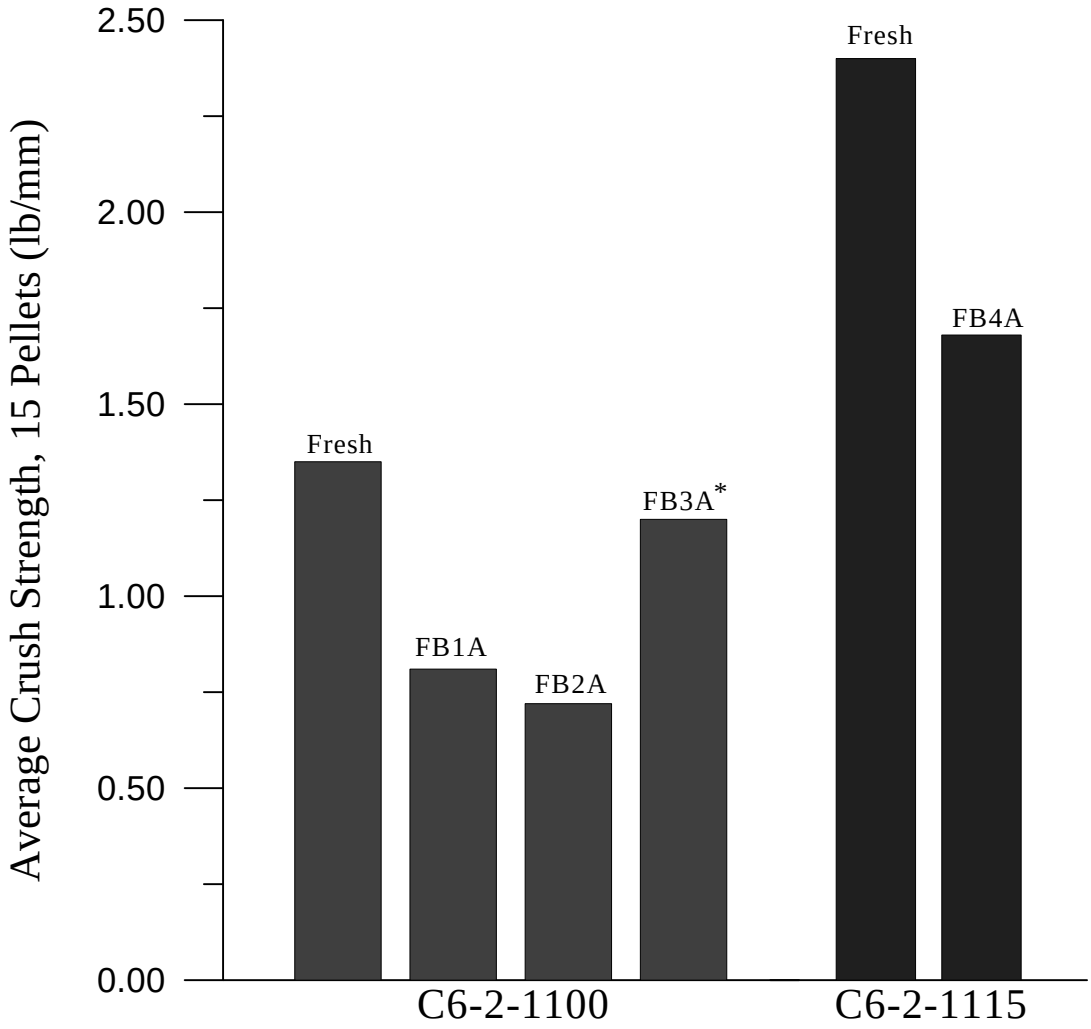

Figure 6.50. Crush strength of sorbents C6-2-1100 and C6-2-1115 after 4 cycles of sulfidation and regeneration in a fixed-bed reactor. *Crush strength of sorbent after 3.5 cycles (sulfided state).

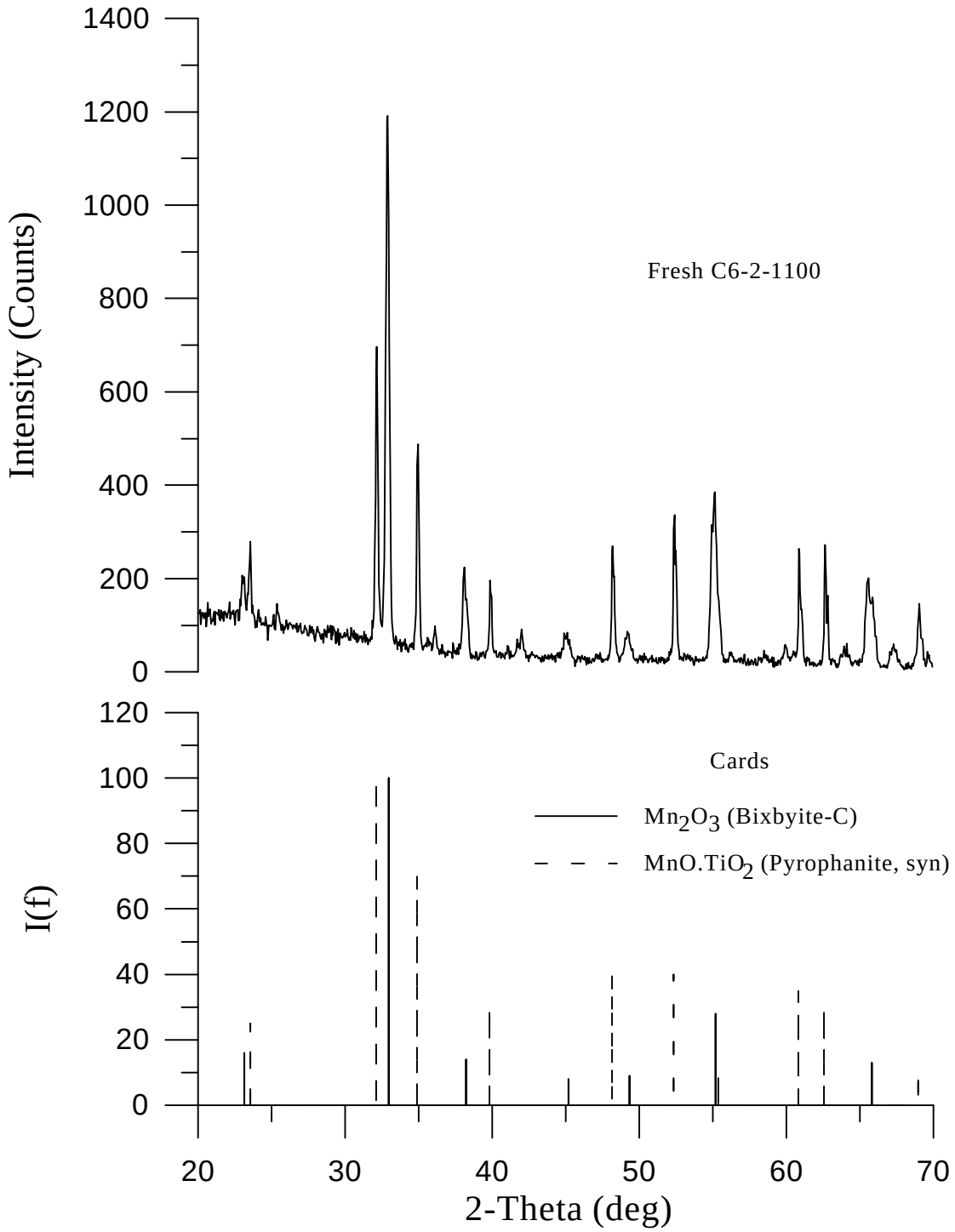

Figure 6.51. X-ray diffraction patterns of fresh C6-2-1100

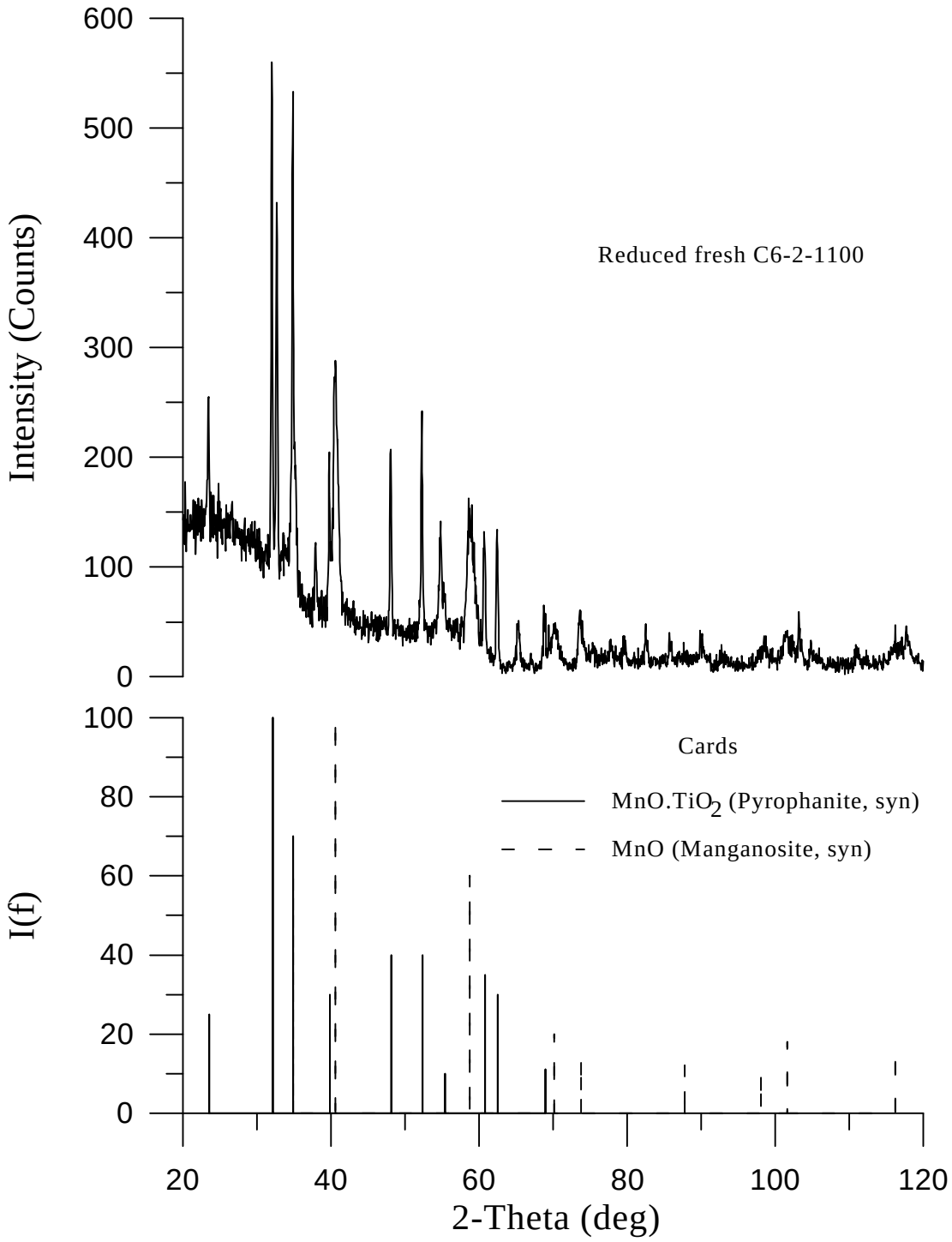

Figure 6.52. X-ray diffraction patterns of reduced fresh C6-2-1100.

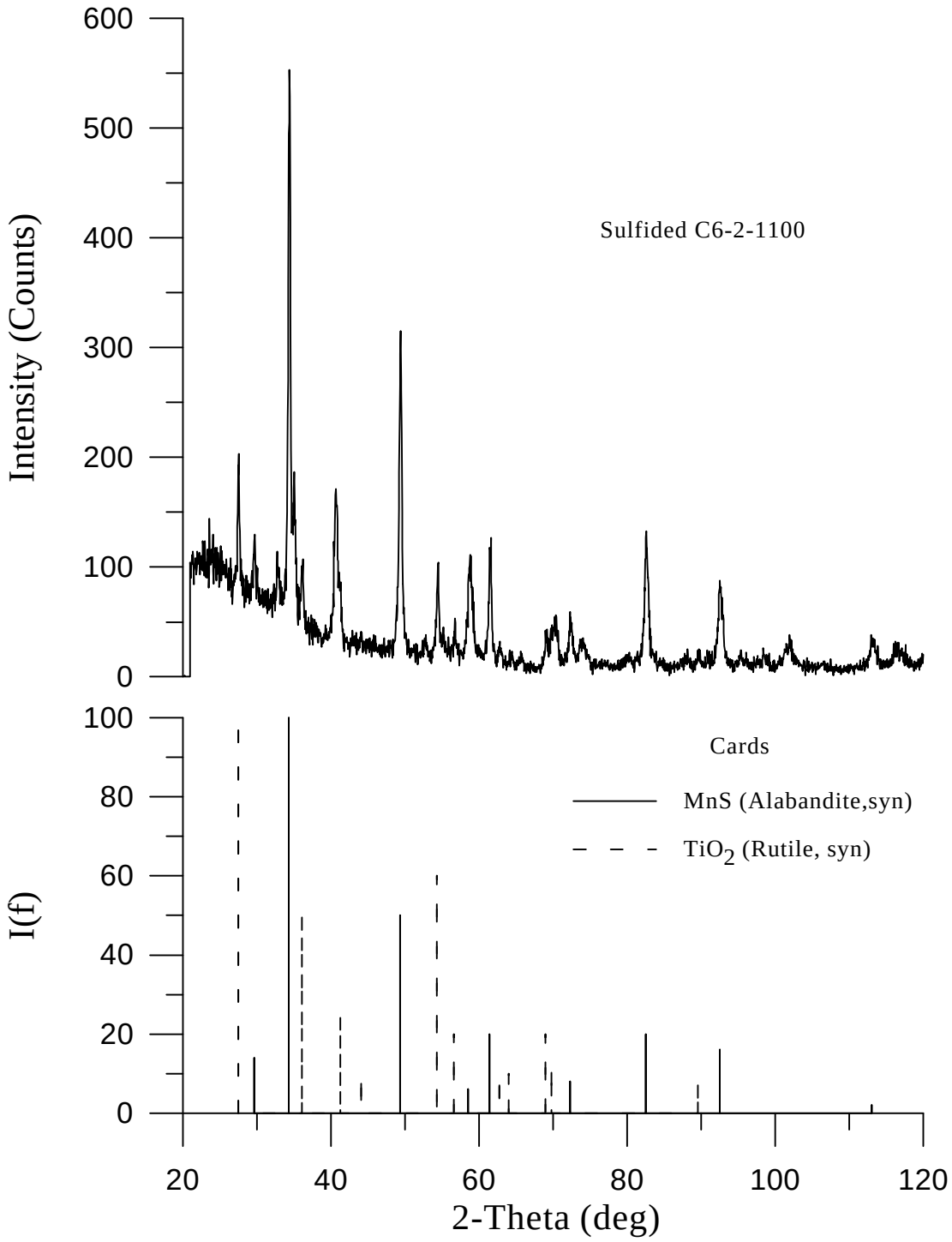

Figure 6.53. X-ray diffraction patterns of sulfided C6-2-1100 from test FB3A, 3.5 cycles.

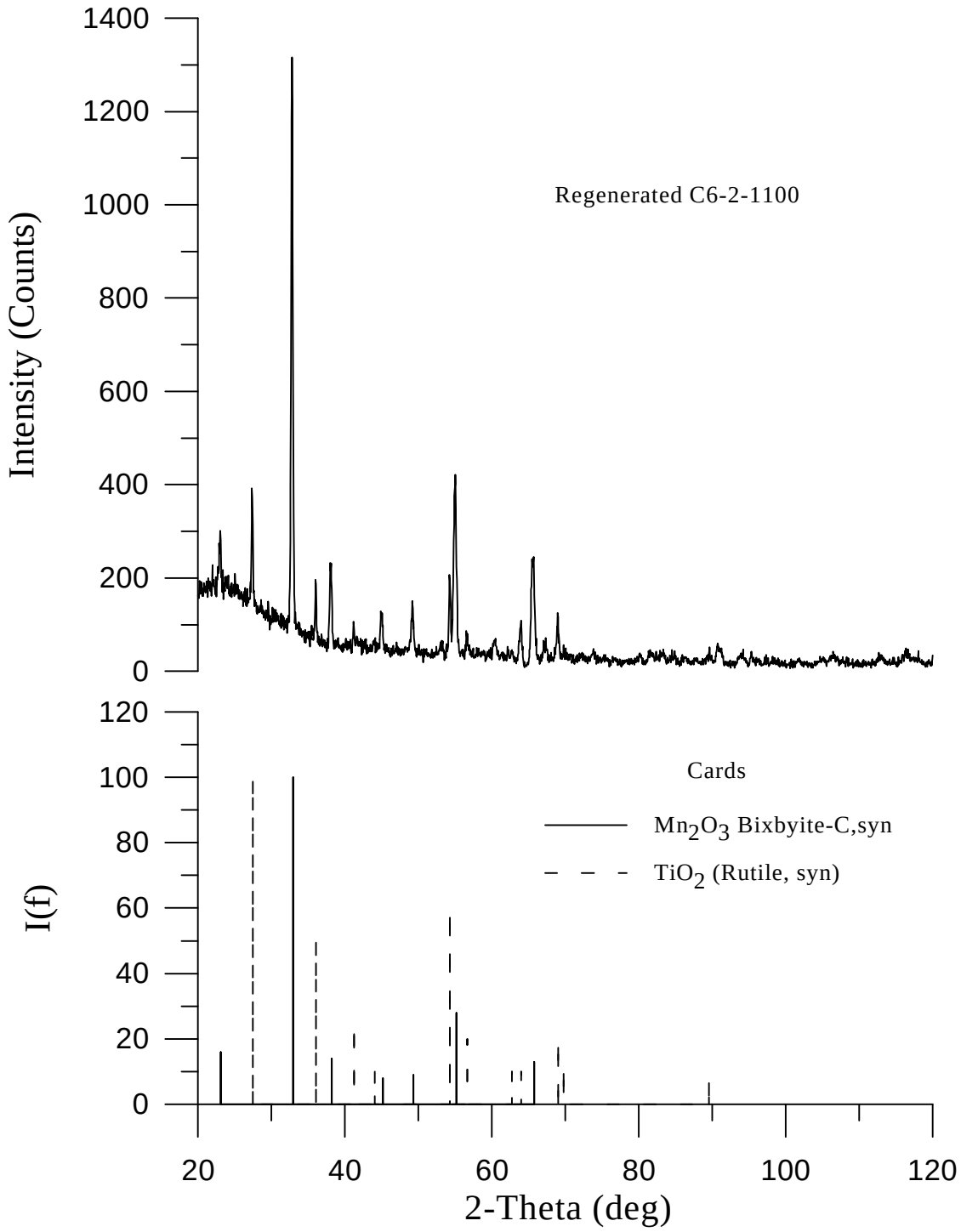

Figure 6.54. X-ray diffraction patterns of regenerated C6-2-1100 from test FB1A after 4 cycles.

CHAPTER 7. CONCLUSIONS

7.1 Theoretical Conclusions

Manganese oxide will theoretically lower the H_2S concentration in Shell coal gas to levels that are acceptable for IGCC applications (<100 ppmv) at reaction temperatures in excess of 900^oC, while a temperature of less than approximately 600^oC is needed to desulfurize KRW gas.

Regeneration should be carried out at a temperature above 900^oC when regenerating in air at ambient pressure to avoid sulfation. It may be possible to lower this temperature using dilute air or air/steam mixture and still keep sulfate formation to a minimum.

7.2 Experimental Conclusions

Preliminary work using TGA testing indicated titania to be a superior substrate than alumina probably because the manganese/titania bond is weaker than the manganese/alumina bond. This means the manganese which is tied up in forming a spinel has a higher activity in the titania form than the alumina form and is more effective in reacting with sulfur.

It is becoming increasingly clear that, current pellet formulations are limited by intra-particle transport resistances. As such, pore structure design and characterization were directed toward higher substrate fractions and no bentonite addition. However, fixed-bed testing showed bentonite addition may be necessary to retain pellet strength over multiple sulfidation and regeneration cycles.

Manganese based sorbents with molar ratios >1:1 Mn:substrate were effective in reducing the H_2S concentration in simulated coal gases to less than 100 ppmv over many cycles in fixed-bed reactor. Actual breakthrough time for formulation C6-2-1100 was as high as 73% of breakthrough time based on wt% Mn in sorbent.

Titania and alundum should be used as a substrate, not as a reactant to combine with manganese, because if combined the manganese becomes much less effective in reaching the low levels of H_2S required by the desulfurization process for hot fuel gas.

Regeneration in steam and nitrogen at 750^oC in fixed-bed operation did not effectively regenerate the pellets. This was true for both titania and alumina supported sorbents. Therefore steam should not be used as a reactant to regenerate the sorbent, rather it should be used as a diluent with air to keep the temperature from rising sharply during regeneration. Regeneration in air produced fast rising temperatures that may have caused sintering of the pellets.

Regeneration in 95% N_2 and 5% O_2, appeared to regenerate the sorbent the best, however, the % SO_2 achieved in the exit gases was low and the time required to achieve complete regeneration was high (approximately 2% and 450 minutes respectively). Regeneration of the sorbent should produce a sulfur

product that is recoverable either directly or indirectly and the time to regenerate should also be considered.

Regeneration in 60% air and 40% steam regenerated the sorbent completely while minimizing sulfate formation and large increases in temperature. Regeneration in 60% air and 40% steam appeared to give the best combination of regenerabilty, sulfate control, length of regeneration and dry SO_2 exit concentrations.

Sorbent C6-2 showed excellent desulfurization performance in the temperature range of 500 to 600^oC with Shell gas flowing between 2 to 3 L/min (STP). The pre-breakthrough concentrations were below 100 ppmv for all tests. The pre-breakthrough concentrations remained below 100 ppmv over 4 consecutive sulfidations.

The sulfidation temperature and sorbent induration temperature greatly affected the sorbent's capacity at breakthrough. The breakthrough sorbent conversion increased only slightly as the superficial gas velocity decreased. The gas velocity also had no significant affect on the pre-breakthrough H_2S concentration.

It has been concluded that the optimum sulfidation temperature should be as high as possible before equilibrium and valve limitations occur. The optimum gas velocity should be as low as economically feasible; however, lowering the gas velocity will probably not improve sorbent performance that much. Finally the optimum sorbent induration temperature should only be as high as needed to achieve pellet strength requirements. Alternatively, a new method for preparing stronger pellets that provide the same level of desulfurization performance could be developed.

A mathematical model was developed that simulates the sulfidation reaction in a fixed-bed reactor. The effective diffusivity, De, was estimated by adjusting its value until a good match could be made between the predicted and experimental breakthrough curves. Using the estimated D_e value, the sorbent conversion as a function of axial position in the packed-bed was predicted and compared well with experimental sulfur analysis.

The crush strength of the manganese-based pellet (C6-2) was highly sensitive to the temperature at which it was indurated. It may be possible to reduce this sensitivity with lower temperatures for longer induration times. All pellets tested in the fixed-bed reactor had the required strength.

Crush strength testing done after 4 or 5 cycles showed decreases in strength from 12.6% to 57.9%. The lowest decrease in crush strength was for sorbent regenerated in a steam/N_2 mixture. However, a steam/N_2 mixture did not completely regenerate the sorbent. The largest decrease in crush strength was for a sorbent that did not contain any bentonite binder. Thus bentonite may be necessary component of the pellets.

Notation

A	gaseous reactant (H_2S)
b	stoichiometric coefficient = 1 for MnO, dimensionless
B	solid reactant (MnO)
C_A	molar concentration of A in the gas phase, mol/cm^3
C_A^*	dimensionless concentration of A, C_{Ab}/C_{AO}
C_{Ab}	bulk molar concentration of A in the gas phase, mol/cm^3
C_{AO}	molar concentration of A at the reactor inlet, mol/cm^3
C_{Ae}	molar concentration of A in equilibrium at the unreacted core interface, mol/cm^3
C_B	molar concentration of B in the solid phase, mol/cm^3
C_{BO}	initial molar concentration of B in the solid phase, mol/cm^3
D_e	effective diffusivity of A in the product layer, cm^2/min
G	gas flowrate (STP), cm^3/min
k	intrinsic reaction rate constant, cm/min
k_g	external mass transfer coefficient, cm/min
J_A	molar flux of A, mol/cm^2·min
L	length of packed-bed, cm
mw_B	molecular weight of B, (grams B)/(mol B)
N_A	moles of gaseous reactant A
N_B	moles of solid reactant B
N_{gfd}	rate of reaction of A when reaction is gas film diffusion controlled
N_{pld}	rate of reaction of A when reaction is product layer diffusion controlled
N_{rxn}	rate of reaction of A when reaction is chemical reaction controlled
Q	amount of sorbent in packed-bed, g
r	radial distance along the product layer, cm
r_A	global reaction rate, mol A/min·cm^3
r_c	radius of the unreacted core, cm
R	radius of particle (pellet), cm
S.S.V.	empty-bed standard space velocity hr^{-1}
t	time, min
t^*	dimensionless time, t/T_{th}
T	temperature, K

T_{th} theoretical breakthrough time, $(QW_B)/[G(C_{AO}-C_{Ae})mw_B]$

u superficial gas velocity, cm/min

V volume of reactor, cm^3

V_p volume of particle (pellet), cm^3

W_B weight percent B in sorbent, (grams B)/(grams sorbent)

X fractional conversion of B, dimensionless

z axial position within reactor, cm

z^* dimensionless axial position, z/L

Greek

ε bed porosity, dimensionless

ρ_B molar density of B, mol/cm^3